Dynamics of Polymers, Colloids and Mixtures close to Hard Wall

by

Vassiliki N. Michailidou

Submitted for the degree of Doctor of Philosophy

Department of Materials Science and Technology
University of Crete

October 2008

Abstract

The main aim of this work is to study the interfacial dynamics of different soft matter systems such as polymer brushes, colloidal particles and mixtures. The main technique employed is the Evanescent Wave Dynamic Light Scattering, used to probe dynamics near a surface.

A complete study on the collective dynamics of end-grafted polystyrene brushes in pure solvents, including good solvents and a theta solvent using the powerful technique of evanescent wave dynamic light scattering will be presented. Synthesis of a wide range of polymer brushes was carried out using the "grafting from" technique. Using different monomers such as polystyrene and polymethylmethacrylate and varying some parameters such as polymerization time and temperature, well – defined polymer brushes were achieved. All brushes had high molecular weight (10^6 g/mol) and different dry thickness, which were measured by ellipsometry as well as atomic force microscopy (AFM). Initially, we examine the dynamics of polymer brushes in good solvent, where the polymer brush is fully swollen and we had identified the theoretically predicted cooperative diffusion. The effect of grafting density in the dynamics was explored as well as the associated intensities. When the solvent quality changes from marginal to poor, the relaxation function was found to exhibit strong effect as compared with the smooth variation of the brush density profile. From a single exponential above 50 °C, the correlation function became a two-step decay function. The fast decay was still assigned to the cooperative diffusion albeit slower than in the good solvent regime whereas the slow non – exponential and non – diffusive process might relate to microsegragated and/or chain dynamics in the present polydisperse brush. The relaxation function of the present three brushes with different grafting density revealed similarities and disparities between wet brushes and semidilute polymer solutions.

Extending these studies on a polymer brush/particle system, we have shown how particle penetration in the brush can be measured and offer an estimate of the brush height and how different degree of penetration affects the measured surface diffusivities. It was shown that the presence of the brush affects the distribution of the particles, especially large hard sphere particles that were not able to penetrate the brush while smaller sized softer particles could partially penetrate the soft layer formed by the polymer brushes. The distribution of the particles was deduced from the penetration depth dependence of the scattering intensities.

In addition, we further investigate the diffusivities of colloidal particles within swollen brushes, focusing on the effect of the brushes grafting density on both particle penetration and diffusivity. The diffusivities themselves of the colloidal particles were also an issue of investigation. Larger non – penetrating particles were seen to be slightly lubricated, the polymer brush providing a screening of

the wall – particle hydrodynamic interactions. The smaller/softer penetrating particles lead to a more complex phenomenology. The slowing down appears to depend very strongly on the size of the particles.

Finally, we use evanescent wave dynamic light scattering to investigate the Brownian motion of colloidal particles near a solid, planar surface. In the dilute regime, the diffusion coefficient near the interface was found to be much smaller than that for free diffusion in bulk solution. This was attributed due to the hydrodynamic interactions between the sphere and the solid wall, which slows down the motion. The wall-induced reduction of the self- diffusion was negligible at higher volume fractions due to interplay between the particle-wall and particle-particle hydrodynamic interactions. A simple model was proposed that captured the basic physical mechanism responsible for such behaviour, while a quantitative prediction of the weaker decay of the near-wall self-diffusion coefficient with volume fraction was offered by Stokesian Dynamics simulations. At high volume fractions, it seems that the particles exhibit similar behaviour either when in close proximity to another particle or to the wall.

The same system was used to study the anisotropic diffusion of colloidal suspensions, varying the volume fraction of the colloidal suspensions, from the dilute to a concentrated regime. The near wall dynamics were compared to the associated bulk dynamics of the hard spheres and the main finding was that the parallel diffusivities in the concentrated suspensions behave similarly to the bulk dynamics in contrast with the perpendicular ones that are affected stronger by the presence of the wall.

Papers included in this thesis

[1] G. E. Yakubov, **V. N. Michailidou**, B. Loppinet, G. Fytas and J. Rühe

Polymeric Materials: Science & Engineering, **2004**, 90, 296

"Evanescent Wave Dynamic Light Scattering from End-Grafted Polymer Brushes"

[2] **V. N. Michailidou**, B. Loppinet, O. Prucker, J. Rühe and G. Fytas

Macromolecules, **2005**, 38, 8960

"Cooperative Diffusion of End-Grafted Polymer Brushes in Good Solvents"

[3] **V. N. Michailidou**, B. Loppinet, D. C. Vo, O. Prucker, J. Rühe and G. Fytas

J. Polym. Sci. Part B: Polym. Phys. **2006**, 44, 590

"Dynamics of End-Grafted Polystyrene Brushes in $\Theta -$ Solvents"

[4] E. Filippidi, **V. N. Michailidou**, B. Loppinet, J. Rühe and G. Fytas

Langmuir Letter. **2007,** 23(9)**,** 5139

"Brownian diffusion close to a polymer brush"

[5] V. N. Michailidou, B. Loppinet, J. Rühe and G. Fytas

Eur. Phys. J. E **2008**, 26, 35

"Observation of slow down of polystyrene nanogels diffusivities in contact with swollen polystyrene brushes"

[6] **V. N. Michailidou**, G. Petekidis, J. W. Swan and J. F. Brady

Submitted to PRL

"Dynamics of concentrated colloidal suspensions near a hard wall"

[7] **V. N. Michailidou**, G. Petekidis, J. W. Swan, J. F. Brady, P. Lang and J. K. G. Dhont

In preparation

"Measurement of anisotropic Brownian motion near an interface by evanescent wave dynamic light scattering"

List of Figures & Tables

List of Tables

Acknowledgments

I would like to express my gratitude to my supervisors, G. Fytas and G. Petekidis, whose expertise, understanding, and patience, added considerably to my experience. I appreciate their vast knowledge and skill in many areas and their assistance in writing. I would like to especially thank Benoit Loppinet for the continuous assistance he provided at all levels all these years. Finally, I would like to thank Maria Vamvakaki for the support and the inspiration.

I must also acknowledge J. Rühe, O. Prücker and Hyun-Kwan Yang from IMTEK, Freiburg, and J. K. G. Dhont and P. Lang from IFF-Soft Condensed Matter in Jülich, for the great experience working with them and the friendly environment. Additionally, J. Brady and J. Swan for the nice collaboration we had.

Of course all these years, good friends were supporting me in different ways. Dafni, Nadia, Maria and Markella are some of my good friends and I cannot forget all my friends and collaborators from the Polymer Group.

I would also like to thank my family for the support they provided me through my entire life and in particular.

to my family

CONTENTS

CHAPTER 1

CHAPTER 2

CHAPTER 3

3. RESULTS & DISCUSSION
DYNAMICS OF POLYMER BRUSHES…………..…....43

CHAPTER 4

4. RESULTS & DISCUSSION

CHAPTER 5

5. CONCLUSIONS

Chapter 1

1. INTRODUCTION

An interface is the boundary between two non-miscible materials. There are interfaces between liquid – solid, liquid – liquid, liquid – gas, solid – solid and solid – gas, but not gas-gas. Interfaces are an important ingredient of mesoscopic systems such as colloids and polymers as well as biological systems such as cells and biomembranes.

With the advance of microfludics and the miniaturisation of processes, a fundamental understanding of how surface properties might affect the overall flow behaviour becomes crucial to the design of micron-sized devices. For large volume-to-surface ratios, surface effects are not essential and simple effective boundary conditions can reliably be used. With increasing surface to volume ratio surface effects become dominant and must be taken into account. They can range from no-slip to slip depending on the surface treatment.

Some of the most important chemical and physical processes on our planet occur at a surface or interface. The surface of a medium whether it is a liquid or a solid has very special

properties, which are often quite distinct from the bulk substance. For example, the surface of water has a very high surface tension, allowing more dense objects to float on top of it. The surface of a semiconductor can have very different electronic properties than the bulk due to the molecular orbitals of the surface atoms, which are left "dangling" as the bulk lattice is terminated. In the biochemical area, most drugs act by interaction with substances at cell surfaces and surface chemistry plays an important role in the events that govern such processes. Several research groups are involved in studies of surfaces and interfaces that examine a range of environmentally, biologically and technologically important surfaces and interfaces using a wide range of methods and techniques.

End grafting macromolecules to solid surfaces represents one of the most popular ways of modifying and functionalizing surfaces, with a breadth of applications in various fields of microsystems engineering such as biochips, microfluidics and sensor construction [1]. At high surface coverage, polymer chains grafted at one end to a planar surface in contact with good solvent are strongly stretched, forming a polymer brush [2]. This high stretching, a result of large excluded volume interaction between monomers can be affected by controlling the grafting density of the latter. Polymer brushes have recently attracted considerable attention and have found application in a broad range of fields, including colloid stabilization, tailoring surface properties and "chemical gates" [2] with numerous studies related to the synthesis and the examination of their structure and novel properties [3-5].

Upon lowering the solvent quality, the brush becomes increasingly compact and finally becomes insoluble. At theta conditions, where the excluded volume interactions vanish, chains adopt Gaussian statistics. Such a switching between an extended and a compact conformation of the surface-attached molecules is very interesting for sensor applications because at such a transition the sensitivity of the sensing layer is highest due to the increased analyte concentration. For sufficiently poor solvents, computer simulations [6, 7] and self-consistent field calculations have predicted lateral inhomogeneities leading to segregation within the grafted layer. Whereas the contraction of model brushes upon lowering solvent quality and the resulting concentration profiles have received considerable attention both theoretically and experimentally, the underlying concentration fluctuations in the brush at thermal equilibrium is essentially unexplored [8].

Colloidal diffusivity close to surface can offer direct information on the nature of these effects. The case of a hard wall has received significant attention and the expected hydrodynamic slow down of particle diffusivity is now well confirmed experimentally [9-12]. More complex surfaces can lead to a strongly different behaviour. A non-wetting, super-hydrophobic surface was reported to lead to a small, hardly measurable slow-down of particle diffusivity close to the surface indicating slip boundary conditions in that case [13].

Polymer brushes, which are formed when macromolecules are densely attached to solid surfaces, can offer a model of soft penetrable surfaces. They are also known to provide very good lubrication conditions [11]. The flow behaviour of particles in contact to such penetrable surfaces should depend on both their size and shape, which is predicted to control the penetration of particles in polymer brushes [14, 15]. The particle – polymer interactions are relevant in nanostructure formation such as in template-driven organization [16] in block copolymer/particle mixtures [17]. It is conceivable that the structure of the chains that ultimately defines the density profile of the brush also controls both how particles penetrate the brush and what their dynamics is. Reciprocally, information on the structure of a brush could be obtained from the particle penetration and diffusion. The latter is useful in view of the lack of scaling arguments on real, polydisperse brushes [7, 11, 18].

Consequently, the Brownian motion of systems such as colloidal particles and polymer chains near a solid or a liquid interface is of central importance and determines their macroscopic properties. Such confined dynamics are affected by direct energetic interactions between the interface and the Brownian diffuser as well as excluded volume and hydrodynamic interactions. Hydrodynamics do strongly affect the diffusion and flow of particles near a hard wall [10, 19, 20] whether between two bounding surfaces [21] or in microfluidic channels [22].

Therefore, Brownian motion of colloidal particles near surfaces is of great interest from both standpoints of fundamental mesoscopic physics and interface science as well as for its high technological relevance. A key question is how particle dynamics are affected by the existence of a non – penetretable wall via hydrodynamic interactions. Experimentally, confocal microscopy and Evanescent wave dynamic light scattering (EWDLS) [9, 19, 23] have been used to study dynamics near surfaces. Confocal microscopy [24] is limited by the size of the particles whilst EWDLS needs a careful interpretation of the intensity time autocorrelation function. Currently, only initial decay of the EWDLS autocorrelation function from dilute

suspensions is well described talking into account both the anisotropic (parallel and perpendicular to the surface) diffusion as well as the particular evanescent wave illumination and wall mirror effect [9, 23].

With increasing volume fraction of the colloidal suspensions, particle – particle hydrodynamics become important and modify the wall – induced drag effect. Furthermore, the liquid to solid transition in confined systems is directly related with the way particles dynamics are highly concentrated suspensions are affected by the presence of a non – penetrable wall [25]. However, near wall dynamics in concentrated suspensions are virtually unexplored either experimentally or theoretically. Thus very little is known about the volume fraction dependence of the particle wall hydrodynamics and near wall diffusivities.

1.1   Introduction to Polymer Brushes

Polymer brushes refer to an assembly of polymer chains which are tethered by one end to a surface or interface [6]. Tethering of the chains in close proximity to each other forces the chains to stretch away from the surface to avoid overlapping (Figure 1.1). Polymer brushes have recently attracted considerable attention and have found application in a broad range of fields, including colloid stabilization, tailoring surface properties and "chemical gates" [26] with numerous studies related to the synthesis and the examination of their structure and novel properties [26-32].

Figure 1.1: Polymer brush systems (a) adsorbed diblock copolymers and (b) end-grafted polymers.

Polymer brushes are typically synthesized by two different methods, physisorption and covalent attachment. Polymer physisorption normally involves absorption of block copolymers onto a substrate, where one block interacts strongly with the surface and the other block forms the brush layer (Figure 1.1a)[33]. The disadvantages of physisorption include thermal and solvolytic instabilities due to the non-covalent nature of the grafting, poor control over polymer chain density and complications in synthesis of suitable block copolymers.

Covalent attachment of polymer brushes can be achieved by either "grafting to" or "grafting from" techniques (Figure 1.1b). The "grafting to" technique involves tethering preformed end-functionalized polymer chains to a suitable substrate under appropriate conditions [34].

This technique often leads to limited grafting density and film thickness, as the polymer molecules must diffuse through the existing polymer film to reach the reactive sites on the surface. The steric hindrance for surface attachment increases as the tethered polymer film thickness increases. To overcome this problem, the "grafting from" approach can be used and has generally become the most attractive way to prepare thick, covalently tethered polymer brushes with a high grafting density. In this method a reactive group is created on the surface that is able to initiate the polymerization, and the propagating polymer chain is growing *from* the surface. It can be employed with all polymerization types, and a number of papers have reported high amounts of immobilized polymer by using radical polymerization with various initiators.

In the past decade the use of controlled/living radical polymerization to prepare nanostructured materials has gained significant attention, as a wide range of functional monomers can be incorporated into polymeric and composite systems [35-37]. Among these, polymer brushes reemerged recently as a particularly fascinating synthetic target [30, 38]. Numerous reports describe polymer brushes prepared from block copolymers synthesized by ionic polymerization and subsequently adsorbed or grafted onto a flat substrate. Since the work of Rühe et al., [8, 39, 40] free-radical polymerization has been widely pursued as a route to grow covalently bound polymer chains from surfaces with high grafting densities. A natural evolution in polymer-brush synthesis led to the use of controlled/living radical polymerization to control film thickness and properties by the surface initiated growth of well-defined (co) polymers [41].

Numerous "living" free radical techniques have been used to produce polymer brushes, these include atom transfer radical polymerization (ATRP) [42-44], reversible addition-fragmentation chain transfer (RAFT) [45] and nitroxide mediated polymerization (NMP) [46] techniques.

Theory of polymer brushes

The study of polymer brushes extends into many fields, including physics, chemistry, material science and engineering. During the last three decades, the behavior of the tethered layers has been investigated using both experimental and theoretical methodologies. The internal structure of polymer brushes has also been illustrated by numerical and analytical self-consistent field calculations and by computer simulations. A characteristic feature of the brush is the grafting density σ, which corresponds to the number of chains per unit surface area grafted to the surface in an athermal solvent [47]. Therefore, the length $d = \alpha \sigma^{-1/2}$ corresponds to the distance between neighboring grafted sites where α is the monomer size. Alexander and de Gennes were the first who, in pioneering research in the 1970's described the scaling of neutral polymer monolayers that were irreversibly attached by one end on a surface. De Gennes [48] discussed the uniform adsorption of chains onto flat surface and found that at equilibrium the coverage density at surface is low and the spread-out chains can be described as a semi-dilute two-dimensional solution. In addition, Alexander [49] predicted the adsorption of polar-head-bearing chains on flat non-absorbing surface and discussed their conformation at a given density. The surface density can now be large and the layer thickness in equilibrium is always larger than the dimensions of the free chain. The chains are considered as linear series of blobs that are confined in a narrow cylinder and the correlation length ξ corresponds to the blob size is $\xi \approx \sigma^{-1/2}$. For a given and fixed density $\sigma \sim 1/d^2$ the thickness of the layer is determined by the opposition of the stretching free energy fs and the excluded volume repulsion fr within the layer [49]. Therefore, the free energy per chain can be expressed (in $k_B T \equiv 1$ units) as $f \sim fs + fr$, with the first term $fs \sim h^2/N$ being related to the conformational entropy and the second $fr \sim w\sigma N^2/h$ corresponding to the osmotic repulsion inside the layer. w is the excluded volume parameter, and by minimizing the free energy f with respect to h, we get the equilibrium brush height $h \approx N (\sigma w^{1/3})$ where N is the degree of polymerization of the

chain. This linear dependence of the brush height on N is a characteristic feature of the brush conformation and indicated that the chains in this state are indeed strongly stretched[49].

De Gennes in a following study [48] treated theoretically the conformational properties of flexible uncharged polymer chains grafted on a solid surface, which are immersed in good solvents and in solutions of the same polymer. In the limit of low σ the chain occupies roughly a half-sphere with radius $r \sim R_g = \alpha N^{3/5}$ as there is no overlapping of chains. In the case of overlapping coils surrounded by good solvent, the distance between neighboring grafted sites d is less than the gyration radius R_g of the polymer in solution, and the grafted chain is subdivided into blobs of linear size d that fill the space densely (Fig 1.1.1).
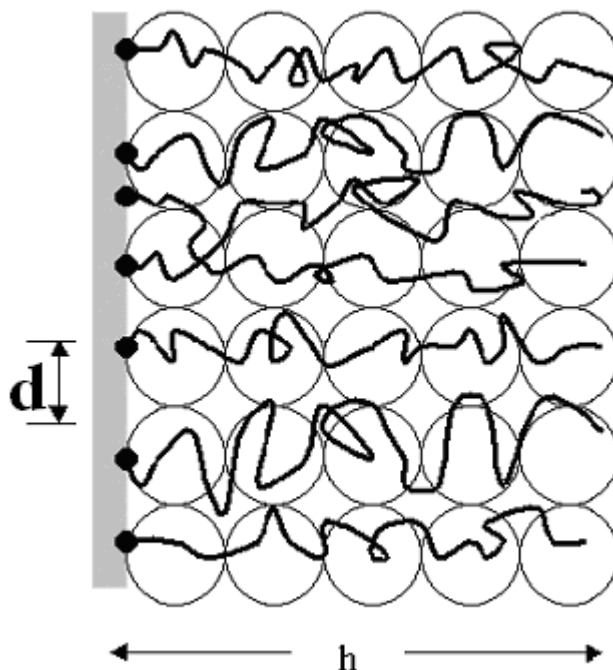
Figure 1.1.1 Schematic representation of the stretched conformation of tethered chains in good solvent as proposed by deGennes.

The polymer concentration is $\varphi_N \sim \sigma^{2/3}$ and the profile predicted shows a depletion layer near the wall. The thickness prediction by Alexander is still valid. If now the surrounding medium is a semi-dilute solution of the same polymer, the degree at which the free chains will penetrate the outer region of the layer depends on the ratio of the concentrations of the grafted and the free chains φ_N / φ_P.

This approximation for the brush as a stretched array of blobs, assumes uniform stretching for the chains, with the free end of each located at the top of the brush at height h from the surface [47]. The brush's corresponding density profile as given by Alexander – de Gennes would be a step function. A more accurate solution to the profile problem was developed by Milner et al. [50] by using a self-consistent field (SCF) approach which is valid in the limit of weak excluded volume and at moderately high surface coverage. Binary repulsions between chain segments are taken into account and the chain ends can be distributed throughout the whole grafted layer.
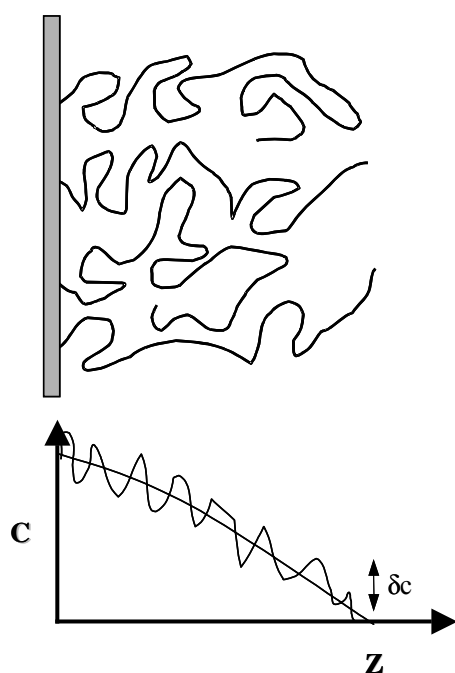
Figure 1.1.1b Schematic representation of an end anchored polymer brush along with its density profile C(z) and the fluctuations δc around the average C(z), where z is the distance from the wall [43].

The calculated density profile is a parabolic profile rather than a step function (Fig.1.1d), that corresponds to a unique global minimum of the free energy [50]. This prediction of a parabolic density profile has been confirmed experimentally for brushes in good solvents by neutron scattering techniques.

While the static properties e.g. density profile of polymer brushes in good and theta solvents have been extensively investigated both theoretically and experimentally [6, 51, 52], their dynamics have received much less attention [4, 7, 53] probably due to the paucity of experimental methods. Several motional mechanisms have been theoretically [48] proposed for the decay of the concentration fluctuations $<(\delta c)^2>^{1/2}$ in a brush in contact with a good solvent. Such motions involve single chain dynamics and collective many chains respiration modes in analogy to semidilute solutions of homopolymer chains [48]. Figure 1.1d shows schematically a snap-shot of an end-anchored polymer brush [51] and the fluctuations $<(\delta c)^2>^{1/2}$ around the average density profile C(z).

1.2 Introduction to Colloids

Colloidal systems are defined as systems consisting of a finely dispersed phase (~10 – 1000 nm) in a dispersion medium. A colloidal system consists of two separate phases: a dispersed phase (or internal phase) and a continuous phase (or dispersion medium). A colloidal system may be solid, liquid, or gaseous. Many familiar materials are colloidal such as milk, fog, paint, and whipped cream. The dispersed-phase particles have a diameter between 1 nm to 1 μm. Suspensions in liquids form the basis of a wide variety of systems of scientific and technological importance, including paints, ceramics, cosmetics, agricultural sprays, detergents, soils, biological cells, and many food preparations [54].

Colloidal particles need to be stabilized to prevent from aggregating. Stabilization can be either steric stabilization or electrostatic stabilization. Colloidal systems have many advantages and can be considered as ideal systems in order to investigate crystallization, glass transition and other phenomena of condensed matter. Interactions between colloidal particles, such as excluded volume interactions or van der Waals forces, can vary, switching the quality of the solvent, tuning the temperature or adding another component such as a polymer.

Hard sphere Colloids

The system studied in this work is the simplest possible particle dispersion. Colloidal hard spheres are ideal microscopic particles that interact with an infinite repulsive potential when they touch and zero elsewhere while moving within a medium with Brownian motion. Figure 1.2.1 below, shows the potential V(r), where R is the particle radius.
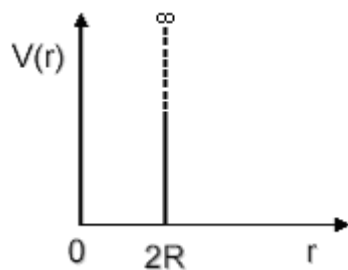
Figure 1.2.1 Pair potential of hard sphere particles

In hard sphere systems the enthalpic part of the free energy is zero and only the entropic term determines the phase behaviour. We can thus characterize this system by the number density

of the particles alone or more precisely by the colloid volume fraction: $$\Phi = \frac{4\pi R^3 N}{3V}$$

Small polymer chains are densely grafted on the surface of the colloidal particles to sterically stabilize these particles so when two particles approach the polymer layers interpenetrate resulting in the reduction of entropy of individual chains. This causes a strong repulsion between the two polymer layers preventing the particles from getting close enough for the Van der Waals forces to become significant. If the grafting density and length of the chains are properly tailored, the resulting potential for sterically stabilized particles is a good approximation of a hard sphere potential.

Hard spheres exhibit a liquid phase at volume fractions below 0.494, where the particles are free to diffuse and explore the whole volume available. A liquid – crystal coexistence phase is observed at volume fractions ranging from 0.494 to 0.545 and a fully crystalline structure between 0.545 and 0.58. As hard spheres cannot overlap, the maximum packing in an ordered state is $\Phi_{max} \approx 0.74$. If the particles form an amorphous random close packed structure then

the maximum packing fraction is $\Phi_{RCP} \approx 0.64$ [55]. The liquid – crystal coexistence phase has a linear dependence of crystal volume to volume fraction that makes it possible from the relevant heights of the phases to accurately determine volume fraction [56, 57].

The driving force behind the crystallization of hard sphere colloids is entropy. The increase of entropy leads to an ordered state, since the crystal structure gives freedom of movement to each particle around their lattice site by increasing individual free volume. Even though the particles are in an ordered state, the increase of entropy is greater than the reduction of the configurationally entropy. By further increasing of the volume fraction, the hard sphere particles reach a metastable state. Over $\Phi = 0.58$ the particles are not unable to move into the entropically favourable crystal positions anymore due to space restrictions and become trapped in a dynamically arrested glass phase [55, 56, 58]. Figure 1.2.2 below shows the hard sphere phase diagram.
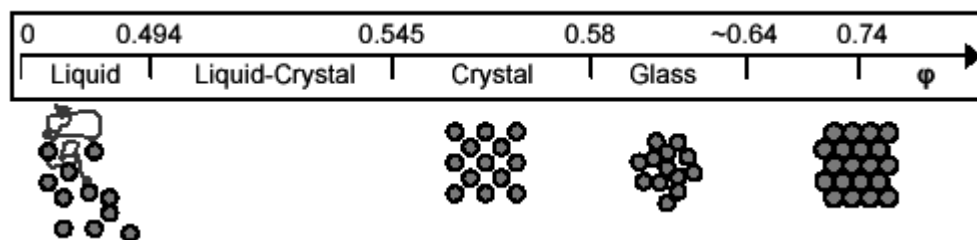
Figure 1.2.2 The Hard – Sphere Phase Diagram

1.3 Preface

In this work, we report a detailed study on the collective dynamics of end-grafted polystyrene (PS) brushes in pure solvents, including good solvents and a theta solvent (cyclohexane) as studied by evanescent wave dynamic light scattering.

We extend then our studies on a polymer brush/particle system, showing how particle penetration[14] in the brush can be measured and offer an estimate of the brush height and how different degree of penetration affects the measured surface diffusivities.

Further, we investigate the diffusivities of colloidal particles within swollen brushes, focusing on the effect of the brushes grafting density on both particle penetration and diffusivity. Three polystyrene brushes with similar molecular weight and different grafting densities are used alongside dilute solutions of two polystyrene nanogels. EWDLS is employed to measure both scattered intensities and relaxation functions of the nanoparticles at the polymer brush. The penetration of the polystyrene nano-gels within the brush layer and the retardation of their mobilities are strong size dependent.

Finally, we investigated the Brownian motion of colloidal particles near a solid, planar surface. Measurements were carried out for various volume fractions of PMMA hard-sphere suspensions over a range of scattering wave vectors. The striking finding of this study is that the dynamics of the dilute suspensions are mush more affected than in concentrated ones. Colloids have much slower dynamics in the presence of the wall in the dilute suspension while in the concentrated suspensions the dynamics of the particles near the wall are virtually the same with the bulk solution. A simple model captures the basic physical mechanism responsible for particles' behaviour, while a quantitative prediction of the weaker decay of the near-wall self-diffusion coefficient with volume fraction is offered by Stokesian Dynamics simulations. The same system was used to study the anisotropic diffusion of colloidal suspensions, utilizing the EWDLS set-up built in Julich (Germany), varying the volume fraction of the colloidal suspensions, from the dilute to a concentrated regime.

1.4 REFERENCES

1.   Advincula, R.C., B. Brittain, J. Rühe, and K. Caster, *Polymer Brushes*. 2004.

2.   Dai, L.L. and S. Granick, *Linear shear viscoelasticity of confined, end-attached polymers in a near-theta solvent*. Journal of Polymer Science, Part B: Polymer Physics, 2005. **43**(23): p. 3487-3496.

3.   Lai, P.Y. and K. Binder, *Structure and dynamics of polymer brushes near the ? point: A Monte Carlo simulation*. The Journal of Chemical Physics, 1992. **97**(1): p. 586-595.

4.   Semenov, A.N. and S.H. Anastasiadis, *Collective dynamics of polymer brushes*. Macromolecules, 2000. **33**(2): p. 613-623.

5.   Huang, J.R. and T.A. Witten, *Universal ratios of characteristic lengths in semidilute polymer solutions*. Macromolecules, 2002. **35**(27): p. 10225-10232.

6.   Milner, S.T., *Polymer Brushes*. Science, 1991. **251**: p. 905.

7.   Yakubov, G.E., B. Loppinet, H. Zhang, J. Ruhe, R. Sigel, and G. Fytas, *Collective Dynamics of an End-Grafted Polymer Brush in Solvents of Varying Quality*. Physical Review Letters, 2004. **92**(11): p. 115501-1.

8.   Prucker, O. and J. Ruhe, *Polymer layers through self-assembled monolayers of initiators*. Langmuir, 1998. **14**(24): p. 6893-6898.

9.   Holmqvist, P., J.K.G. Dhont, and P.R. Lang, *Anisotropy of Brownian motion caused only by hydrodynamic interaction with a wall*. Physical Review E - Statistical, Nonlinear, and Soft Matter Physics, 2006. **74**(2).

10. Lobry, L. and N. Ostrowsky, *Diffusion of Brownian particles trapped between two walls: Theory and dynamic-light-scattering measurements*. Physical Review B - Condensed Matter and Materials Physics, 1996. **53**(18): p. 12050-12056.

11. Milner, S.T., *Polymer brushes*. Science, 1991. **251**(4996): p. 905-914.

12. Garnier, N. and N. Ostrowsky, J. Phys. II (France), 1991. **1**: p. 1221.

13. Joly, L., C. Ybert, and L. Bocquet, *Probing the nanohydrodynamics at liquid-solid interfaces using thermal motion*. Physical Review Letters, 2006. **96**(4).

14. Kim, J.U. and B. O'Shaughnessy, *Morphology selection of nanoparticle dispersions by polymer media*. Physical Review Letters, 2002. **89**(23): p. 238301/1-238301/4.

15. Kim, J.U. and B. O'Shaughnessy, *Nanoinclusions in dry polymer brushes.* Macromolecules, 2006. **39**(1): p. 413-425.

16. Lee, J.Y., R.B. Thompson, D. Jasnow, and A.C. Balazs, *Entropically driven formation of hierarchically ordered nanocomposites.* Physical Review Letters, 2002. **89**(15): p. 155503/1-155503/4.

17. Bockstaller, M.R., Y. Lapetnikov, S. Margel, and E.L. Thomas, *Size-selective organization of enthalpic compatibilized nanocrystals in ternary block copolymer/particle mixtures.* Journal of the American Chemical Society, 2003. **125**(18): p. 5276-5277.

18. Karim, A., S.K. Satija, J.F. Douglas, J.F. Ankner, and L.J. Fetters, *Neutron reflectivity study of the density profile of a model end-grafted polymer brush: Influence of solvent quality.* Physical Review Letters, 1994. **73**(25): p. 3407-3410.

19. Lan, K.H., N. Ostrowsky, and D. Sornette, *Brownian dynamics close to a wall studied by photon correlation spectroscopy from an evanescent wave.* Physical Review Letters, 1986. **57**(1): p. 17-20.

20. Squires, T.M. and M.P. Brenner, *Like-charge attraction and hydrodynamic interaction.* Physical Review Letters, 2000. **85**(23): p. 4976-4979.

21. Pesche, R. and G. Nagele, *Stokesian dynamics study of quasi-two-dimensional suspensions confined between two parallel walls.* Physical Review E - Statistical Physics, Plasmas, Fluids, and Related Interdisciplinary Topics, 2000. **62**(4 B): p. 5432-5443.

22. Beatus, T., R. Bar-Ziv, and T. Tlusty, *Anomalous microfluidic phonons induced by the interplay of hydrodynamic screening and incompressibility.* Physical Review Letters, 2007. **99**(12).

23. Holmqvist, P., J.K.G. Dhont, and P.R. Lang, *Colloidal dynamics near a wall studied by evanescent wave light scattering: Experimental and theoretical improvements and methodological limitations.* Journal of Chemical Physics, 2007. **126**(4).

24. Carbajal-Tinoco, M.D., R. Lopez-Fernandez, and J.L. Arauz-Lara, *Asymmetry in colloidal diffusion near a rigid wall.* Physical Review Letters, 2007. **99**(13).

25. Nugent, C.R., K.V. Edmond, H.N. Patel, and E.R. Weeks, *Colloidal glass transition observed in confinement.* Physical Review Letters, 2007. **99**(2).

26. Y. Ito, S.N., Y. S. Park, Y. Imanishi, *Oxidoreduction-Sensitive Control of Water Permeation through a Polymer Brushes-Grafted Porous Membrane* Macromolecules, 1997. **30**: p. 5856.

27.   X. Kong, T.K., J. Abe, T. Iyoda, *Amphiphilic Polymer Brushes Grown from the Silicon Surface by Atom Transfer Radical Polymerization* Macromolecules, 2001. **34**(6): p. 1837.

28.   Y. S. Park, Y.I., Y. Imanishi, *Photocontrolled Gating by Polymer Brushes Grafted on Porous Glass Filter* Macromolecules, 1998. **31**: p. 2606.

29.   Zhao, B. and W.J. Brittain, *Synthesis, characterization, and properties of tethered polystyrene-b-polyacrylate brushes on flat silicate substrates.* Macromolecules, 2000. **33**(23): p. 8813-8820.

30.   Zhao, B. and W.J. Brittain, *Synthesis of polystyrene brushes on silicate substrates via carbocationic polymerization from self-assembled monolayers.* Macromolecules, 2000. **33**(2): p. 342-348.

31.   Zhulina, E.B., C. Singh, and A.C. Balazs, *Self-assembly of tethered diblocks in selective solvents.* Macromolecules, 1996. **29**(25): p. 8254-8259.

32.   Zhulina, E.B., C. Singh, and A.C. Balazs, *Forming patterned films with tethered diblock copolymers.* Macromolecules, 1996. **29**(19): p. 6338-6348.

33.   Belder, G.F., G. Ten Brinke, and G. Hadziioannou, *Influence of anchor block size on the thickness of adsorbed block copolymer layers.* Langmuir, 1997. **13**(15): p. 4102-4105.

34.   Mansky, P., Y. Liu, E. Huang, T.P. Russell, and C. Hawker, *Controlling polymer-surface interactions with random copolymer brushes.* Science, 1997. **275**(5305): p. 1458-1460.

35.   Hawker, C.J., *"Living" Free Radical Polymerization: A Unique Technique for the Preparation of Controlled Macromolecular Architectures.* Accounts of Chemical Research, 1997. **30**(9): p. 373-382.

36.   Patten, T.E. and K. Matyjaszewski, *Atom transfer radical polymerization and the synthesis of polymeric materials.* Advanced Materials, 1998. **10**(12): p. 901-915.

37.   Pyun, J. and K. Matyjaszewski, *Synthesis of nanocomposite organic/inorganic hybrid materials using controlled/"living" radical polymerization.* Chemistry of Materials, 2001. **13**(10): p. 3436-3448.

38.   Lodge, T.P. and M. Muthukumar, *Physical chemistry of polymers: Entropy, interactions, and dynamics.* Journal of Physical Chemistry, 1996. **100**(31): p. 13275-13292.

39.   Prucker, O. and J. Ruhe, *Mechanism of radical chain polymerizations initiated by azo compounds covalently bound to the surface of spherical particles.* Macromolecules, 1998. **31**(3): p. 602-613.

40.   Prucker, O. and J. Ruhe, *Synthesis of poly(styrene) monolayers attached to high surface area silica gels through self-assembled monolayers of azo initiators.* Macromolecules, 1998. **31**(3): p. 592-601.

41.   Ejaz, M., S. Yamamoto, K. Ohno, Y. Tsujii, and T. Fukuda, *Controlled graft polymerization of methyl methacrylate on silicon substrate by the combined use of the Langmuir-Blodgett and atom transfer radical polymerization techniques.* Macromolecules, 1998. **31**(17): p. 5934-5936.

42.   Kamigaito, M., T. Ando, and M. Sawamoto, *Metal-catalyzed living radical polymerization.* Chemical Reviews, 2001. **101**(12): p. 3689-3745.

43.   Patten, T.E., J. Xia, T. Abernathy, and K. Matyjaszewski, *Polymers with very low polydispersities from atom transfer radical polymerization.* Science, 1996. **272**(5263): p. 866-868.

44.   Wang, J.S. and K. Matyjaszewski, *Controlled/"living" radical polymerization. Atom transfer radical polymerization in the presence of transition-metal complexes.* Journal of the American Chemical Society, 1995. **117**(20): p. 5614-5615.

45.   Baum, M. and W.J. Brittain, *Synthesis of polymer brushes on silicate substrates via reversible addition fragmentation chain transfer technique.* Macromolecules, 2002. **35**(3): p. 610-615.

46.   Husseman, M., E.E. Malmstrom, M. McNamara, M. Mate, D. Mecerreyes, D.G. Benoit, J.L. Hedrick, P. Mansky, E. Huang, T.P. Russell, and C.J. Hawker, *Controlled Synthesis of Polymer Brushes by "Living" Free Radical Polymerization Techniques.* Macromolecules, 1999. **32**(5): p. 1424-1431.

47.   Rubinstein, M. and R.H. Colby, *Polymer Physics.* 2003: Oxford University Press.

48.   deGennes, P.G., J. Physique, 1976. **37**: p. 1445.

49.   Alexander, S., J. Physique, 1977. **38**: p. 583.

50.   Milner, S.T. and T.A. Witten, *1988.* Europhys. Lett. **413**(5).

51.   Binder, K., *Scaling concepts for polymer brushes and their test with computer simulation.* European Physical Journal E, 2002. **9**(3): p. 293-298.

52.   Milner, S.T., T.A. Witten, and M.E. Cates, *Theory of the grafted polymer brush.* Macromolecules, 1988. **21**(8): p. 2610-2619.

53.   Fytas, G., S.H. Anastasiadis, R. Seghrouchni, D. Vlassopoulos, J. Li, B.J. Factor, W. Theobald, and C. Toprakcioglu, *Probing collective motions of terminally anchored polymers.* Science, 1996. **274**(5295): p. 2041-2044.

54.   Russel W. B., S.D.A., and. Schowalter W. R., *Colloidal Dispersions.* 1989, Cambridge: Cambridge University Press.

55.   Snook, I., W. Van Megen, and P. Pusey, *Structure of colloidal glasses calculated by the molecular-dynamics method and measured by light scattering.* Physical Review A, 1991. **43**(12): p. 6900-6907.

56.   Pusey, P.N. and W. Van Megen, *Phase behaviour of concentrated suspensions of nearly hard colloidal spheres.* Nature, 1986. **320**(6060): p. 340-342.

57.   Pusey, P.N. and W. Van Megen, *Observation of a glass transition in suspensions of spherical colloidal particles.* Physical Review Letters, 1987. **59**(18): p. 2083-2086.

58.   Van Megen, W., S.M. Underwood, and P.N. Pusey, *Dynamics of hard spherical colloids from the fluid to the glass.* Journal of the Chemical Society, Faraday Transactions, 1991. **87**(3): p. 395-401.

Chapter 2

2. TECHNIQUES & MATERIALS

A. Techniques

2.1 Dynamic Light Scattering

Principles of DLS

The interaction of light with matter can be used to obtain important information both about the structure and the dynamics of matter. Light scattering experiments are based on such light – matter interactions. When light impinges on matter, the electric field of the light induces an oscillating polarization of the electrons in the molecules. The molecules then can serve as a secondary source of radiation and thus "scatter" light.

Dynamic light scattering is measuring particle motion moving due, for example, to Brownian diffusion. In a typical light scattering system the temporal fluctuation of the scattered intensity, I(t), will be measured, originating from the movement of the molecules. The intensity of scattered light will vary as the particles move around under Brownian motion causing constructive and destructive interference of the light. The dynamic information of the particles is derived from an autocorrelation of the intensity, $<I(t)I(0)>/<I(t)>^2 = G^{(2)}(t)$ recorded during the experiment.

When light irradiates matter the state of polarization of the molecules oscillates at the frequency of the irradiating light. This results in an electric field $\mathbf{E}$ (q, t) associated with the position of the molecules at a given time. This oscillating electric field produces light of the same wavelength as the incident light that is irradiated from the molecules essentially in a uniform manner in space. Constructive interference between the emitted light from two molecules or parts of a polymer results in the scattering pattern. The observed intensity is proportional to the square of the resulting electric field associated with the combination of light emanating from the irradiated volume. $I(q,t) = \left| E(q,t)^2 \right|$

Photon Correlation Spectroscopy - Set-up

In a photon correlation experiment the measured quantity is the normalized autocorrelation function of the scattered intensity. The relaxation time of the fluctuations is examined, providing information in the reciprocal space for the spatial Fourier length $2\pi/q$, where q is the scattering vector. In a typical dynamic-light-scattering set-up, light from a laser passes through a polarizer, which defines polarization of the incident beam and then impinges on the scattering medium. The scattered light passes then through an analyzer that selects a given polarization, and finally enters the detector. The position of the detector defines the scattering angle θ [1].

The autocorrelation function of the polarized light scattering intensity which is given by the following equation $G_{vv}(q,t) = \dfrac{<I(q,t)I(q,0)>}{<I(q,0)>^2}$, was measured at different scattering angles, θ, using an ALV spectrophotometer and an ALV-5000 full digital correlator over the time range 10^{-7}-10^3 s; I(q,0) is the mean scattering intensity. Generally both the incident and the

scattered beam were polarized perpendicular to the scattering plane (VV geometry). Here, a Torus diode-pumped Nd:YAG laser was used as the light source with wavelength $\lambda= 532$ nm and single mode intensity 170 mW. The magnitude of the scattering wavevector is $q = (\frac{4\pi n}{\lambda})\sin\left(\frac{\vartheta}{2}\right)$, where n is the refractive index of the medium. All measurements were performed at room temperature.
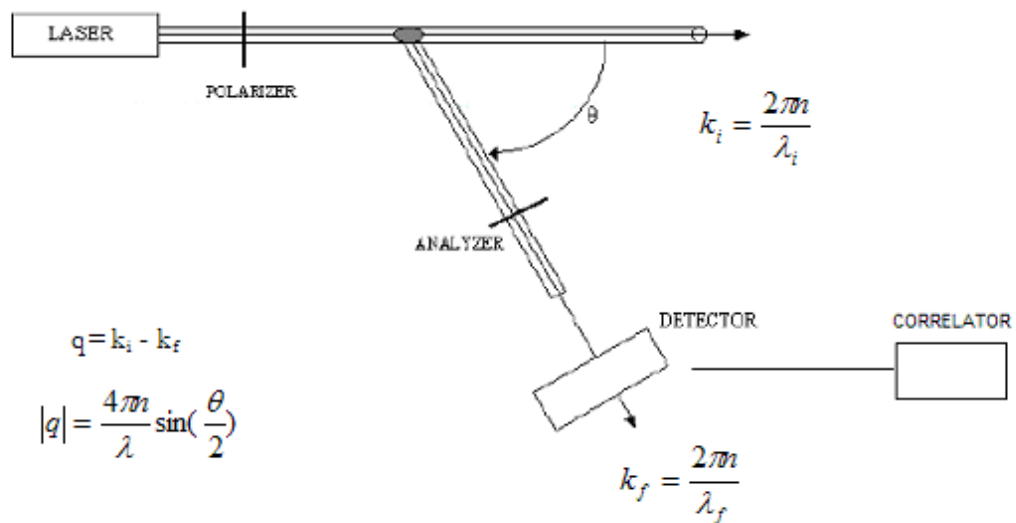
Figure 2.1 Typical dynamic light scattering set-up

2.2 Evanescent Wave Dynamic Light Scattering

Total Internal Reflection

An optical method that has been developed the last years for investigating dynamics close to a surface is Evanescent Wave Dynamic Light Scattering technique. The principle of this technique is the generation of the evanescent waves under total internal reflection conditions. Evanescent waves are formed when a light beam impinges at an interface at an angle greater than the critical angle so that total internal reflection occurs.

Etymologically, the word "Evanescent" means "tending to vanish", which is appropriate because the intensity of evanescent waves decays exponentially with distance from the interface at which they are formed [2-8].

Total internal reflection occurs when the incidence angle is greater than a critical angle, which is defined by the Snell's Law: $\theta_c = \sin^{-1}\left(\dfrac{n_1}{n_2}\right)$

where n_1 and n_2 are the refractive indices of the two media with $n_1 < n_2$.
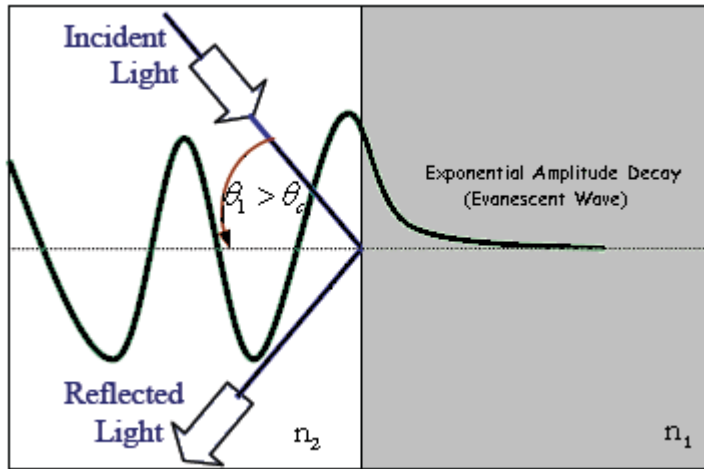
Figure 2.2a   Generation of evanescent waves under total internal reflection conditions.

In the case of the formation of the evanescent waves, at least one component of the wavevector **k** becomes imaginary or complex and the wave experiences exponential damping when propagating in this region. The magnitude of the imaginary part of the wavevector component defines the penetration depth Ξ [9] inside the forbidden region as:

$$\Xi = \frac{\lambda}{2\pi n}(\sin^2\theta_1 - \sin^2\theta_c)^{-1/2} = \frac{1}{\text{Im}(k)}$$

where θ_c is the critical angle an n is the refractive index of the medium of the higher refractive index which is usually a solid surface.
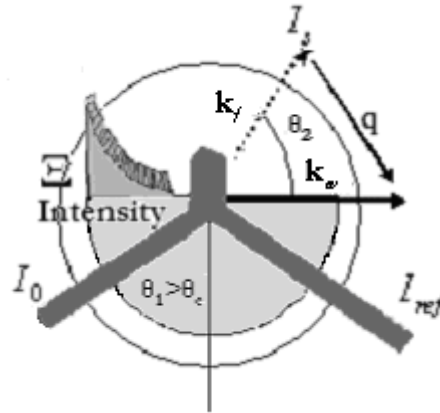
Figure 2.2b Geometry of evanescent waves

Generally, in a light scattering experiment, the scattered intensity is detected by a photomultiplier detector (PMT). When only scattered light falls on the PMT, we have homodyne conditions. On the other hand, when unscattered light is mixed with scattered light, we have heterodyne conditions. Under heterodyne conditions, we measure directly the $G^{(1)}(t)$. In some cases, we may have mixed homodyne and heterodyne conditions since the scattering intensity I_s is mixed with the I_0. So in this case using the following equation, we normalize the autocorrelation function within the homodyne limit [7].

$$G^{(2)}(t) = 1 + \frac{1}{(1+\alpha)^2}\left|G^{(1)}(t)\right|^2 + \frac{2}{(1+\alpha)^2}\mathrm{Re}[G^{(1)}(t)]$$

$$where: \alpha = \frac{E_0^2}{E_s^2} = \frac{I_0}{I_s}$$

Two evanescent wave dynamic light scattering set-up were used during this work. These are described below in detail.

EWDLS IESL-FORTH *Set-up*

This experimental set-up, allows for the probing of the Fourier component of the concentration fluctuations $c_q(t)$ with wave vector q at thermal equilibrium by the evanescent wave with a penetration depth Ξ inside the polymer brush layer. The evanescent light was generated by total internal reflection of the laser ($\lambda = 532$ nm) at the interface of a semi-cylindrical high refractive index prism, F2 glass by Schott, with a refractive index n = 1.627 in the wavelength of our source.

In an evanescent wave dynamic light scattering experiment, we have independent rotation of both the cell and a single mode optical fiber that in turn, permits to define both the angle θ_2 of the goniometer and the penetration depth Ξ, which was defined earlier. Hence the scattering wave vector is $\mathbf{q} = \mathbf{k}_f - \mathbf{k}_{ev}$ with $\mathbf{k}_{ev}$ and $\mathbf{k}_f$ being the wave vectors of the evanescent and scattered light. The autocorrelation function $G^{(1)}(q,t)$ of the scattered intensity was recorded over a broad time range by the ALV-5000 fast correlator under mainly heterodyne conditions due to the strong elastic scattering from the rough glass substrate. The whole set-up is illustrated in Figure 2.2c. Laser

The intermediate scattering function $C(q,t)$ at a given q was computed from the experimental $G^{(1)}(q,t)$ under heterodyne conditions i.e. $C(q,t) = [G^{(1)}(q,t)-1]/a$ where a is the short time amplitude of $G^{(1)}(q,t)$.
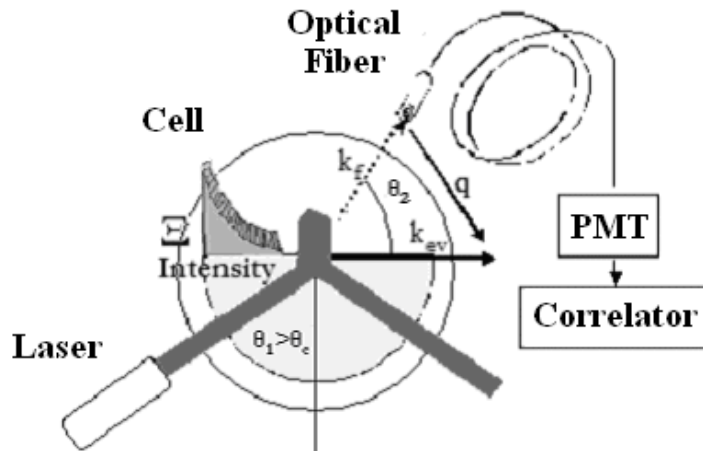
Figure 2.2c   Schematic representation of the evanescent wave dynamic light scattering instrumentation.

EWDLS Jülich Set-up *(Forschugszentrum Jülich, Institut für Festkörperforschung)*

This set-up was used to study the anisotropic diffusion of colloidal suspensions, varying the volume fraction of the colloidal suspensions, from the dilute to a concentrated regime.

A triple axis goniometer and a spherical sample cell to construct a scattering geometry as shown in Figure 2.2d was used. The cell consists of a massive SF10-glass semispherical lens covered by a dome, which contains the sample solution. The incident beam is totally reflected from the interface between the bottom part and the solution, if the angle of incidence is larger than the critical angle of total reflection θ_c. Since we can change the observation angle in –plane θ_2 and off – plane θ_c, $q_\perp = 2\pi \sin \alpha_r / \lambda$ can be changed while $q_{II} = 2\pi \sqrt{1 + \cos \alpha_r^2 - 2 \cos \alpha_r \cos \theta_2} / \lambda$ is kept constant and vice versa. The total scattering vector magnitude is given by $q = \sqrt{q_{II}^2 + q_\perp^2}$. In our experiments the illuminating beam comes from a He-Ne laser with a power of 35 mW and a vacuum wavelength of λ =632.8 nm, which is mounted on the source arm of the triple axis goniometer. Scattered light is collected with a single mode fiber and detected with an avalanche diode (ALV-APD, ALV-Laservertriebsgesellschaft, Germany). The diode's transistor-transistor logic (TTL) output is correlated with an ALV-6010 multiple tau correlator. Varying the angle of incidence, the penetration depth of the evanescent wave Ξ can be changed approximately in the range $100 nm < \Xi < 1 \mu m$. The upper limit is mainly set by focusing of the incoming beam in the bottom part of the sample cell and the divergence of the penetration depth at the critical angle. The nominal critical angle of total reflection θ_c can be calculated from the refractive index of the SF10 glass n_1=1.723 and of the solution n_2=1.497 for the sample solution. [10, 11]
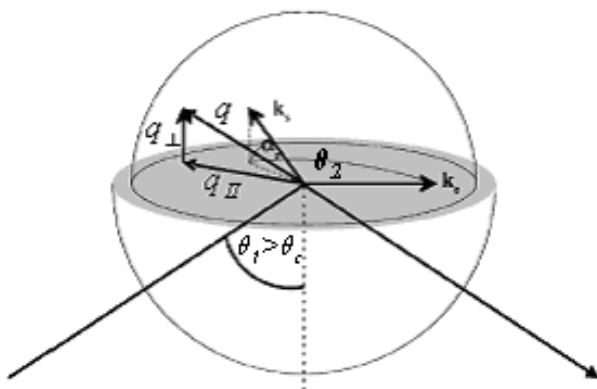
Figure 2.2d Spherical sample cell with total scattering vector q and scattering vector components parallel $q_{//}$ and normal $q_{\perp}$ to the reflecting interface.

Data Analysis

In many cases, the correlation function was described by an exponential decay and was fitted with a function of the form $C(q,t) = a\exp^{-(\frac{t}{\tau})}$ which gives the intensity (∞ α) and the relaxation time (τ), while the relaxation rate of the process is $\Gamma = 1/\tau$. In other cases nevertheless, the correlation function had a broader than exponential shape that required a different fitting function. In these cases the correlation function can be analyzed by the Kohrlausch-William-Watts (KWW) function fit, which is described as the following equation proposes: $C(q,t) = a\exp^{-(\frac{t}{\tau})^{\beta}}$ where β is the exponent parameter that takes values between 0 and 1. For $\beta = 1$ the relaxation is exponential whereas for $\beta < 1$ there is a distribution of characteristic times.

In other cases, where only a small part of the full correlation function was exponential, first cumulant analysis was chosen for the fitting of the data.

In every case, we can deduce the diffusion coefficient of either the polymer brushes or the colloidal particles, since:

$$\Gamma = \frac{1}{\tau} = Dq^2$$

Also, from the diffusion coefficient through the Stokes – Einstein – Sutherland's equation the hydrodynamic radii were calculated in each case using the following equation:

$$R_h = \frac{K_B T}{6\pi\eta D}$$

where η is the viscosity of the solvent, K_B is the Boltzmann's constant and T is the temperature of the sample.

As far as the colloidal particles concern, it is already known that they undergo Brownian motion, which is relatively simple in the dilute case and more complicated in the concentrated suspensions. In the dilute suspension, for a single particle that diffuses we can write:

$$< \Delta r^2(t) >= 6D_0 t$$

where $<\Delta r^2(t)>$ is the mean square displacement and D_0 is the diffusion coefficient of a single particle.

In the concentrated suspensions the dynamics of the colloids are more complicated. Other interactions such as hydrodynamics are involves in particles' motion. We will only investigate the time diffusion, determined by the initial slope of the correlation functions that will give an effective diffusion coefficient D_{eff} that is related to D_0, with the equation that follows:

$$D_{eff} = D_0 \frac{H(q)}{S(q)}$$

Where $H(q)$ is the hydrodynamic factor and $S(q)$ is the structure factor [12].

Thus the short time diffusion in general is affected by both hydrodynamics and thermodynamics.

In every part of this work, the fitting of the data will be discussed separately.

2.3 Brownian Motion

If we now consider the Brownian motion of a spherical particle suspended in a solvent at a given time t, we can divide the time in small intervals Δt, that correspond to $\Delta r(t)$ shifts. Then, the probability a particle to move around has a Gaussian distribution and is given by the following equation[1]:

$$P(r,t) = [\frac{2\pi}{3} < \Delta r^2(t) >]^{-3/2} \exp[-\frac{3r^2}{2} < \Delta r^2(t) >]$$

where $< \Delta r^2(t) >$ is the mean square displacement of the particle at a given time t.

Using this density probability the autocorrelation function will be given by the following equation:

$$g(t) = \exp(-q^2 \frac{<\Delta r^2(t)>}{6})$$

As also mentioned earlier, for a single particle that diffuses we can write: $<\Delta r^2(t)> = 6D_0 t$

where $\Delta r^2(t)$ is the mean square displacement and D_0 is the diffusion coefficient.

Finally, the autocorrelation function can be written as: $g(t) = \exp(-Dq^2 t)$

Brownian motion close to a wall

The 3D Brownian motion close to a wall can be analyzed in two independent motions; a parallel and a vertical to the surface. The parallel movement obeys the 2D statistics of the Brownian motion, while the latter one includes the "mirror effect" with the surface[13].
The probability density in this case can be given by the following equation:

$$P(r_{//}, z, z_0, t) = (4\pi Dt)^{-3/2} e^{-\frac{r_{//}^2}{4Dt}} \left[e^{\frac{-(z-z_0)^2}{4Dt}} + e^{\frac{(z+z_0)^2}{4Dt}} \right]$$

where (O, Z_0) and $(r_{//}, z)$ are the parallel and perpendicular coordinates of the particle at time 0 and t, respectively. The theoretical form of the surface correlation function g_{2D} is thus given by the following integral:

$$g_{2D} = \int\int\int P(r_{//}, z, z_0, t) e^{iq_{//}r_{//}} e^{iq_z(z-z_0)} d^2 r_{//} dz$$

where $q_{//}$ and q_z are the components of the scattering vector parallel and perpendicular to the wall.
This integral has been found to be equal to[14]:

$$g_{2D} = \exp(-Dq_{//}^2 t)g_z(q_z, \xi, D, t)$$

where $g_z(q_z, \xi, D, t)$ is an analytical function. The effect of the hydrodynamics

To account for this position dependence of the diffusion coefficient in the computation of the correlation function $g_s(t)$ is not a trivial matter, apart from short times compared to the correlation function relaxation time. In this limit, a limited expansion of the previous equation will yield to the following:

$$g_s^{(1)}(t) \cong \left[1 - Dq_{//}^2 t - D_z \left(q_z^2 + \frac{1}{\xi^2} \right) t \right]$$

Also, it can be assumed for short times, that a given scattering Brownian particle is confined to a volume small enough so that its diffusion coefficients $D_{//}(z)$ and $D_z(z)$ can be considered as constant. The observed correlation function is an average of the previous equation over all the Brownian particles contained in the scattering volume.

Taking into account the fact that the particles closer to the wall accept and thus scatter a higher intensity according to the exponential law $\exp(\frac{-2z}{\xi})$ that would lead to the following approximation:

$$g_s^{(1)}(t) \cong \frac{\int_0^\infty \left[1 - D_{//}(z)q_{//}^2 t - D_z(z)(q_z^2 + \frac{1}{\xi^2})t \right] \exp(\frac{-2z}{\xi}) dz}{\int_0^\infty \exp(\frac{-2z}{\xi}) dz}$$

$$g_s^{(1)}(t) \cong \left[1 - \bar{D}(\xi)(q^2 + \frac{1}{\xi^2}) \right]$$

This approach is only valid for short times, and the above result should be compared only with the very begging of the measured correlation function, i.e. initial slope at the origin. Further analysis at high φ's show that a similar equation for the average diffusion coefficient may be written.

B. Materials

2.4 Polymer Brushes

The polymer brushes used in this work are the following; three polystyrene (PS) brushes, a poly(*n*-butyl acrylate) [P(*n*-BuA)] brush, a poly(methyl methacrylate) (PMMA) brush and a mixed PS-PMMA brush.

PS   PMMA

P(*n*-BuA)
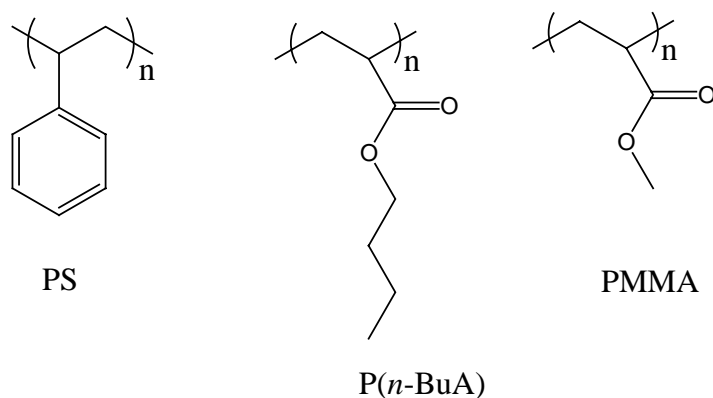
Figure 2.4 Chemical structures of the brushes used.

Additionally, a range of solvents were used in this work and their chemical structures can be seen in a table at the end of this chapter.

2.4.1 Synthesis of Polymer Brushes *(IMTEK, University of Freiburg)*

In this part, formation of mainly polymer monolayers covalently attached to silica surface will be discussed. The polymer layers are formed by radical polymerization *in situ* from a self-assembled monolayer of a chlorosilane group containing azo initiator. The azo compound is linked to the surface of the substrate through a base-catalyzed condensation reaction. The synthesis of the azo initiator, the immobilization of the initiator layer onto the surface of the silica, and the principles of the radical-chain polymerization of styrene started from this layer are described.[15-20]
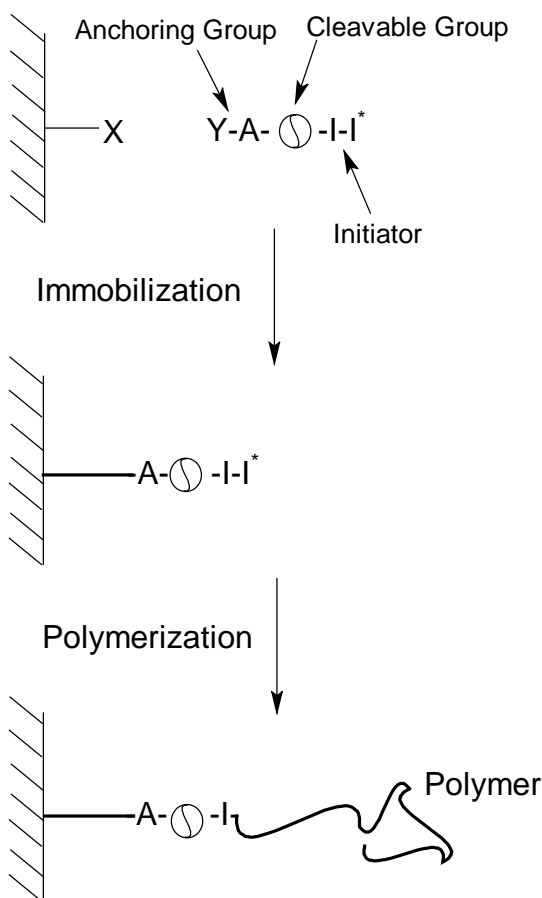
Figure 2.4.1a Schematic description of the concept for the preparation of terminally attached polymer monolayers using covalently bonded initiators for radical-chain polymerizations ("grafting from").

Synthesis of Asymmetric Azo Initiators

A mixture of 100 g (0.86 mol) of neutralized laevulic acid and 50 g (0.86 mol) of acetone was added dropwise to a solution of 112 g (1.72 mol) of KCN and 112 g (0.86 mol) of hydrazine sulfate in 1.5 L of water maintained at 50 $^\circ$C. After complete addition, the solution was stirred for 3 h and then allowed to cool. It was then acidified (pH = 4) and cooled to 0 $^\circ$C. At this temperature bromine was added dropwise until it remained in excess and the mixture was stirred for 30 min. The excess of bromine was destroyed with sodium hydrogen sulfite and a white precipitate collected. The filtrate was extracted twice with methylene chloride, and 11 g of **1** could be isolated (see fig. 2.4.1b). The solid was suspended in about 500 mL of 1 N NaOH, stirred for 30 min and filtered. The non-soluble part (24 g) consisted of the symmetric coupling product 2,2'-azobis(isobutyronitrile) (AIBN). After filtration the solution was acidified, causing the precipitation of 17 g of **1**. To a suspension of 40 g (200 mmol) of phosphorus pentachloride (PCl$_5$) in 50 mL of methylene chloride cooled with an ice-bath was added dropwise a solution of 10 g (45 mmol) of **1** in 50 mL of methylene chloride. The mixture was allowed to warm to room temperature and stirred overnight. The excess of PCl$_5$ was filtered off, and the remaining solution was concentrated until no more PCl$_5$ separated. The mixture was filtered again, and the filtrate was added to 300 mL of cold hexane, causing the separation of **2** as a white solid (9.5 g, 90%). To a solution of 40 mmol of the respective alcohol and 6.5 mL (80 mmol) of pyridine in 50 mL of methylene chloride at 0 $^\circ$C was added dropwise a solution of 8 g (33 mmol) of **2** in 50 mL of methylene chloride. The mixture was allowed to warm to room temperature and stirred overnight. Then the solution was washed twice with 2 N H$_2$SO$_4$, aqueous NaHCO$_3$, and water. The organic layer was dried over Na$_2$SO$_4$, and the solvent was evaporated. The resulting pale yellow oil was dissolved in a small amount of methylene chloride and poured into 300 mL of cold hexane. Thus, the respective ester **3** or **4** (fig. 2.4.1b) separated as a white solid (90% yield).

Hydrosilation Reactions

To a suspension of 3 g of the respective ester **3** or **4** in 30 mL of the respective chlorosilane was added a solution of 30 mg of hexachloroplatinic acid in 0.5 mL of dimethyl ether/ethanol (1/1 v/v), and the mixture was heated to reflux for 3 h. After that time the entire solid dissolved, indicating the completion of the reaction. The excess of the silane was recovered by distillation, and the product was dried in vacuum, yielding pale green oils in quantitative yields. Residual platinum catalyst was removed by filtration of a CH_2Cl_2 solution of the product over anhydrous sodium sulfate.
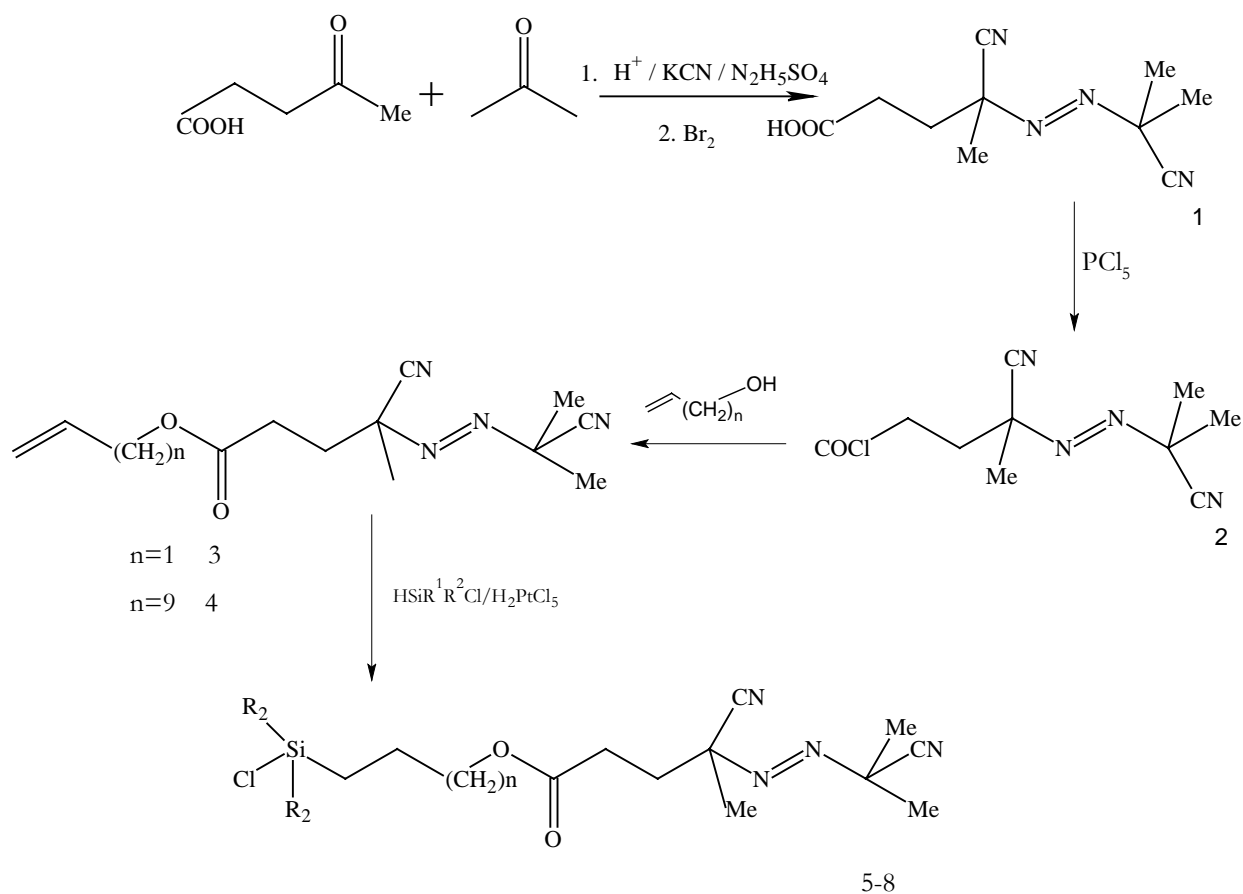
Figure 2.4.1b Synthesis of self-assembled monolayers of azo initiators.

Immobilization of the Chlorosilanes to Silica Surface

Under an atmosphere of dry nitrogen a solution of 0.5 g of the respective azochlorosilanes 5-8 in 50 mL of toluene and 5 mL of triethylamine was added in a flask where the silicon wafers were placed. The flask was stored in a dry and dark place overnight. The modified silica wafers were then washed with toluene, acetone, methanol and acetone and dried under N_2 flow.
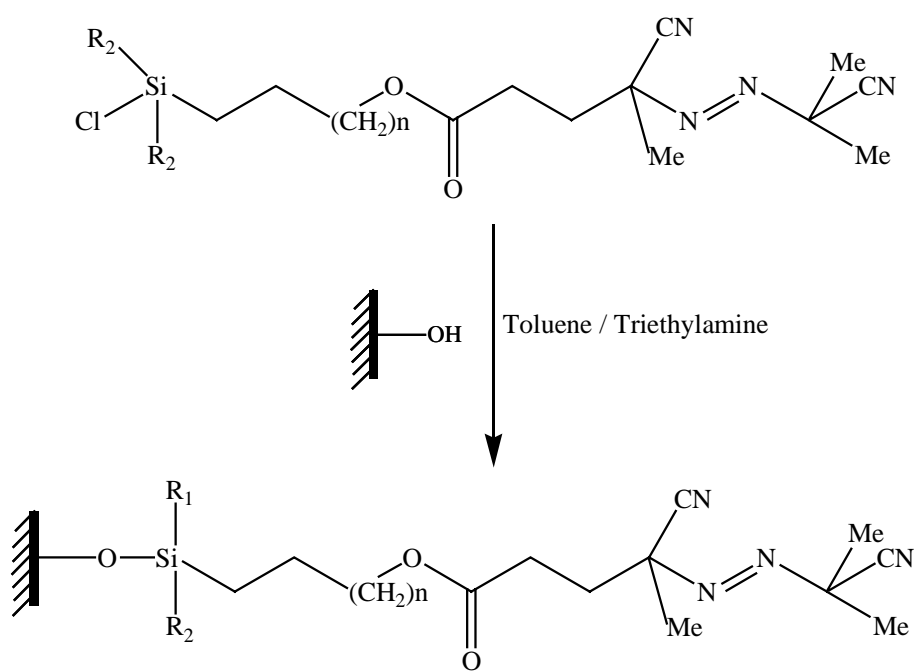
Figure 2.4.1c Immobilization of the chlorosilanes to silica surface.

Formation of Polymer Monolayers
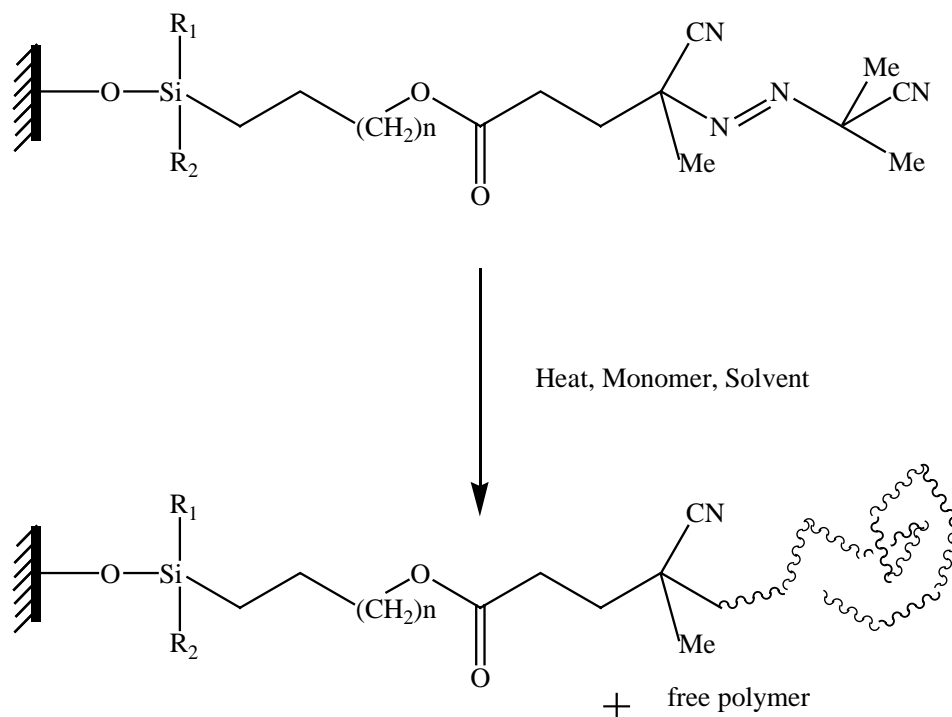
Figure 2.4.1d Reaction scheme for the synthesis of covalently attached polystyrene monolayers on silica surfaces using immobilized AIBN-type azo initiators.

Under an atmosphere of dry nitrogen, a silicon surface sample was placed in a flask where 100 mL of styrene/toluene (varying the content) were added. The solution was degassed in vacuum through repeated freeze-thaw cycles, and heated to $60.0 \pm 0.1\ ^{\circ}C$ in a thermostat. After chosen periods of time (0.5 – 24 h) the flask was opened allowing air to terminate the polymerization. The samples was washed with toluene and then dried under N_2 flow.

Results and Discussion

In this part of the work a wide range of PS brushes were prepared varying the molecular weight and the grafting density of the brush. Additionally, a few attempts were carried out using *n*-butyl acrylate and methyl methacrylate as the monomers. Finally, mixed brushes were prepared using styrene and MMA as the co-monomers.

The thickness of the dry polymer brushes was measured by ellipsometry and was in a good agreement with the thickness measured by AFM. An AFM picture of a 25 nm PS brush is illustrated in the figure below.
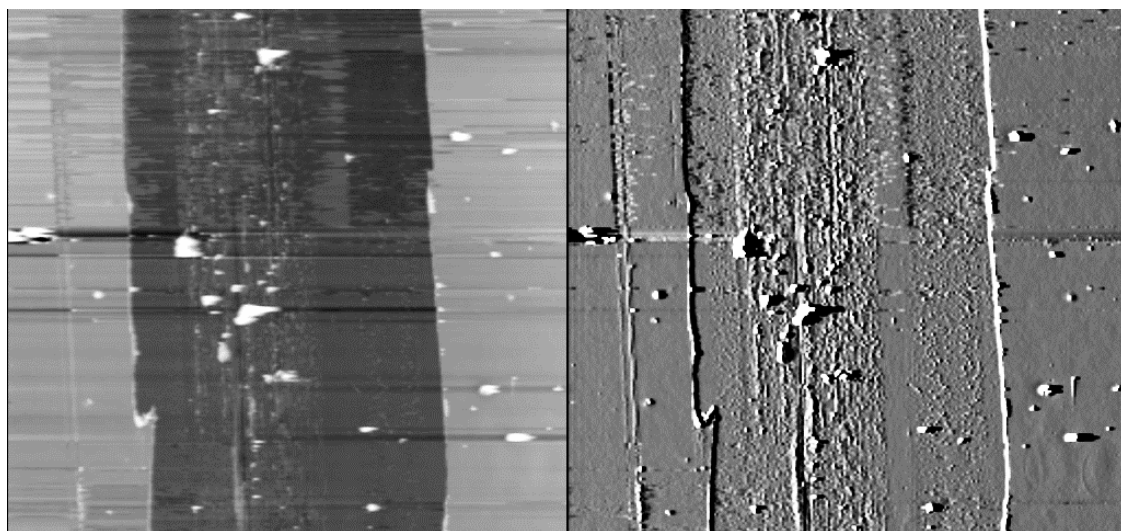
Figure 2.4.1e AFM picture of a 25 nm PS polymer brush.

The following tables describe in detail some of the samples that were prepared, including the polymerization time, the volume content of the monomer and the solvent as well as the calculated molecular weight and the grafting density. The dry thickness was measured by ellipsometry.

Code	Sample	Polymerisation T (°C)	Polymerisation Time (hrs)	Monomer : Toluene	Molecular Weight (*10^{-6}) Mw (g/mol)	Dry Thichness (nm)	Grafting Density (nm^{-2})
VM19	P(*n*-BuA)	60	0.5	bulk	1.10	7	0.0065
VM20	P(*n*-BuA)	60	1	bulk	1.30	5	0.013
VM21	P(*n*-BuA)	60	0.5	bulk	1.20	15	0.007
VM22	P(*n*-BuA)	60	2	bulk	1.00	35	0.03
VM26	P(*n*-BuA)	60	5	5:3	1.00	17	0.04

Table 2.4.1f: Synthesis of p(n-BuA) brush using asymmetric azo initiator.

Code	Sample	Polymerisation T (°C)	Polymerisation Time (hrs)	Monomer : Toluene	Molecular Weight (*10^{-6}) Mw (g/mol)	Dry Thichness (nm)	Grafting Density (nm^{-2})
VM01	PS	60	3	1:1	1.45	9	0.04
VM02	PS	60	5	1:1	1.40	24	0.06
VM04	PS	RT	24	1:1	0.25	9	0.22
VM06	PS	60	3	1:1	0.90	18	0.04
VM07	PS	60	16	1:1	1.20	33	0.16
VM08	PS	60	24	1:1	1.80	65	0.21
VM17	PS	60	2	1:1	1.30	14	0.03
VM18	PS	60	3	1:1	1.20	20	0.04
VM23	PS	60	24	2:1	0.85	30	0.22
VM24	PS	60	24	3:1	1.70	60	0.22
VM29	PS-PMMA	60	5/2	(1:1)/(2:1)	1,4/1	24-109	0,06/0,025
VM30	PS-PMMA	60	18/3	(1:1)/(1:1)	1.1/1	92-40	0,18/0,04
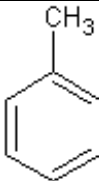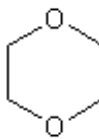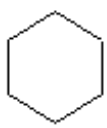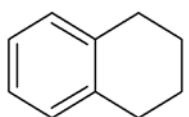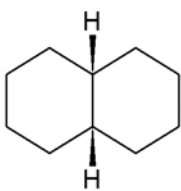
Table 2.4.1g: Synthesis of PS and PS-PMMA brushes using symmetric azo initiator.

2.5 Colloidal Particles

The colloid particles used consist of nearly mono disperse spheres of poly-methyl-methacrylate (PMMA), sterically stabilized by a chemically grafted monolayer of poly-12-hydroxystearic acid (P.H.S.A.) polymer chains [21]. The volume fraction was determined from the random closed packing which is assumed to be $\varphi=0.65$ and from crystallization. The particles (suspended in cis-decahydronaphalane) were synthesized in dodecane initially. We used suspensions of PMMA particles with different but close radii in a refractive index matching tetralin (1, 2, 3, 4 - Tetrahydronaphthalene)/cis-decalin (30%/70%) mixture, and in a variety of other different solvents such as cis-decalin, octadecene and bromo-cyclohexane. It was assumed that the colloids behave as hard spheres in this mixture of solvents since they are poor solvents for PMMA polymer chains and there is low swelling of the particle cores, but good solvents for P.H.S.A., to force them into extended conformation. Nevertheless, it has been reported a small swelling of PMMA particles in this mixture of solvents [22, 23]. Thus all the samples have been left for at least two days to equilibrate and reach the maximum swelling before measuring them. All samples were kept in the dark and were wrapped in aluminum foil since tetralin's photosensitivity and exposition to light gives the solution a yellow tint.
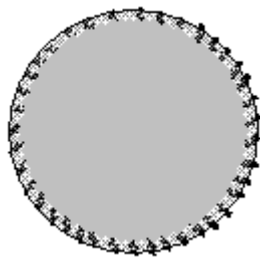
Figure 2.5: Schematic representation of a PMMA (dark) colloidal particle with a PHSA (gray) layer.

Chemical Structure	Name	Refractive Index	Viscosity (cP)	Density (gr/ml)
	Toluene	1.497	0.59	0.867
	1, 4 Dioxane	1.422	1.2	1.034
	Cyclohexane	1.429	0.98	0.778
	Tetralin	1.54	2.03	0.973
	Cis-Decalin	1.48	3.23	0.897
	Mixture Tetralin/Decaline (30%/70%)	1.497	2.35	0.92

Table 2.5: Chemical structures and characteristic properties of all the solvents used in this work.

Sample Preparation

In order to determine the volume fraction for a monodisperse hard sphere sample, the standard procedure is to reach the coexistence regime through dilution or evaporation and derive a value from the crystal to liquid ratio of the sample. Because of high refractive index mismatch in dodecane, in which the particles were initially synthesized the coexistence region in those cases could not be found in this solvent. The particles were then "cleaned" a few times (typically eight times) with a mixture of cis-decaline/tetraline, a refractive index matching solution as mentioned earlier. Thus in order to have the same conditions for all the samples used, they were first centrifuged until all the excess solvent was expelled from the colloid and the sample was separated to a randomly close packed colloid and solvent. The rest of the sample concentrations were determined by successive dilutions of the same sample batch.

The following equation was used to calculate volume fractions when dilution or evaporation occurred:

$$\Phi = \Phi_0 [1 + \frac{m_s}{m_c}(1 + \frac{\Phi_0(\chi - 1)}{1 + \alpha\chi})],$$

$$where \chi = \frac{\rho_c}{\rho_s}$$

with Φ as the new volume fraction, Φ_0 the old volume fraction, m_s the mass of the added solvent, mc the mass of the colloidal suspension, ρ_c the density of the dry colloid and ρ_s the density of the solvent. α is a parameter used to compensate for the fact that the spheres do not have the same density when in solvent, but have an increased radius due to the stabilizing layer.

For the colloidal particles, the density was ρ_c=1.188 gr/cm^3 in all cases, and for the solvents the associated densities are listed in the Table 2.5a. For α we used a typical value of α=0.12.

2.6 REFERENCES

1. Berne, B.J. and R. Pecora, *Dynamic Light Scattering*, New York: Dover Publications.

2. Sornette, D. and N. Ostrowsky, *Repulsive steric interactions between membranes of finite size.* Journal de physique Paris, 1984. **45**(2): p. 265-271.

3. Lan, K.H., N. Ostrowsky, and D. Sornette, *Evanescent wave photon correlation spectroscopy to study brownian diffusion close to a wall*, in *Progress in Colloid & Polymer Science*. 1987. p. 185.

4. Fytas, G., S.H. Anastasiadis, R. Seghrouchni, D. Vlassopoulos, J. Li, B.J. Factor, W. Theobald, and C. Toprakcioglu, *Probing collective motions of terminally anchored polymers.* Science, 1996. **274**(5295): p. 2041-2044.

5. Loppinet, B., G. Petekidis, G. Fytas, R. Rulkens, and G. Wegner, *Dynamics of adsorbed hairy-rod polymer solutions.* Langmuir, 1998. **14**(18): p. 4958-4960.

6. Marcus, A.H., J. Schofield, and S.A. Rice, *Experimental observations of non-Gaussian behavior and stringlike cooperative dynamics in concentrated quasi-two-dimensional colloidal liquids.* Physical Review E - Statistical Physics, Plasmas, Fluids, and Related Interdisciplinary Topics, 1999. **60**(5 B): p. 5725-5736.

7. Ostrowsky, N.L.a.N., *Diffusion of Brownian particles trapped between two walls: Theory and dynamic-light-scattering measurements.* Physical Review B, 1996(53): p. 12050 - 12056.

8. Arauz-Lara, J.S.-S.a.J.L., *Short-time dynamics of colloidal particles confined between two walls.* Phys. Rev. E, 2002. **021406** (65).

9. Michailidou, V.N., B. Loppinet, D.C. Vo, O. Prucker, J. Ruhe, and G. Fytas, *Dynamics of end-grafted polystyrene brushes in theta solvents.* Journal of Polymer Science, Part B: Polymer Physics, 2006. **44**(24): p. 3590-3597.

10. Holmqvist, P., J.K.G. Dhont, and P.R. Lang, *Anisotropy of Brownian motion caused only by hydrodynamic interaction with a wall.* Physical Review E - Statistical, Nonlinear, and Soft Matter Physics, 2006. **74**(2).

11. Holmqvist, P., J.K.G. Dhont, and P.R. Lang, *Colloidal dynamics near a wall studied by evanescent wave light scattering: Experimental and theoretical improvements and methodological limitations.* Journal of Chemical Physics, 2007. **126**(4).

12. Petekidis, G., J. Gapinski, P. Seymour, J.S.v. Duijneveldt, D. Vlassopoulos, and G. Fytas, *Dynamics of core-shell particles in concentrated suspensions.* Physical Review E -

Statistical Physics, Plasmas, Fluids, and Related Interdisciplinary Topics, 2004. **69**: p. 042401.

13.   Garnier, N. and N. Ostrowsky, J. Phys. II (France), 1991. **1**: p. 1221.

14.   Lan, K.H., N. Ostrowsky, and D. Sornette, *Brownian dynamics close to a wall studied by photon correlation spectroscopy from an evanescent wave.* Physical Review Letters, 1986. **57**(1): p. 17-20.

15.   Prucker, O. and J. Ruhe, *Synthesis of poly(styrene) monolayers attached to high surface area silica gels through self-assembled monolayers of azo initiators.* Macromolecules, 1998. **31**(3): p. 592-601.

16.   Akgun, B., D.R. Lee, H. Kim, H. Zhang, O. Prucker, J. Wang, J. Ru?he, and M.D. Foster, *Self-affine surfaces of polymer brushes.* Macromolecules, 2007. **40**(17): p. 6361-6369.

17.   Murata, H., O. Prucker, and J. Ruhe, *Synthesis of functionalized polymer monolayers from active ester brushes.* Macromolecules, 2007. **40**(15): p. 5497-5503.

18.   Raghuraman, G.K., R. Dhamodharan, O. Prucker, and J. Ruhe, *A robust method for the immobilization of polymer molecules on SiO 2 surfaces.* Macromolecules, 2008. **41**(3): p. 873-878.

19.   Prucker, O. and J. Ruhe, *Polymer layers through self-assembled monolayers of initiators.* Langmuir, 1998. **14**(24): p. 6893-6898.

20.   Prucker, O. and J. Ruhe, *Mechanism of radical chain polymerizations initiated by azo compounds covalently bound to the surface of spherical particles.* Macromolecules, 1998. **31**(3): p. 602-613.

21.   Jardine, R.S. and P. Bartlett, *Synthesis of non-aqueous fluorescent hard-sphere polymer colloids.* Colloids and Surfaces A: Physicochemical and Engineering Aspects, 2002. **211**(2-3): p. 127-132.

22.   Ackerson, B.J. and P.N. Pusey, *Shear-induced order in suspensions of hard spheres.* Physical Review Letters, 1988. **61**(8): p. 1033-1036.

23.   Bagchi, B. and D. Thirumalai, *Freezing of a colloidal liquid subject to shear flow.* Physical Review A, 1988. **37**(7): p. 2530-2538.

Chapter 3

3. RESULTS & DISCUSSION - Dynamics of Polymer Brushes

In this first part, the case of polymer brushes, their dynamics in various solvents and their effect on colloidal particle diffusion is reported

Though polymer brushes have long been studied, both experimentally and theoretically, little was known on their dynamics and their comparison to solutions dynamics and to existing theory. Therefore we studied the dynamics of large brushes, with varying grafting density, as this is the parameter expected to govern the concentration profile of brushes (within the simple Alexander-DeGennes model)

Initially, we examine the dynamics of polymer brushes in good solvent, where the polymer brush is fully swollen and we identify the theoretically predicted cooperative diffusion. The effect of grafting density in the dynamics will be explored as well as the associated intensities.

Then, the dynamics of the same polymer brushes in theta solvent, cyclohexane, and the temperature dependence of the dynamics of the polymer bushes, as well as the grafting density dependence will be discussed. When the solvent quality changes from marginal to poor, the relaxation function $C(q, t)$ exhibits strong effects as compared with the smooth variation of the brush density profile. From a single exponential above 50 °C, $C(q, t)$ becomes a two-step decay function. The fast decay is still assigned to the cooperative diffusion albeit slower than in the good solvent regime whereas the slow non – exponential and non – diffusive process might relate to microsegragated and/or chain dynamics in the present polydisperse brush. The relaxation function of the present three brushes with different grafting density reveals similarities and disparities between wet brushes and semidilute polymer solutions.

A second line of studies goes towards the diffusion of colloidal particles in the vicinity of the polymer brushes. Since the diffusion of tracer particles in semi dilute solution is not a fully settled issue, the simplest view envisaged the semi dilute solution as a network of mesh size ξ and therefore particle lower than ξ should penetrate the network easily and diffuse with a diffusion only slightly slowdown compare to the diffusion coefficient in solvent.

After that the effect of polymer brush to non-adsorbing colloidal particles is reported. It is shown that the presence of the brush affects the distribution of the particles, especially large hard sphere particles that are not able to penetrate the brush while smaller sized softer particles can partially penetrate the soft layer formed by the polymer brushes. The distribution of the particles was deduced from the penetration depth dependence of the scattering intensities.

The diffusivities themselves of the colloidal particles were also an issue of investigation. Larger non – penetrating particles were seen to be slightly lubricated, the polymer brush providing a screening of the wall – particle hydrodynamic interactions. The smaller/softer penetrating particles lead to a more complex phenomenology. The slowing down appears to depend very strongly on the size of the particles.

The following text reproduces the 4 recently published articles that make the core of this chapter concerning dynamics of polymers brushes as studies by evanescent wave dynamic light scattering.

3.1 Polymer Brushes in Good Solvents

(Macromolecules 2005, 38, 8960)

The most stable situation of terminally attached soft layers is achieved by covalent bonding of polymer chains at one end to a solid surface. For sufficiently high grafting densities $\sigma = d^{-2}$, the distance d between grafted sites is less than the size of the polymer coil and the tethered layer falls into the brush regime where chains adapt an extended conformation. Polymer brushes have recently attracted considerable attention and have found application in a broad range of fields, including colloid stabilization [1], tailoring surface properties and "chemical gates" [2] with numerous studies related to the synthesis and the examination of their structure and novel properties [3]. While the static properties e.g. density profile of polymer brushes in good and theta solvents have been extensively investigated both theoretically and experimentally [4-8], their dynamics have received much less attention [9] probably due to the paucity of experimental methods. Several motional mechanisms have been theoretically [10, 11] proposed for the decay of the concentration fluctuations $<(\delta c)^2>^{1/2}$ in a brush in contact with a good solvent. Such motions involve single chain dynamics and collective many chains respiration modes in analogy to semidilute solutions of homopolymer chains [10, 11].

Here, we report on the collective dynamics of end-grafted polystyrene and poly (n-butylacrylate) brushes in a good solvent as studied by evanescent wave dynamic light scattering, extending the measurements of a recent report [12] towards different grafting densities and polymer material. The cooperative diffusion of the polymer brushes has been identified, confirming the theoretical predictions [10, 11] and illustrating some universal behavior of polymer brushes in good solvents. The present evanescent wave dynamic light scattering experiment reveals a thermally driven process, the breathing of the brush.

The polymer brushes were prepared by the "grafting from" technique/surface-initiated polymerization where the polymer chains were covalently attached to a glass surface. The chains are grown via free radical polymerization from an azo initiator previously covalently attached to the glass surface [13, 14]. Molecular weight and grafting density are varied by controlling the polymerization time and the monomer concentration. The grafting density is estimated from the measured dry film thickness and the average molecular weight. The

molecular weight can reach up to a few millions g/mol with an estimated polydispersity of $M_n/M_w \sim 2$. Four different brushes consisting of polystyrene (PS) and one poly (n-butyl acrylate) (PBuA) with high and low glass transition temperature were used and their molecular characteristics are summarized in Table 3.1.1 below.

Good solvent conditions were obtained by immersing these PS and PBuA brushes in dioxane and 1-butanol respectively. Under good solvent conditions, the thickness of the polymer brush can be as high as 1 µm[13, 14] with a concentration profile much broader than the parabolic profile of monodisperse brushes[7, 8, 15].
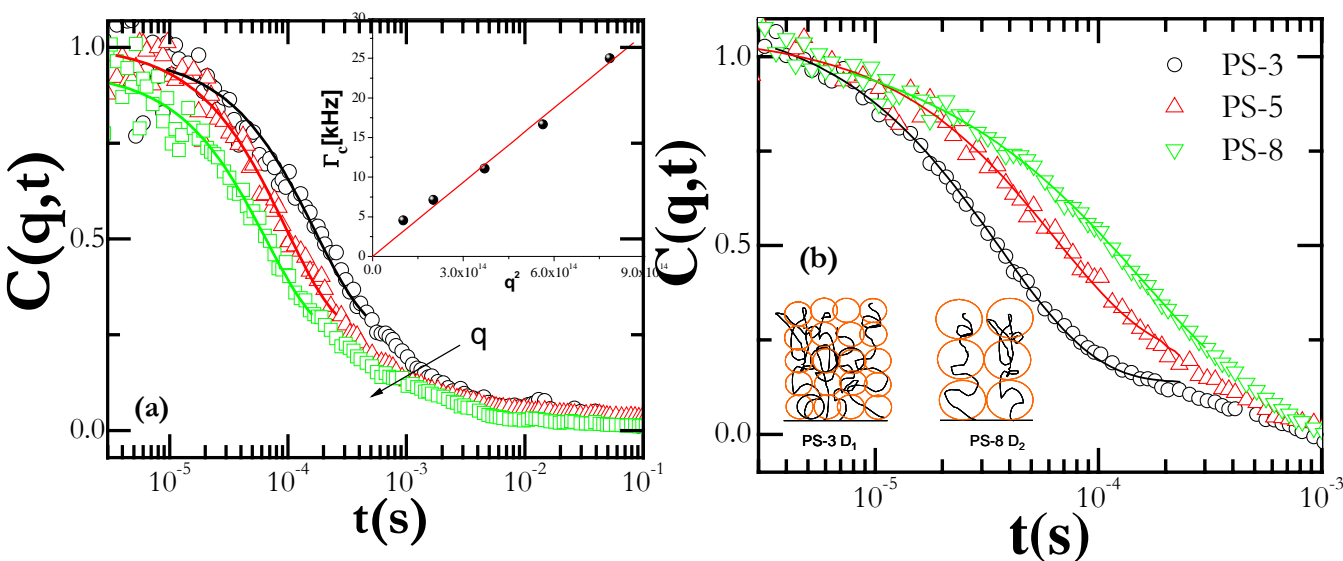
Figure 3.1.1: Normalized intermediate scattering function C (q,t) of the PS brushes in dioxane at 20°C (a) C(q,t) at three different q values between 0.01 and 0.04 nm^{-1} increasing in the direction of the arrow, represented by single exponential functions (solid lines) for the PS-5 brush. Inset: The diffusive nature of the relaxation rate $\Gamma(q)$ is indicated by the solid line. (b) C (q,t) at q = 0.03 nm^{-1} for all three PS/dioxane brushes at 20°C, where the solid lines denote a single exponential fit. Inset: A schematic representation of the linear cigars of blobs for the two extreme grafting densities.

Code	Molecular weight (g/mol)	Dry thickness d (nm)	Grafting density σ (nm^{-2})
PS-3	1.6×10^6	90	0.16
PS-5	1.1×10^6	30	0.05
PS-8	1.6×10^6	9	0.016
PBuA	1.2×10^6	90	0.06

Table 3.1.1: Molecular characteristics of the polymer brushes.

Figure 3.1.1a above shows the relaxation function C(q,t) for the PS-5 brush immersed in dioxane at three different q's. In the good solvent regime, C(q,t) can be represented by a fast exponential function ,$f_c$exp[-Γ_c(q)t], followed by a tail at long decay times,[16] this is more clearly shown (solid lines) in the presentation of Fig.3.1.1b.The relaxation rate Γ_c(q) (inset to Fig.3.1.1a) is found to be purely diffusive and hence the fast diffusion coefficient $D_c=\Gamma_c(q)/q^2$ describes the dynamics of the collective concentration fluctuations.

Good solvent conditions were obtained by immersing these PS and PBuA brushes in dioxane and 1-butanol respectively. Under good solvent conditions, the thickness of the polymer brush can be as high as 1 μm[13, 14] with a concentration profile much broader than the parabolic profile of monodisperse brushes[4, 7, 8].

The relaxation function C(q,t) displays qualitatively the same behavior in the other two PS/dioxane and in PBuA/1-butanol brushes at 20°C.The concentration fluctuations c_q of a given q decay slower with increasing spacing d between neighboring chains as suggested by the experimental C(q,t) in Fig.3.1.1b. (D_c decreases from 10 10^{-7} cm^2/s in PS-3 to 3.2 10^{-7} cm^2/s in PS-5 to D_c=2.5 10^{-7} cm^2/s in PS-8 in dioxane at 20°C). For the PBuA brush, the slower value of D_c (= 8 10^{-8} cm^2/s) is partly attributed to the different viscosities η of the two solvents. Theoretically[11], fast and diffusive Γ_c(q) was originally predicted for a simple step like density profile envisaged as linear "cigars" of blobs with uniform diameter *d* as described earlier. In this case, $D_c=kT/6\pi\eta\xi$ describes the longitudinal mode of an ideal monodisperse step-like brush with correlation length ξ=d as illustrated in the inset to Fig.3.1.1b. The relation

$D_c \propto \eta^{-1}$ was confirmed in the case of PS-5 in three different good solvents (toluene, dioxane and carbon tetrachloride) and conforms the previous findings[12]. For real and polydisperse brushes, however, the blob size increases towards the edge and hence the value of ξ should depend on the experimental probe. Since light scattering intensity is determined by both size and concentration of the blobs, in this experiment ξ should be of the order of $\sigma^{-1/2}$.

The high concentration of segments in the brush implies to collective dynamics similar as in gels or semi dilute solutions of homopolymers. The relaxation rate is diffusive with respect to the magnitude of q (inset to Fig.3.1.1a). This observation suggests that the probed concentration fluctuations decay via a cooperative motion in the sense that all attached coils move together like a swelling and shrinking of a sponge. In this picture, this motion resembles the cooperative diffusion in semi dilute solution of homopolymers driven by an osmotic force and the diffusive object is the mesh size (blob) $\xi \sim c^{-3/4}$.

In the present end-anchored brush, however, the kinetics of such collective process is correlated with the grafting density. The dynamics become faster with increasing grafting density suggesting faster breathing of the chains as the system becomes stiffer.
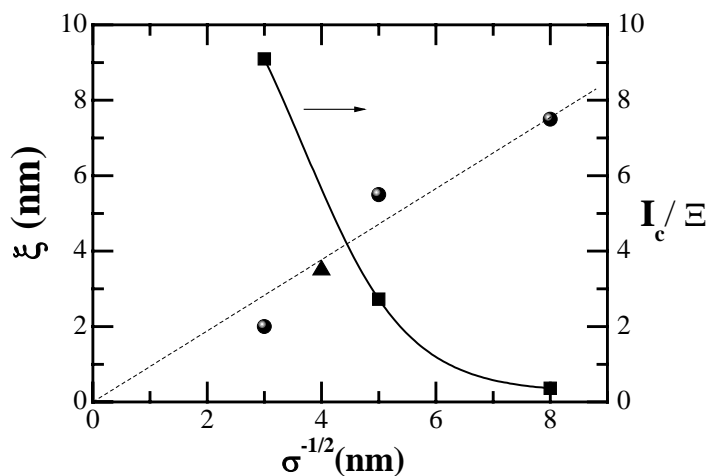
Figure 3.1.2: Variation of the correlation length ξ in the four brushes and the reduced intensity I_c/Ξ (squares) with the average grafting density of the three PS brushes. The circles and the triangle symbols refer to PS and PBuA brushes respectively whereas the diagonal dotted line and the solid line are to guide the eye.

The effect of the different grafting densities (and hence d) is clearly seen in the C (q,t) of Fig.3.1.1b , since the dynamics at a given q become faster with increasing grafting density. Figure 3.1.2, demonstrates this predicted effect in the plot ξ vs $\sigma^{-1/2}$ for all four brushes where ξ was computed from the experimental D_c and σ was estimated from the dry brush thickness (Table 3.1.1). The intensity I_c associated with the fast cooperative process in the wet brushes under good solvency can be estimated from its amplitude (af_c) and total scattering intensity I(q) i.e. $I_c=af_cI(q)$. I_c is found to be insensitive to q-variations as expected for very short correlation length ξ (qξ<<1) and grow linearly with the penetration depth Ξ suggesting a smoothly decaying concentration profile in a polydisperse brush[4, 7, 8].

Further, the reduced intensity I_c/Ξ displays an unexpectedly strong increase with grafting density (Fig.3.1.2). From very simple scaling arguments, a much moderate dependence ($I \sim c^2\xi^3 \sim \sigma^{1/2}$) is predicted[11] for a monodisperse and step like brush.

In conclusion, we have exploited an experimental light scattering configuration to study the dynamic structure of layers of polymers anchored on planar surfaces. Using chemically end grafted polydisperse polymer brushes (three polystyrene and one poly (n-butylacrylate) samples), synthesized by the "grafting from" technique, in good solvent, we have identified the theoretically predicted cooperative diffusion[11]. The concentration fluctuations of a given wave vector q decay slower with decreasing grafting density σ and the associated intensity I_c increases rather strongly with σ.

3.2 Polymer Brushes in Θ - Solvent

(J. Polym. Sci. Part B: Polym. Phys. 2006, 44, 590)

End grafting macromolecules to solid surfaces represents one of the most popular ways of modifying and functionalizing surfaces, with a breadth of applications in various fields of microsystems engineering such as biochips, microfluidics and sensor construction [1]. At high surface coverage, polymer chains grafted at one end to a planar surface in contact with good solvent are strongly stretched, forming a polymer brush [1, 10]. This high stretching, a result of large excluded volume interaction between monomers can be affected by controlling the grafting density of the latter. Upon lowering the solvent quality, the brush becomes increasingly compact and finally becomes insoluble as schematically shown in Figure 3.2.1[4]. At theta conditions, where the excluded volume interactions vanish, chains adopt Gaussian statistics. Such a switching between an extended and a compact conformation of the surface-attached molecules is very interesting for sensor applications because at such a transition the sensitivity of the sensing layer is highest due to the increased analyte concentration.
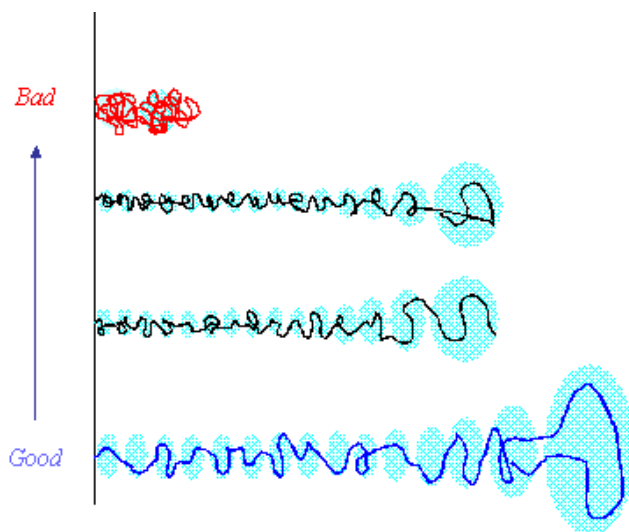
Figure 3.2.1: Schematic representation of an end-anchored polymer chain at different solvent conditions ranging from "good" to "bad".

Whereas the contraction of model brushes upon lowering solvent quality and the resulting concentration profiles have received considerable attention both theoretically and experimentally, the underlying concentration fluctuations in the brush at thermal equilibrium is essentially unexplored[17].

The evolution of the time correlation function C (q,t) at q = 0.02 nm^{-1} and at constant penetration depth (Ξ = 400 nm) for the three brushes with temperature between 26 °C and 50 °C is shown in Figure 3.2.2 (a), (b) and (c).
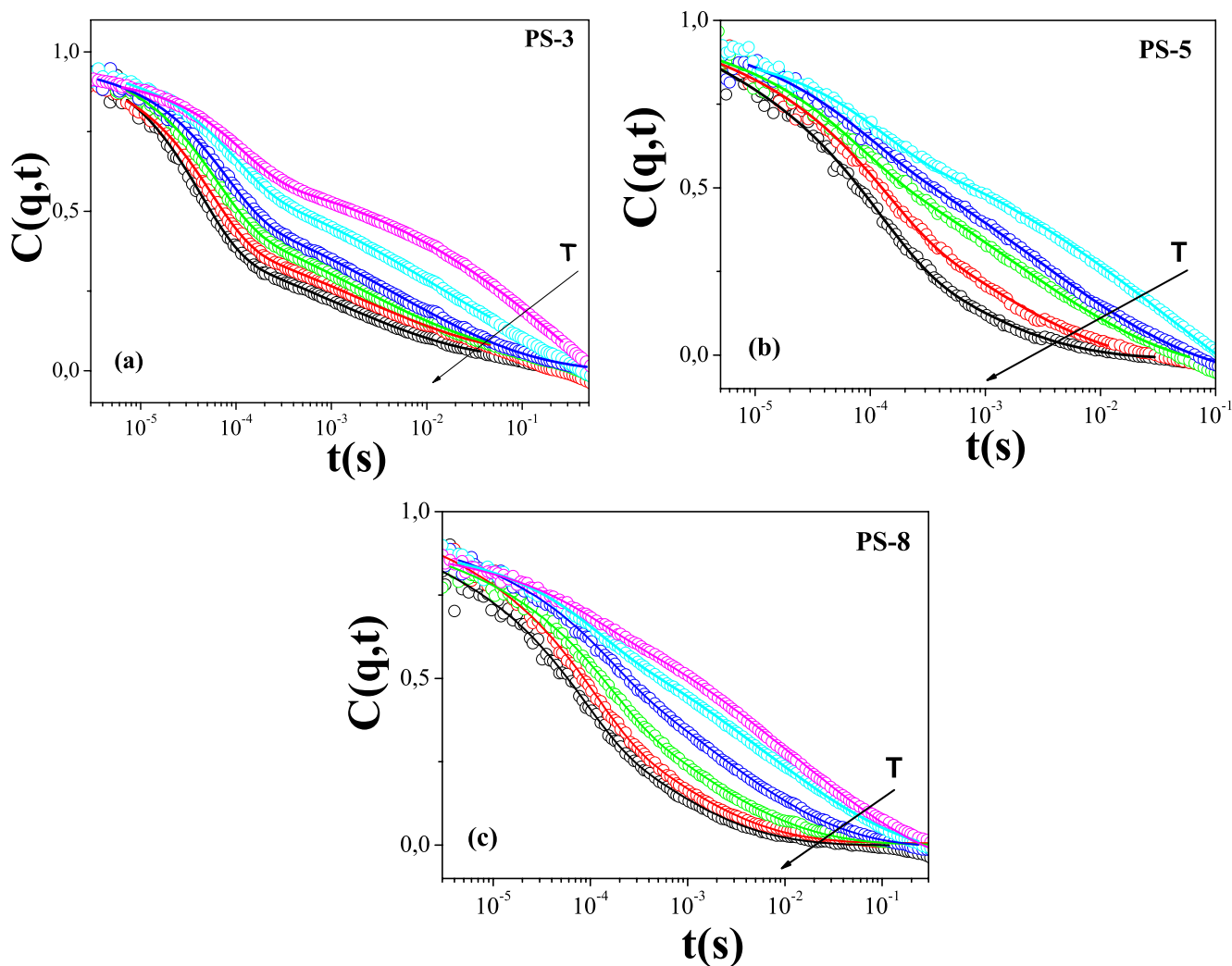
Figure 3.2.2: The normalized intermediate scattering function C(q,t) for the PS-3 brush (a), PS-5 brush (b) and PS-8 brush (c) in cyclohexane at q = 0.02 nm^{-1} and penetration depth Ξ = 400 nm for a range of temperatures (26 °C ≤ T ≤ 50°C) increasing in the direction of the arrow. The solid lines denote the fit of eq. (1) to the experimental functions.

The slowing down of the overall relaxation upon cooling is apparent for the three brushes, in agreement with the previous reported data [12]. The overall shape of the correlation function also shows a similar temperature evolution for the three measured brushes. Starting at high temperatures from an almost single decay, it clearly assumes two-step decay at lower temperatures. A sum of a single exponential function, $\exp[-\Gamma_c(q)t]$ and a stretched exponential $\exp[-\Gamma_s(q)t]^\beta$ was chosen to represent the experimental normalized time correlation function:

$$C(q,t) = A\exp[-\Gamma_c(q)t] + (1-A)\exp[-\Gamma_s(q)t]^\beta \qquad (1)$$

using the relative amplitude A and the two rates $\Gamma_c(q)$ and $\Gamma_s(q)$ as adjustable parameters. The shape parameter β of the slow mode was represented by a fixed value of $\beta = 0.32$. The intensity I_i associated with the fast and slow process (i = f, s) are given by $I_i = A_i \bullet <I>$ where $<I>$ is the total scattering intensity at a given q. The broad shape of the curve of the slow process for all three PS brushes at all examined temperatures might be partly influenced from the presence of a tail [18] in $C(q,t)$ at long times.

The obtained relaxation times and associated intensities for the fast and slow relaxation are presented in Figure 3.2.3. For the $C(q,t)$, the characteristics of the fast process resemble the single process of $C(q,t)$ for the same brushes in dioxane (good solvent)[19]. It is therefore attributed to the cooperative diffusion $D_c = \Gamma_c/q^2$ (breathing of the brush) [11] that slows down with decreasing temperature, in analogy to the behavior of semidilute solutions of PS in cyclohexane[20]. In contrast to the latter solutions, τ_c (= $1/\Gamma_c$) does not diverge up to the lowest (20 °C) examined temperature (well below the nominal Θ of the bulk PS/cyclohexane solutions). The relaxation time $\tau_s(q)$ is found to exhibit a stronger temperature dependence than $\tau_c(q)$ which nonetheless slows down upon cooling. Below 25 °C, the slow process runs out of the experimental time window.
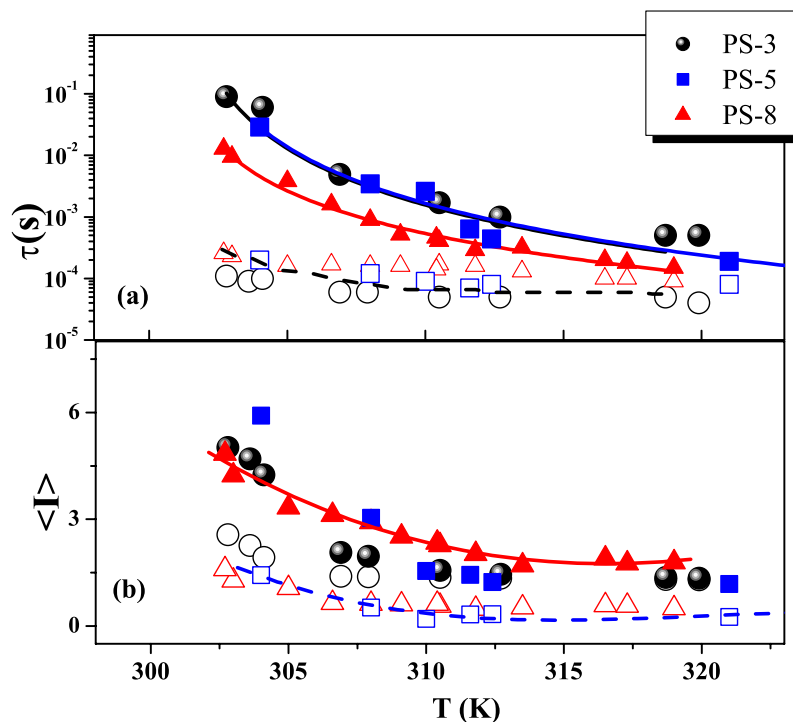
Figure 3.2.3: (a) The relaxation time for the slow (τ_s, solid symbols) and the fast cooperative (τ_c, open symbols) processes in the three polystyrene brushes; PS-3 brush (●), PS-5 brush (■) and PS-8 brush (▲) in cyclohexane at q = 0.02 nm^{-1} plotted vs temperature. The solid lines indicate a power law fit as described in the text. (b) The intensity of the slow (I_s solid symbols) and the fast (I_f open symbols) plotted as a function of temperature. The relaxation times and the intensities were obtained from the fit of Eq.1 to the experimental C (q,t) of Fig 2. The dashed lines (for the fast process) are to guide the eye.

The slowing down of τ_s with decreasing temperature can be described by power law $\tau_s \sim$ (T-T_c)$^{-x}$ (solid lines in Fig. 3.2.3) with $T_c \sim$ (299 $\pm$ 1) K and x = 2.6 $\pm$ 0.2 for all three PS brushes. This value is clearly larger than the critical exponent reported for the mutual diffusion in critical polymer solutions [21]. Based on the intensity plot of Fig. 3.2.3, the contribution of the induced slow process is evidently increased below T_θ. The increase of I_s (T) with decreasing temperature in all three samples is a signature of the diminishing solvent quality for the end-grafted PS chains.

In contrast to the PS/cyclohexane solutions, which phase separate below T_θ, the brush can only accommodate unfavorable thermodynamic interactions by adjusting its thickness as it looses the ability to macrophase separate. Furthermore, the intensity I_s was found to increase with grafting density of PS.
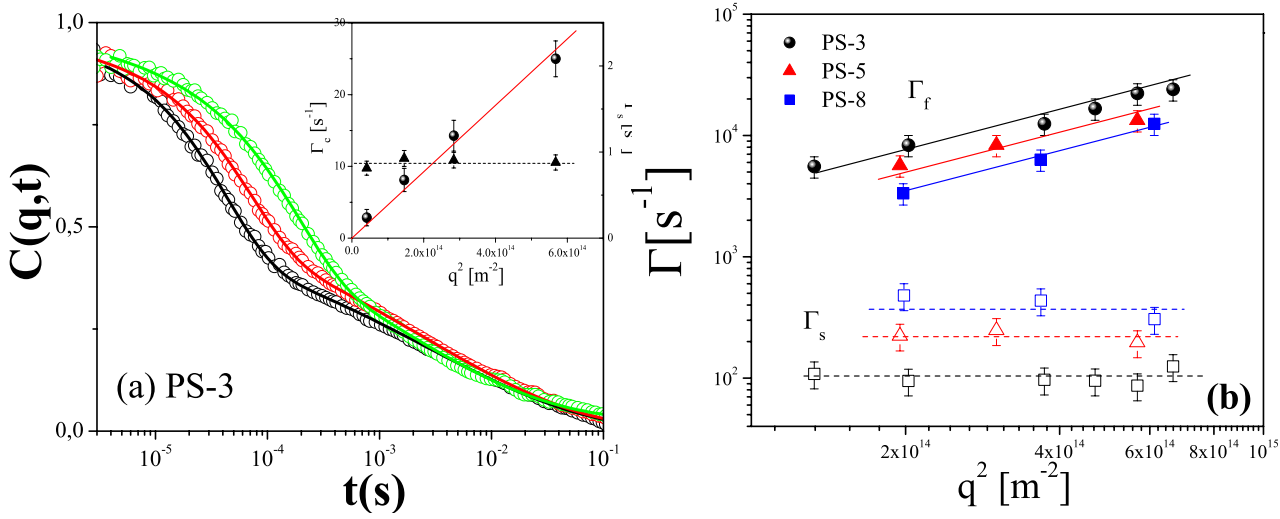
Figure 3.2.4: (a) Normalized intermediate scattering functions C (q,t) of the PS-3 brush in cyclohexane at 32 °C at three different q values between 0.01 and 0.025 nm^{-1} increasing in the direction of the arrow. The solid lines denote the fit of eq. (1) to the experimental functions. Inset: The diffusive nature of the relaxation rate $\Gamma_c(q)$ where the solid line denotes the diffusive ($\Gamma_c(q) = D_c q^2$, $D_c = 3.7 \times 10^{-7}$ cm^2/s) behavior and the insensitivity of the rate $\Gamma_s(q)$ of the slow process to the variation of q indicated by the dashed line. **(b)** The relaxation rate $\Gamma_c(q)$ of the fast process in the three polystyrene brushes immersed in cyclohexane as a function of q^2 at T = 35 °C. The solid lines denote the diffusive ($\Gamma_c(q) = D_c q^2$) behavior and the dashed lines indicate the insensitivity of the rate $\Gamma_s(q)$ of the slow process to the variation of q.

Turning to the wave vector dependence of the correlation function, Figure 3.2.4a shows the experimental C (q,t) for the brush with the highest grafting density, PS-3, at Ξ = 400 nm and three q's (0.01, 0.02 and 0.025 nm^{-1}) at 32° C. The fast decay shifts to shorter time with q whereas the slow decay of C (q,t) appears to be insensitive to the variation of q.

The representation of C (q,t) by eq.(1) reveals the diffusive (q^2-dependent) nature of the relaxation rate of the fast process in contrast to the slow mode that is found to display no apparent q-dependence for its characteristic rate Γ_s. This q-dependence of C (q,t) also applies to the other two PS brushes as shown in Fig.3.2.4b. The fast diffusion D_c (= Γ_f / q^2) increases with grafting density as found for the same brushes in good solvents, while the slow rate Γ_s shows the opposite trend. The q-independent rate appears different from the diffusive slow mode reported earlier [12].

We may attribute this discrepancy to the very broad relaxation time distribution, which results the q-dependent measurements somewhat ambiguous. In the present study, the insensitivity of Γ_s to q-variations was found for all three brushes.

To examine possible surface segregation, the dynamic behavior of the three polystyrene brushes was investigated around T_θ for a wide range of the penetration depth Ξ in the range 150 nm to 750 nm. According to the experimental C (q,t) of the PS-5 and the PS-8 brushes in Figure 3.2.5a and 3.2.5b, there is no apparent penetration depth dependence.
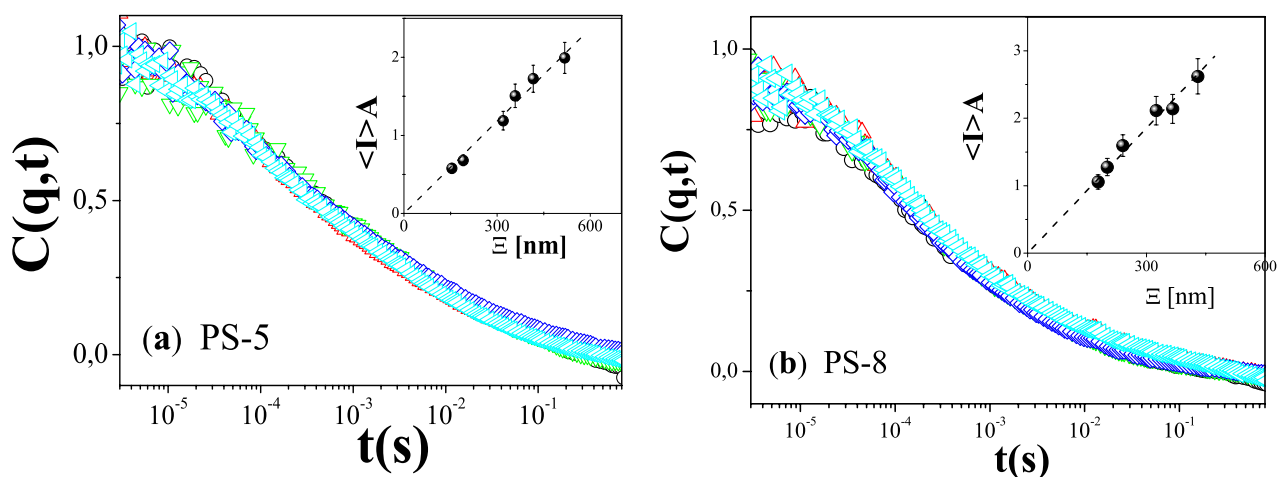
Figure 3.2.5: Normalized intermediate scattering functions C (q,t) for (a) PS-5 brush in cyclohexane and (b) PS-8 brush in cyclohexane at 35 °C at q = 0.02 nm^{-1} for a range of penetration depths (150 nm $\leq \Xi \leq$ 750 nm). Insets: The intensity <I>A, associated with the two processes ($\bullet$) is plotted as a function of Ξ.

Eq. (1) represents well the experimentally obtained normalized C (q,t)· The total intensity I associated with both processes plotted as a function of Ξ is shown in the insets of Fig. 3.2.5a and 3.2.5b. In both brushes, the total intensity increases linearly with the penetration depth. Conversely, the brush PS-3 with the highest grafting density exhibits a quite different behavior as depicted in Figure 6a. Strong penetration depth dependence of the dynamics was observed in the vicinity of T_θ with an apparent slowing down at larger Ξ's. Fits obtained by Eq 1 return a constant slow time independent of Ξ and associated intensities of the fast (solid symbols) and the slow mode (open symbols) plotted as a function of Ξ as shown in Fig. 3.2.6b.
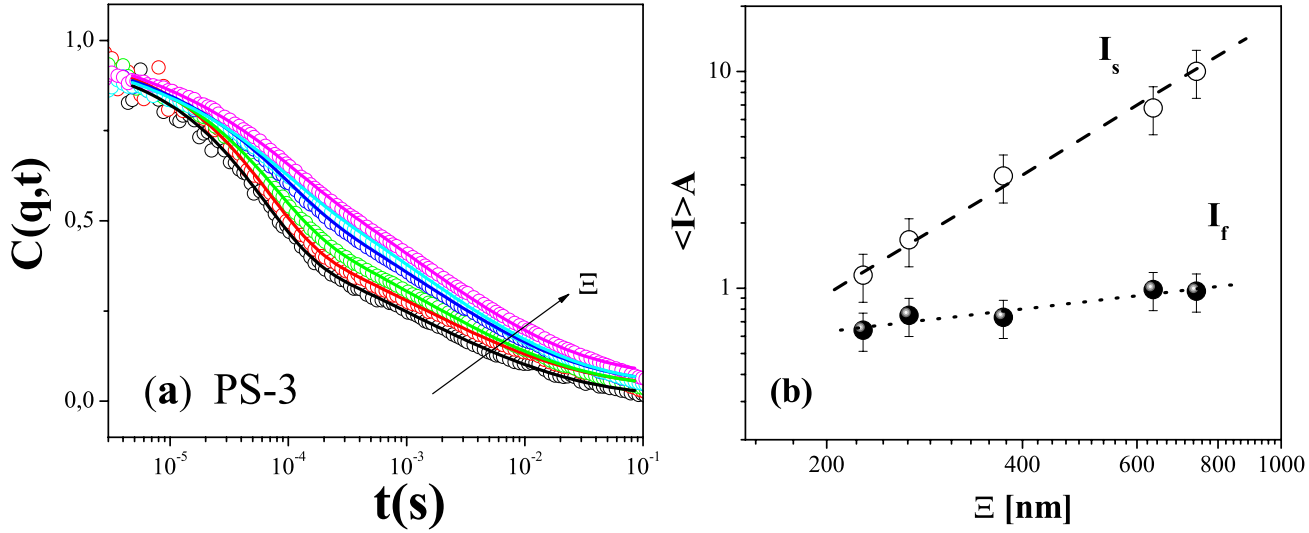
Figure 3.2.6: (a) Normalized intermediate scattering functions C (q,t) for the PS-3 brush in cyclohexane at: (a) 35 °C at $q = 0.02$ nm^{-1} for a range of penetration depths (150 nm $\leq \Xi \leq$ 750 nm). **(b)** The intensity of the slow (I_s ○) and the fast (I_f ●) contributions to the experimental C (q,t) at 35 °C plotted as a function of Ξ.

As it can be seen in Fig. 3.2.6b, the associated intensity of the slow mode displays stronger Ξ dependence than the associated intensity of the fast mode, i.e. the inside part (nearer to the hard wall) relaxes proportionally less through the slow process than the outside part (closer to the brush/solvent interface), leading to the overall slowing down of the relaxation.

Summing up, the measured relaxation functions for the three brushes can be represented by eq. (1) leading to a diffusive Γ_c (q) of the fast mode and virtually q-independent Γ_s of the slower process. The hydrodynamic size ($kT/6\pi\eta D_c$, with η being the solvent viscosity) is found to increase upon cooling whereas the characteristic rate Γ_s of the slower mode is strongly temperature (swelling) dependent. This is the case for all three brushes with different grafting densities, which, however, appear to be distinguished in the dynamic heterogeneity towards the brush edge.

The emergence of a slow mode as solvent quality decreases is reminiscent of the dynamics of entangled polymer solutions. The issue of concentration fluctuation dynamics in semidilute solutions is not entirely understood but there is a consensus on the overall behavior. The major modification as compared to the good solvent case is the extra length scale introduced by the visco-elasticity of the solution. This was first noticed by Brochard and de Gennes [22] and soon supported by dynamic light scattering experiments[20, 21, 23, 24].

Brochard and de Gennes [22] have developed scaling expressions for θ systems. They propose two limiting regimes: at low scattering vectors *(q)* (such that $Dq^2 < \tau_r^{-1}$, where τ_r, is the characteristic disentanglement time for the chains or the terminal time from viscoelastic measurements) the restoring force for the concentration fluctuations, originating from the osmotic compressibility, leads to a cooperative diffusion coefficient that is linearly proportional to the polymer concentration. At high scattering vectors (corresponding to $Dq^2 > \tau_r^{-1}$), they predict that the correlation function is bimodal. The fast mode characterizes the cooperative diffusion and the other mode, which is independent of the scattering vector, characterizes the structural relaxation of the transient network. The time autocorrelation function of the scattered field was found to be bimodal and the results concerning the slow relaxation process could be accounted for by the theoretical models describing the coupling of concentration fluctuations to the viscoelasticity[23] . In these reports, the correlation function was analyzed at large scattering vectors in terms of two modes as had been predicted by Brochard and de Gennes: the fastest mode was found to be diffusive and the slowest was independent of the scattering vector and close to the longest relaxation time obtained by viscoelastic measurements.

This "ideal picture" may not be observed for all systems as other works [24] have reported more complex (in various   systems) spectrum. Besides the diffusive mode they observed a number of slower modes that were independent of the scattering vector. The slowest of these modes was of the order of τ_r.

Keeping the simplest approach of a step-like brush that still captures qualitatively all features, the situation in theta solvents should be represented by Gaussian chains of blobs when the structure inside the blob is also Gaussian, whereas in good solvent the conformation inside the blob is extended. Dynamically, the brush may be visualized as a slice of semidilute polymer solution, where the concentration is set by the grafting density. As it now appears, the brush case may well be understood from the 3D bulk solutions in theta solvent.

The modification compared to the bulk solution case relates the terminal relaxation time, since such a time does not exist for grafted chain. The slowest time for one chain is the "disentanglement time" and that has to be long and given the polydispersity extremely broadly distributed. Therefore the broad range of times may find its origin in the "branched" geometry

and the large polydispersity of the PS brushes. The brush specificity also lies in its ability to shrink and hence the reduced dimension in the z-direction. Based on these two distinct features some modification of the solution picture is expected. No phase separation occurs and the measurements of D_c can be extended well below T_θ as the brush adjusts its height with decreasing solvent compatibility and the increase of the characteristic length scale can not exceed the brush thickness; part of the solid surface would be fully uncovered, which is not feasible for grafted chains. As far as the viscoelastic mode and the polydispersity concern, large distribution of relaxation time is expected from a comb like structure of polydisperse-entangled chains. A theoretical treatment would be needed for grafted chains including the specificity described above.The two brushes with lower graft density, PS-5 and PS-8, show no penetration depth dependence, which suggests similar fluctuations throughout the brush. For the denser PS-3, stronger slow fluctuations at higher penetration depths are an evidence of inhomogeneity within the thickness.

We have extended our previous studies [12, 19] to polystyrene brushes in contact with solvents of varying solvent quality. We studied slow and broad dynamics when the solvent environment changes, from good to theta conditions. The decay of the relaxation function for the polymer density fluctuations becomes bimodal and is well described by a sum (eq.1) of one single exponential and a broad stretched exponential decay with $\beta = 0.32$. For the three brushes, the diffusive relaxation rate $\Gamma_c(q)$ of the fast mode relates to the cooperative diffusion whereas the origin of q-independent Γ_s of the slower process with a q-independent rate is not certain. The brush specific behavior concerns both the non-divergence of Γ_c and the heterogeneous dynamics associated with Γ_s. Based on the current documentation of the structural behavior of brushes their rich and complex dynamics is rather unexpected given the smooth variation of the average density profile[5].

In agreement with expectations close to theta-conditions concentration fluctuations become stronger. Interestingly, we observe under solvent conditions around theta (even for solvent qualities slightly below the theta-point, where in bulk solution phase separation occurs) cooperative diffusion i.e. a "breathing" of the brush. The results of the study show that measurements of the brush dynamics provide detailed local structural information and allow quantifying the solvent quality directly, which is not possible based on static measurements (i.e. reflectivity measurements) alone[5, 25].

3.3 Diffusion of micro gels close to Polymer Brush (a)

 (Langmuir 2007, 23(9), 5139)

With the advance of microfludics and the miniaturisation of processes, a fundamental understanding of how surface properties might affect the overall flow behaviour becomes crucial to the design of micron-sized devices. For large volume-to-surface ratios, surface effects are not essential and simple effective boundary conditions can reliably be used. With increasing surface to volume ratio surface effects become dominant and must be taken into account. They can range from no-slip to slip depending on the surface treatment [1]. Colloidal diffusivity close to surface can offer direct information on the nature of these effects. The case of a hard wall has received significant attention and the expected hydrodynamic slow down of particle diffusivity is now well confirmed experimentally [26-28]. More complex surfaces can lead to a strongly different behaviour. A non-wetting, super-hydrophobic surface was reported to lead to a small, hardly measurable slow-down of particle diffusivity close to the surface indicating slip boundary conditions in that case.

Polymer brushes, which are formed when macromolecules are densely attached to solid surfaces, can offer a model of soft penetrable surfaces. They are also known to provide very good lubrication conditions [7]. The flow behaviour of particles in contact to such penetrable surfaces should depend on both their size and shape, which is predicted to control the penetration of particles in polymer brushes [6]. The particle – polymer interactions are relevant in nanostructure formation such as in template-driven organization [29] in block copolymer/particle mixtures [30]. It is conceivable that the structure of the chains that ultimately defines the density profile of the brush also controls both how particles penetrate the brush and what their dynamics is. Reciprocally, information on the structure of a brush could be obtained from the particle penetration and diffusion. The latter is useful in view of the lack of scaling arguments on real, polydisperse brushes [5, 7, 12].

The soft compliant surface should act as a region of increased friction for penetrating particles and as a lubricant for non-penetrating ones, therefore introducing a size dependent dynamic threshold. We now show how particle penetration [6, 30] in the brush can be measured and

offer an estimate of the brush height and how different degree of penetration affects the measured surface diffusivities.

The polystyrene (PS) brush was grown using an azo initiator covalently attached to a glass surface. The grafting density (0.05 nm^2) was estimated from the dry film thickness (30 nm) using the number average molecular weight of the polymer chains. With a molecular weight above 10^6 g/mol and an estimated polydispersity of $M_w/M_n = 2$, which leads to a concentration profile broader than the parabolic profile of monodisperse brushes[8], the PS brush can reach a thickness up to 1µm in a good solvent such as toluene [14]. Both hard spheres and soft particles were used. The hard spheres are poly (methylmethacrylate) particles with a hydrodynamic radius R = 120 nm (in decalin). The soft particles are 64-armed star polystyrene - polybutadiene (PS-PB) diblock copolymers with the PS forming an outer shell so that is no chemical interaction between the stars and the PS brush. Their hydrodynamic radius was determined by quasi-elastic light scattering to be 20 ± 1 nm in decalin. All experiments were performed at 25 °C. The Evanescent wave dynamic light scattering technique was used and has been already discussed earlier. Figure 3.3.1 below, illustrates in detail the experimental set-up as well as the three different cases studied.
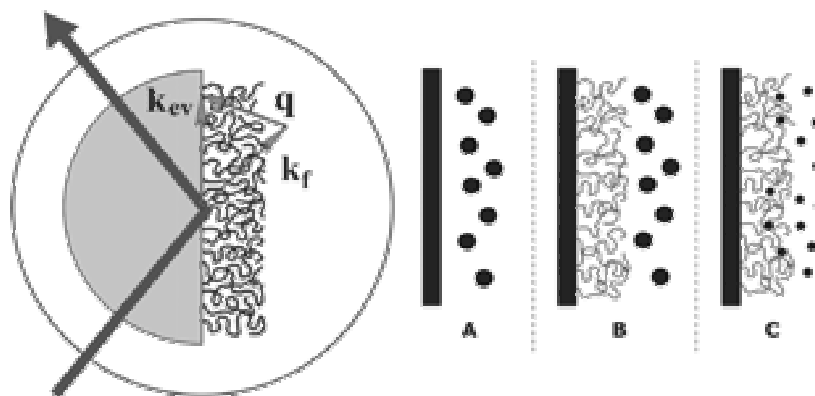
Figure 3.3.1: Schematic diagram of the evanescent wave dynamic light scattering setup with the laser beam undergoing a total reflection and the evanescent field penetrating within a distance Ξ from the surface .The wave vectors k_{ev} and k_f refer to the incident and scattered beams with q being the scattering wave vector. A, B illustrate respectively the case of the PMMA spheres close to the collapsed PS brush in dodecane and to the soft surface of the swollen PS brush in cis-decalin, and C illustrates PS-PB stars close to the PS brush in cis- decalin.

Particle penetrability

We first examine the proximity of the large PMMA spheres to the collapsed brush in dodecane, a non-solvent for PS (but good solvent for the PMMA particles). Measurement of $I(q,\Xi)$ provides an efficient way to assess the concentration profile, $c(z)$, of the particles perpendicular to the wall as: $I(\Xi) = I(0)\int_z c(z)\exp(-\frac{2z}{\Xi})dz$

It was early on recognized [19, 31] as a way to estimate the density profile close to a surface (i.e. depletion enrichment; albeit it was not successfully applied to the best of our knowledge). It should be mentioned that the intensity $I(\Xi)$ exhibits the q-dependence anticipated from the form factor of individual PMMA particles excluding any particle aggregation both in the free solution and in the presence of the brush. For the PMMA particles in contact with the collapsed (PS/dodecane) brush, $I(\Xi)$ was found to be well fitted adopting a simple step $c(z)$ profile as shown in Fig.3.3.2 (solid squares).
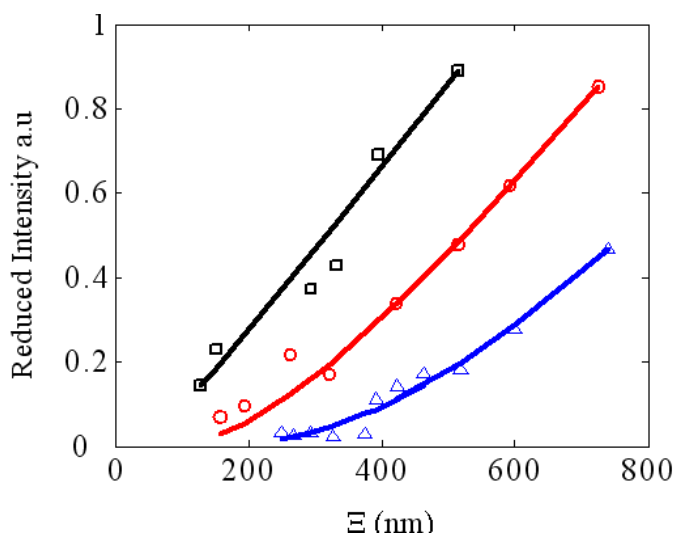
Figure 3.3.2: Reduced Intensity I(Ξ) profiles for the 120nm PMMA hard sphere in contact with the collapsed brush in dodecane (squares) and the swollen PS brush in cis-decalin (triangles). Circles correspond to the PS-PB stars close to the PS brush in cis- decalin (circles). The solid lines indicate the data representation by eq.(1) using a step density profile with thickness of 30 nm , 160 nm , 420 nm .

The sample had an excluded layer too small to be accurately measured (30 nm for the line in Fig 3.3.2 in agreement, with the thickness of the PS layer). In contrast to these test case experiments, a good fit of the experimental *I(Ξ)* for the PMMA particles in contact with the swollen brush in decalin (a marginal solvent for PS), (open triangles in Figure 3.3.2) requires to assume an excluded volume of a height L = 430 ± 30 nm, clearly demonstrating the exclusion of the particles from the brush .

This exclusion of 2R = 240 nm PMMA spheres from a dense wet brush which has a very small averaged mesh size ξ~5 nm [19, 31] is to be expected [29]. The excluded thickness value is in agreement with the expected brush thickness (less than 1 µm) and ellipsometry measurements [5, 13].The level of particle penetration should however depend on their size [29, 30]. Three regimes might be expected (i)) exclusion for particles with R > $\xi(z)$, (ii) complete mixing for particles with 2R< $\xi(z)$ and (iii) partial penetration the upper part of the brush for $\xi(z)$ and 2R in the same order of magnitude, owing to the z-dependent brush density profile [4].

The case (iii) of partial penetration is illustrated by the smaller soft diblock star particles (R_h = 20nm), in the same PS brush /decalin system. The fit of I(Ξ) by a step profile in Figure 2a leads to excluded layer of size 160 ± 20 nm , much smaller than the 430 nm layer from the PMMA spheres , indicating incomplete penetration of the brush by the particles. We may therefore deduce a mesh size of ~$2R_h$ = 40 nm at a distance z ~ 160 nm from the wall, which is otherwise theoretically hard to deduce for a polydisperse brush. Besides this exclusion behavior of the brush and the related structural characterization, the dynamics of the particles inside the brush up to about 160 nm close to the solid wall can be addressed and is discussed below.

Particle Diffusion
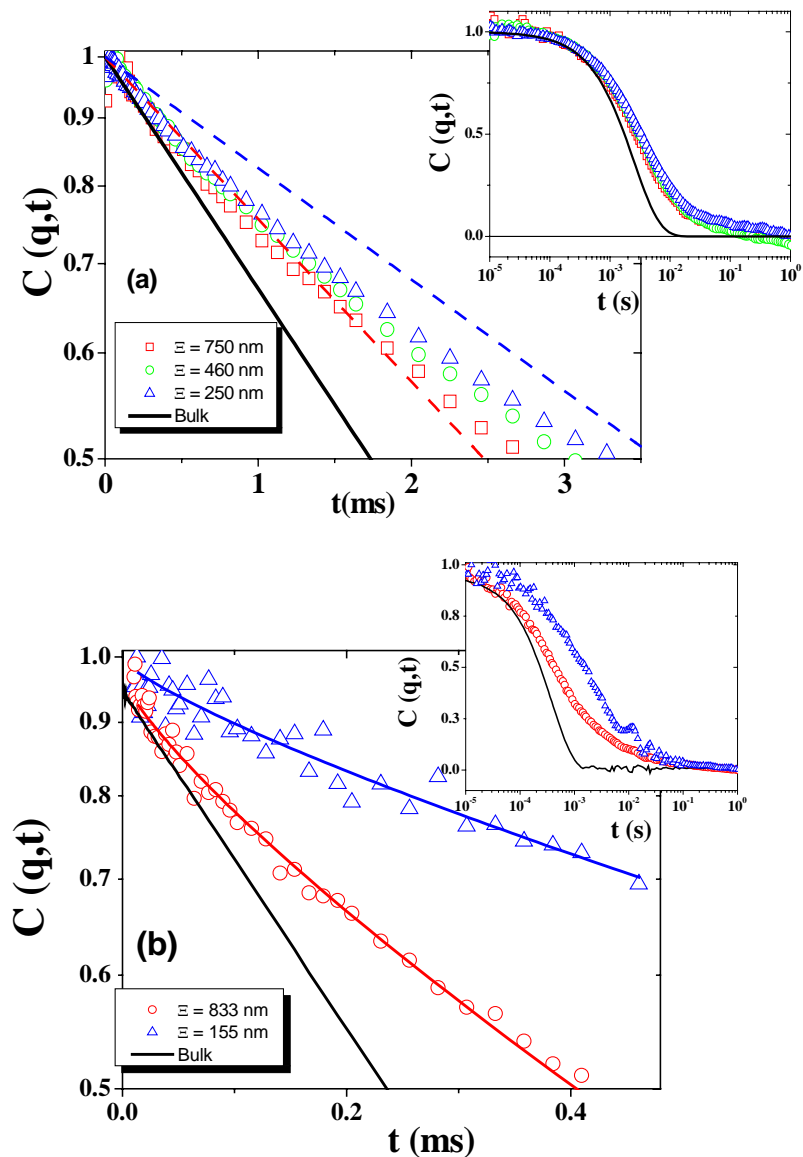
Figure 3.3.3: Normalized intermediate scattering function C(q,t) at q=0.025nm^{-1} for the particles in contact with the swollen brush in cis decalin at different indicated penetration depth Ξ he bulk C(q,t) is shown in full line for comparison . (a) The PMMA spheres. A moderate slow down effect is indicated by the comparison to the free diffusion far from the wall (in the bulk solution) (solid line) Dashed lines represent theoretical early decay of C(q,t) for diffusion close to hard wall for penetration depth 750 nm and 250 nm . (b) PS-PB stars. Both insets present the same correlations on a wider time range presented on a logarithmic scale.

We first examine the translational dynamics of the PMMA spheres to validate this expulsive situation since particle mobility is a sensitive index of the environment. Figure 3a displays the normalized $C(q,t)(=g(q,t)/a)$ relaxation functions at $\theta = 90°$ for a range of Ξ's for this system in decalin. The overall shape and dynamics of $C(q,t)$ (inset of Fig. 3.3.3a) is nearly independent to the variation of Ξ and slower and broader than the bulk $C(q,t)$ (solid line) for the particle diffusion away form the brush. In evanescent wave dynamic light scattering experiments of diffusion close to surface, quantitative analysis is generally restricted to the short time decay [27, 28]. In that case the decay rate obtained from the early decay is related to a diffusivity averaged over the scattering volume of size [28]. However, deviations from an exponential shape, unexpected for simple diffusion, are observed even at short decay times (Fig. 3.3.1).

Despite the non-exponential shape, the good data quality allows some unambiguous conclusions. Fig. 3.3.3a clearly illustrates the slower decay of the surface correlation (open symbols) compared to the bulk one (solid line) at the same wave vector q. Also shown in Fig. 3.3.3a are the early exponential decays predicted for diffusion close to a hard wall (broken lines) for two penetration depths. The value for the decay rate has been taken from ref. [28] where the averaged diffusivities for $\Xi = 250$ nm and 750 nm (corresponding to $\Xi/R = 2.1$ and 6.2) are $0.5\ D_0$ and $0.7\ D_0$ respectively; D_0 denotes the diffusion in the free bulk solution. For $\Xi = 750$ nm, short time particle diffusion near brush and hard wall cases is similar, whereas for $\Xi = 250$ nm, the diffusion dynamics near the brush (open triangles) is visibly faster than near the hard wall (blue dashed line in Fig.3.3.3a).

The slow down of the short time diffusion imposed by the brush on the non-penetrating PMMA particles (compared to D_0) appears to be different than the slow down near to a hard wall. Indeed the weak Ξ-dependence observed in the case of the brush implies that $D(z)/D_0$ is larger for the brush than for a hard wall. This reduced slowing down of non-penetrating sphere coming into contact with the permeable wall could originate from the rather large hydrodynamic penetration in a real brush predicted by theory[8].

Turning to the partially penetrating particles, the low scattered intensity from the smaller particles lead to more noisy correlation functions (Fig. 3.3.3b) that nonetheless can provide clear information on the diffusivity of the partially penetrating smaller PS-PB particles. The short time diffusion (symbols) clearly exhibits strong dependence on the penetration depth, in

clear distinction to the previous expelled larger particles (Fig.3.3.3a). It is also found to be slower than the unconstrained diffusion far from the brush, in the bulk solution (solid line). The origin of the observed retarded particle mobility has to be a manifestation of the penetration of the particles within the brush and might be attributed to an increased friction experienced by the smaller PS-PB particles within the brush. As to the microscopic origin of this increased friction, different possibilities arise, but topological confinements trapping the particles in the brush appears the most likely. A quantitative evaluation of the slow down (out of the scope of the present paper) should lead to a determination of "trapping" time and/or of viscoelastic like relaxation within the brush in a micro-rheology type of approach.

We have investigated, using evanescent wave dynamic light scattering, the penetration and diffusivities of particles of different sizes in contact with a swollen polymer brush. The penetration depth dependence of the scattered intensity evidenced a size selective penetration of the particles within the brush. The larger (120 nm) hard spheres are found to be largely expelled from the brush and their diffusivities are only slightly slowed down, reflecting a certain drag reduction from the brush. The smaller 20 nm softer particles show a partial penetration of the brush. The slower diffusivities of the penetrating particles reflect their increased friction within the brush, providing an indirect structural characterization of the brush.

3.4 Diffusion of micro gels close to Polymer Brush (b)

(Eur. Phys. J. E 2008, 26, 35)

Recent developments in the area of microfluidics have fostered the regain of interest into the longstanding problem of flow and diffusion close to surfaces [32, 33] as the movement of particles close to functionalized surfaces is of importance in many practical devices. The case of the hard wall as one special case has received significant attention and the boundary condition are now well established and understood. However, more complex situations may arise for example in the case of polymer decorated surfaces, like the for many applications highly desired slippery boundaries that increase the near wall flow velocity [33]. On the opposite side, sticky surfaces may also be desirable in some cases in order to attract particles or to reduce surface slip, like in the case of polymer melt flow, where surface grafted polymer chains are used to reduce the slip of flowing polymer melts.

Grafting polymer chains on a surface [1] constitutes a popular way to modify surfaces. Polymer brushes refer to ensembles of end grafted macromolecules attached to a solid surface with high enough grafting densities so that the polymeric coils adopt a stretched conformation perpendicular to the surface. Their structure is governed by two main parameters, the molecular weight and the grafting density as they determine the segment density profile of the polymer layer close to the surface. The surface-attached chains modify the interaction of particles present in a contacting solution with such surfaces. The particle organization by the polymer brushes has recently been theoretically described [6, 34].and the authors predicted that polymer-soluble particles smaller than a brush-determined threshold should penetrate in the brush up to a given depth that scales inversely with particle volume.

In recent experimental work [35], we observed that the permeability of swollen polymer brushes to colloidal particles depended on the particles size and nature and that the diffusivities of the particles in the vicinity of the brush were influenced by the brush presence: Whereas large hard spheres were found to not penetrate the brush and exhibited solution like diffusivities with a certain drag reduction from the brush, smaller and softer particles were found to partially penetrate the brush and to exhibit slower diffusivities reflecting the increased friction within the brush.

Following up the previous studies on particles' dynamics close to a polymer brush, we extend our studies reporting results about the diffusion of dilute colloids in contact with swollen polymer brushes as studied by evanescent wave dynamic light scattering. Two polystyrene nanogels with 16 nm and 42 nm radius were put into contact with three polystyrene brushes with varying grafting densities. Partial penetration of the nanogels within the brushes was revealed by the evanescent wave penetration depth dependent scattering intensities,. The experimental short time diffusion coefficients of the penetrating particles were measured and found to strongly slow down as the nanoparticles get deeper into the brushes. The slow down is much more marked for the smaller (16 nm) nanogels, suggesting a size exclusion type of mechanism and the existence of a characteristic length scale present in the outer part of the brush

Brush penetrability

As discussed earlier, the distribution of the particles normal to the glass wall can be estimated from the evanescent wave penetration depth dependence of the evaluated scattered intensity. Figure 3.4.1 displays the reduced scattered intensities obtained for varying penetration depth at a constant $q = 0.02$ nm^{-1} (corresponding to 90° scattering angle) for the two microgels suspended in toluene, in contact with the three swollen brushes as well as a bare glass prism. Remarkably, the experimental data obtained for the two nanogels in contact with a given brush are almost superimposed for all three brushes. It suggests that within the explored particle size range and the technique's resolution, the brush penetrability is controlled by the brush rather than the particle radius.

The lines in figure 3.4.1 represent the best fits of the experimental points obtained for a hypothetical step like concentration profile, i.e. z>h, $n(z)=n_0$ and z<h , $n(z)=0$, corresponding to a hard core /excluded volume potential:

$$I(\kappa) = \frac{1}{2} I_0 \kappa^{-1} n_o \exp(-2h\kappa)$$
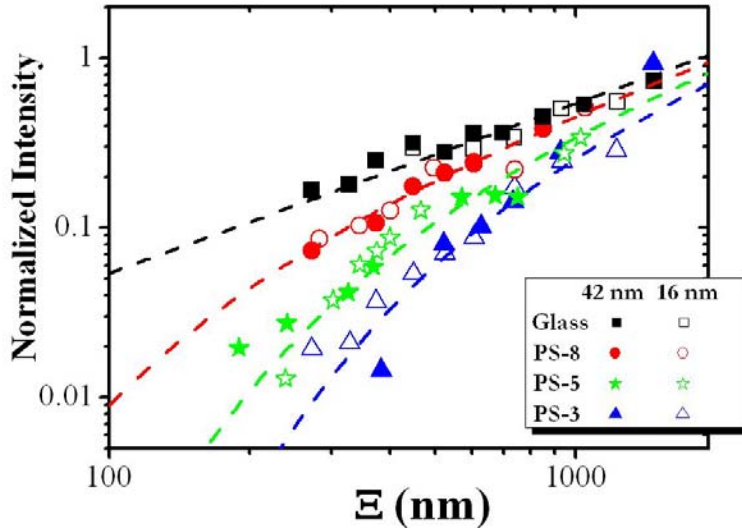
Figure 3.4.1: Intensity I(Ξ) profile for the PS nanogel particles in the case of a solid surface (■) and in contact with the three brushes; PS-3 (▲), PS-5 (★) and PS-8 (●) for the larger (solid symbols) and the smaller particles.(open symbols). The lines are the best fit of step concentration profiles.

Clearly the agreement with this simple profile is rather satisfactory. The obtained values for the excluded layer thickness h, which is a measure of how close to the glass surface the particle can travel, are L_{PS-3} = 375 ± 30 nm, L_{PS-5} = 230 ± 25 nm and L_{PS-8} = 100 ± 10 nm. These values demonstrate the overall exclusion of the particles with $2R_1$ = 84 nm and $2R_2$ = 32 nm from the brushes.

The same brushes were found to present an average dynamic mesh sizes $3 \leq \xi \leq 8$ nm, and exclusion of particles with radius of the order of 10x ξ from the brush might be expected, [10]. When reported as a function of the grafting density (Fig.3.4.2), the deduced h values are expectedly found to increase with the grafting density. Assuming power law dependence, we obtain $h \sim \sigma^{0.57}$. This exponent is clearly larger than the theoretical scaling exponent for the brush thickness ($h_0 \sim \sigma^{1/3}$ within the Alexander-DeGennes model).[10]
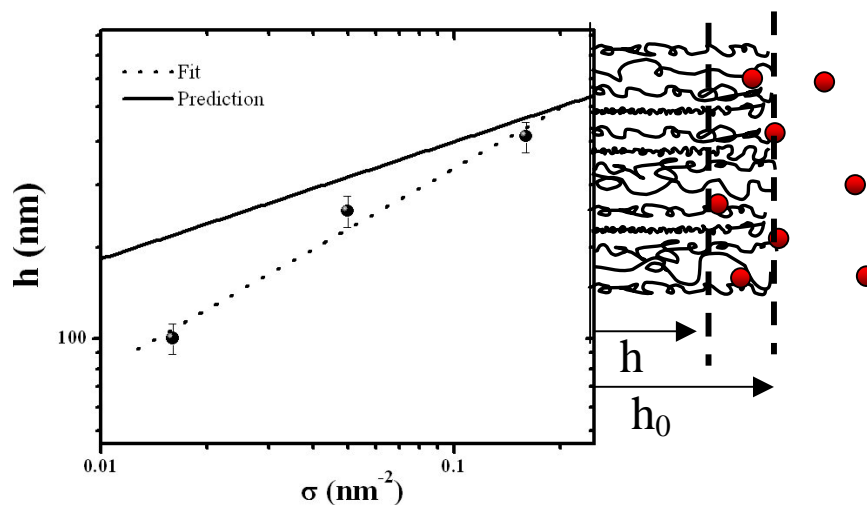
Figure 3.4.2: Excluded heights h obtained from the fit in a) as a function of the brush grafting density. The line is the expected scaling for brush height h_0.

Particle diffusion

We now turn to the diffusion of the nanoparticles in the vicinity of the polymer brushes. Normalized correlation functions measured for different particle-brush systems at a given wave vector ($q=0.02$ nm^{-1}) are reported in Figures 3.4.3 and 3.4.4 both in C vs log(time) (inset) and log C vs time representations highlighting respectively the overall decay over the full time scale and the early part of the decay used to determine the fast relaxation rate Γ.

Figure 3.4.3 presents the normalized correlation functions measured at the largest 900 nm evanescent wave penetration depth for the smaller 16 nm nanogels (top) and the larger 32 nm ones (bottom). The different symbols correspond to the different brushes, and the solid line to the bulk nanogel solution.
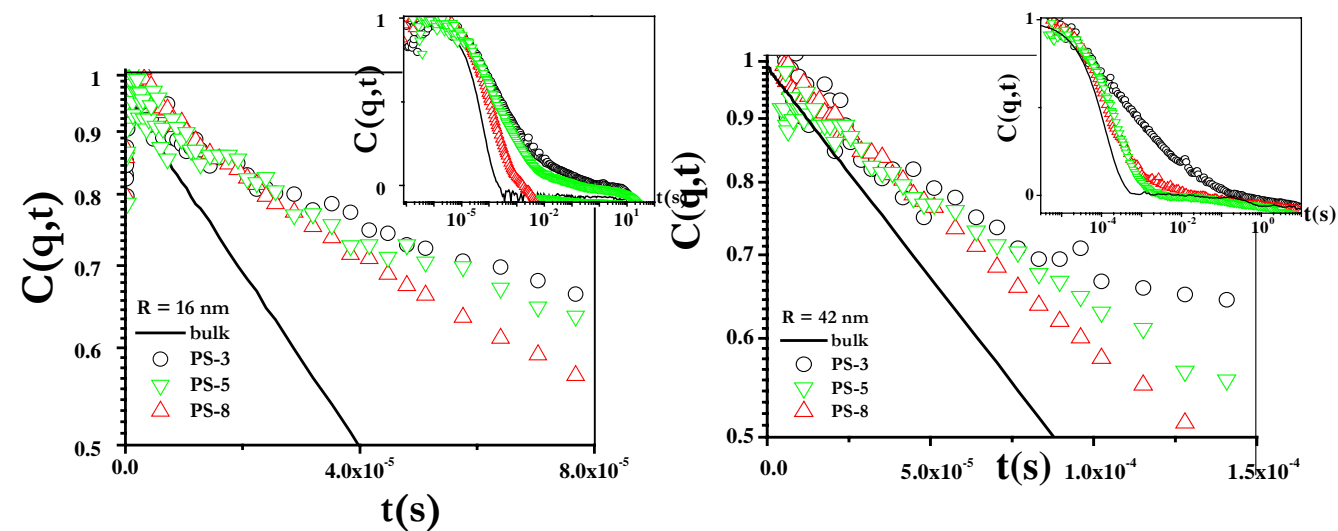
Figure 3.4.3: Normalized intermediate scattering functions C(q,t) of the PS nanogels in contact with the 3 brushes at the same q (*q = 0.02 nm⁻¹*)and the same large penetration depth (*Ξ = 900 nm*) in toluene at room temperature with (a): dilute solutions of 42 nm and (b) 16 nm nanogel particles. Inset: The same full correlation functions on a wider time range presented on a logarithmic scale are shown in insets.
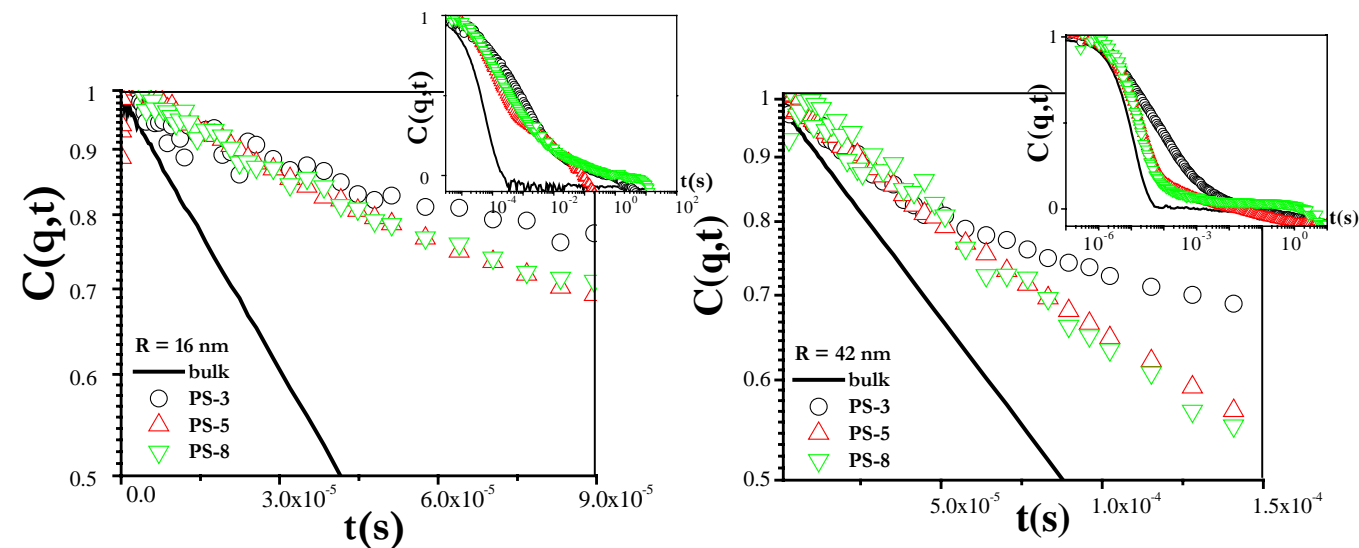
Figure 3.4.4: Normalized intermediate scattering functions C(q,t) of the PS nanogels in contact with the 3 brushes at the same q (*q = 0.02 nm⁻¹*)and the same large penetration depth (*Ξ = 700 nm*) in toluene at room temperature with (a): dilute solutions of 42 nm and (b) 16 nm nanogel particles. Inset: The same full correlation functions on a wider time range presented on a logarithmic scale are shown in insets.

Figure 3.4.4 presents in a same way the data at a shorter 700 nm penetration depth. In order to allow easy comparisons, the same scaling has been adopted for the four cases, in the main figures correlation scale is from 1 to 0.5 and the time scale is from 0 to $2\ln2/\Gamma_0$ where Γ_0 is the bulk decay rate. The decays measured for the nanogels in contact with the brushes (points) are clearly slower than the decays of the bulk solution (lines), clearly revealing the slow down of the nanogels dynamics at contact with the brushes. Evaluating the different brush/nanogel cases, a comparison of top and bottom graphs of figure 3.4.3 and 3.4.4, clearly reveals that the smaller 16 nm particles experience a stronger slow down than the larger 42 nm ones at both penetration depths. Similarly, a comparison between fig 3.4.3 and 3.4.4 shows that for a given nanogel the decays are slower for the shorter 700 nm penetration depth than for the larger 900 nm one. Finally, we note that in each graph the decays of the three different symbols (corresponding to the same nanogel at the three different brushes) almost superimpose in the early part (correlation from 1 down to 0.8). Therefore, the early decay rates for a given nanogel in contact with the three different brushes are very similar.

The slow and broad decays observed in the presence of the brushes clearly reflects the slower particles diffusion due to the presence of polymeric environment and can be taken as a confirmation of some level of interaction/interpenetration of the particles within the brushes, as inferred from the penetration depth dependence of the scattered intensities (Fig. 3.4.1).

The early decay rates Γ obtained from initial slope analysis are transformed into the apparent short time diffusivities defined as:

$$D_{eff}(\kappa^{-1}) = \frac{\Gamma}{q^2 + \kappa^{-2}}$$

Figure 3.4.5 reports the short time diffusion coefficient normalized by the free bulk solution diffusion coefficient D_o as a function of the evanescent wave penetration depth $\Xi = \kappa^{-1}$ for the different brush/nanogel systems, as well as well as for the nanogels/bare glass systems. The normalized apparent fast diffusion coefficients are expectedly found to increase with the evanescent wave penetration depth in all cases and to approach 1 at the larger Ξ. The data in Figure 3.4.5 fall into three groups: the bare glasses for the two nanogels (full and empty squares) present the weakest Ξ dependence, the large 42 nm nanogel at the three brushes (full

other symbols) fall together with an intermediate Ξ dependence and the small 16 nm nanogel at the three brushes (empty other symbols) present the strongest Ξ dependence. The insensitivity of D_{eff}/D_0 to the brush grafting density confirms the earlier observation of the similar early decays in Fig 3.4.3 &3.4.4.

The Ξ dependence is a consequence of the slowing down of the particles as they move closer to the glass surface and reflects a strong z dependence of D, much stronger than the hydrodynamic slow down at a solid surface. In the hard surface case, the observed slow down is known to be the result of the hydrodynamic slow down induced by the presence of the hard wall [1, 2, 15, 19]. The polymer has a stronger effect on the nanogels mobility than the hard wall. The Ξ dependence is much more marked for the smaller 16 nm nanogels than for the larger 42 nm particles. At the shorter penetration depth, the D_{eff} is down to $D_0/25$ compare to $D_0/2$
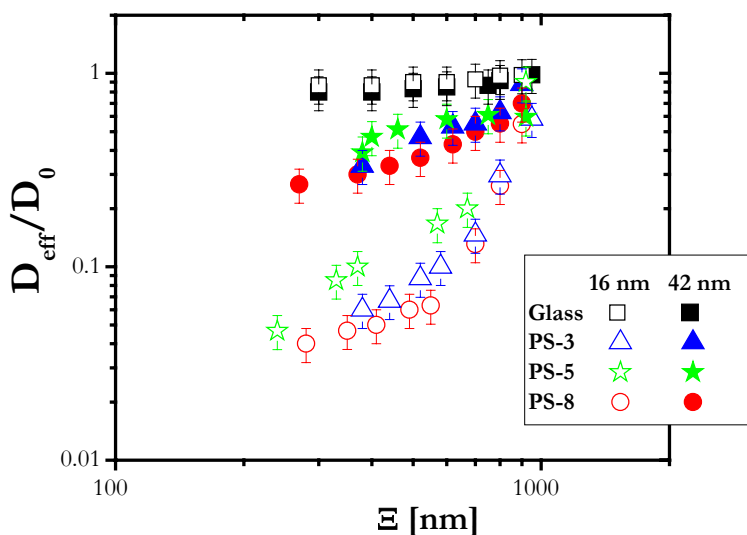
Figure 3.4.5: **N**ormalized apparent diffusivities D_{eff}/D_o ratio where D_0 is the diffusion coefficient of the bulk vs penetration depth Ξ. Solid surface is represented by squares and the three brushes; PS-3 (▲), PS-5 (★),and PS-8 (●). Larger 42nm nanogels are represented by solid symbols and smaller 16 nm nanogels by open symbols.

Beside the fast diffusivities quantified in Figure 3.4.5, the measured correlation functions of Figure 3.4.3 and 3.4.4 also provide a qualitative picture of the long time behavior. Indeed the stronger slow down of the short time diffusion also leads to the broader long time decay of the correlation function. Upon closer inspection of the correlation functions, the departures from the linear regime appear more marked for the denser brush and reveal systematic differences between the three brushes. The tendency is more evident for the 42 nm nanogels, but also present in the 16 nm ones. These deviations could be interpreted as a arising from a strong gradient of diffusion coefficient D(z) [27, 28]. In extreme cases, correlation functions spanning four decades of time can be observed for the 16 nm particles in contact with the denser brush, whereas the C(q,t) decay remains narrow for the 42 nm particles in contact with the same brush. Since the decay reflects the self-diffusion of the particles over characteristic distances of $1/(q^2+k^{-2})$, the very broad decays signify that this motion at the brush contact can be slow down up to 4 orders of magnitude compare to the diffusion in solvent. This extremely large slow down of the particles has to be envisaged as a trapping of the particles by the brush. The experimental results obtained for the spatial distribution of the nanogels within the brushes decorated interfaces (Fig. 3.4.1) and the nanogels short time diffusivities (Fig. 3.4.5) can be rationalized within the following scenario. Dense polymer brushes remain partially impenetrable to the nanogels, with a region in the outer part of the brush where the nanogels can penetrate and "feel" the polymer brush and where they experience a slower diffusion as schematically depicted in the inset of Fig 3.4.3b.

With increasing the brush grafting density the particles are kept at a further and further distance from the glass surface. The volume inaccessible to the particles increases faster with increasing grafting density than the expected brush height, which means that the exclusion of the particles becomes stricter with increasing grafting density. Within the technique resolution, the extent of the visited region in a given brush appears to be similar for both nanogels (16 and 42 nm).

The partial impenetrability of the brush is somehow confirm by a complementary experiment where the nanogels were dispersed in a PS solutions of 1M molecular weight and concentration of 10 % by weight, which is the order of magnitude of the averaged concentration in the brush. The nanogels were found to slowly segregate from the polymer solution, forming macroscopic domains over very large time scale (days to weeks).

Within this outer interaction region, the nanogels diffusion is significantly slower than the diffusion in the pure solvent, and more so as the nanogels get deeper into the brush, as the z-dependence of the diffusion coefficient is at the origin of the observed Ξ dependence of the D_{eff} (eq(7))(Figure 3.4.5) . The slow diffusion has to be attributed to an increased interaction/friction of the nanogels in the brush environment.

At this point we may note that the parent case of colloidal particles in solutions and gels of non adsorbing polymers has received much attention from theory, experiments and simulations. Many possibilities have been considered but despite the large efforts the diffusion of colloids in such environment is still not fully understood. It is generally admitted that the experienced friction should lie in between the solvent and overall polymer solution viscosity [36].

The striking finding in Figure 3.4.5 is that the smaller 16 nm nanogels are much more affected than the larger 42 nm nanogels. This is somewhat counter intuitive since larger tracer particles are usually expected to be more affected than smaller particles. For example this is the case in semi-dilute polymer solutions with colloids dispersed in it. A noticeable exception is the case of gel permeation chromatography (GPC), were larger polymer chains are eluted faster than shorter one [37]. This is generally believed to arise from the "tortuosity" of the used gels, so that the smaller chains can explore a larger volume of pores and have a slower overall velocity [reference], leading to the size exclusion mechanism. A further possibility for the two distinct behaviours in the case of the two nanogels lies in the possible differences in the nanogels structures. They might have different cross-linking densities and accordingly a different hardness. In addition the surface chemistry of the particles might also be different. If only the nanoparticles size is involved, the very strong slow down experienced by the 16 nm nanogels, and not present to the same extend in the larger 42 nm ones will have to be explained by some commensurate topological interaction within the brush, This would imply the presence of a specific length scale in the outer part of the three brushes. Further experiments with nanoparticles of similar sizes and different chemistry should help to corroborate one or the other possibility, i.e. the friction or the interaction origin of the slow down.

Due to the chain stretching in the direction perpendicular to the surface, we may expect an anisotropic experienced friction, which will result in a motion with different diffusion

coefficients in plane and in the perpendicular direction. Such anisotropy has been evidenced in the case of flat hard surfaces. With the used set-up, the anisotropy of the diffusion cannot unambiguously be resolved, however we did not observe any angular dependence that will imply large anisotropic motion.

Using EWDLS and the penetration dependence of the scattered intensity and the early decay rate, we have observed the partial exclusion of PS nanogels from swollen PS brushes and the nanogel slowdown as they penetrated the polymeric environment, using three different brushes with different grafting densities in combination with two different colloidal nanogels. The measured dynamics clearly uncovered some large differences in the motion of the particles when in contact with the swollen brushes, where the larger particles are less trapped. The role of the nature of the particles remains to be resolved, and could be of importance. On the practical side, these findings suggest that polymer brush could be used for size exclusion purposes. EWDLS appears as a powerful technique for study of the diffusivities of small particles near soft interfaces [20] that will not be feasible by the more standard optical microscopy [24].

The simple case of non-interacting particles in contact with polymer brushes reveals a rich dynamic behavior; form lubricating condition for fully non-penetrating hard sphere [6] to the almost trapped smaller nanogels reported in this paper. Support of theory of the type of [5] as well as of computer simulations will be needed to shed some more lights on those swollen brush/particle specificities and to uncover the penetration of non-adsorbing particles within a polymer brush. Such progresses will allow the quantification of the observed phenomena and permit to identify whether their origin is purely entropic or required specific interactions between the brush and the particles.

3.5 REFERENCES

1.   Advincula, R.C.B., B.; Rühe, J.; Caster, K, *Polymer Brushes.* 2004.

2.   Minko, S., S. Patil, V. Datsyuk, F. Simon, K.J. Eichhorn, M. Motornov, D. Usov, I. Tokarev, and M. Stamm, *Synthesis of adaptive polymer brushes via "grafting to" approach from melt.* Langmuir, 2002. **18**(1): p. 289-296.

3.   Zhao, B., W.J. Brittain, W. Zhou, and S.Z.D. Cheng, *AFM study of tethered polystyrene-b-poly(methyl methacrylate) and polystyrene-b-poly(methyl acrylate) brushes on flat silicate substrates.* Macromolecules, 2000. **33**(23): p. 8821-8827.

4.   Binder, K., *Scaling concepts for polymer brushes and their test with computer simulation.* European Physical Journal E, 2002. **9**(3): p. 293-298.

5.   Karim, A., S.K. Satija, J.F. Douglas, J.F. Ankner, and L.J. Fetters, *Neutron reflectivity study of the density profile of a model end-grafted polymer brush: Influence of solvent quality.* Physical Review Letters, 1994. **73**(25): p. 3407-3410.

6.   Kim, J.U. and B. O'Shaughnessy, *Morphology selection of nanoparticle dispersions by polymer media.* Physical Review Letters, 2002. **89**(23): p. 238301/1-238301/4.

7.   Milner, S.T., *Polymer brushes.* Science, 1991. **251**(4996): p. 905-914.

8.   Milner, S.T., T.A. Witten, and M.E. Cates, *Theory of the grafted polymer brush.* Macromolecules, 1988. **21**(8): p. 2610-2619.

9.   Fytas, G., S.H. Anastasiadis, R. Seghrouchni, D. Vlassopoulos, J. Li, B.J. Factor, W. Theobald, and C. Toprakcioglu, *Probing collective motions of terminally anchored polymers.* Science, 1996. **274**(5295): p. 2041-2044.

10.   De Gennes, P.G., *Conformations of polymers attached to an interface.* Macromolecules, 1980. **13**(5): p. 1069-1075.

11.   de Gennes, P.G., *Polymers at an interface; a simplified view.* Advances in Colloid and Interface Science, 1987. **27**(3-4): p. 189-209.

12.   Yakubov, G.E., B. Loppinet, H. Zhang, J. Ruhe, R. Sigel, and G. Fytas, *Collective Dynamics of an End-Grafted Polymer Brush in Solvents of Varying Quality.* Physical Review Letters, 2004. **92**(11): p. 115501-1.

13.   Prucker, O. and J. Ruhe, *Polymer layers through self-assembled monolayers of initiators.* Langmuir, 1998. **14**(24): p. 6893-6898.

14. Prucker, O. and J. Ruhe, *Synthesis of poly(styrene) monolayers attached to high surface area silica gels through self-assembled monolayers of azo initiators.* Macromolecules, 1998. **31**(3): p. 592-601.

15. Muthukumar, M. and J.S. Ho, *Self-consistent field theory of surfaces with terminally attached chains.* Macromolecules, 1989. **22**(2): p. 965-973.

16. Mukhopadhyay, A., J. Zhao, S.C. Bae, and S. Granick, *Contrasting friction and diffusion in molecularly thin confined films.* Physical Review Letters, 2002. **89**(13): p. 1361031-1361034.

17. Dai, L.L. and S. Granick, *Linear shear viscoelasticity of confined, end-attached polymers in a near-theta solvent.* Journal of Polymer Science, Part B: Polymer Physics, 2005. **43**(23): p. 3487-3496.

18. Semenov, A.N., *Dynamics of entangled polymer layers: The effect of fluctuations.* Physical Review Letters, 1998. **80**(9): p. 1908-1911.

19. Michailidou, V.N., B. Loppinet, O. Prucker, J. Ruhe, and G. Fytas, *Cooperative diffusion of end-grafted polymer brushes in good solvents.* Macromolecules, 2005. **38**(21): p. 8960-8962.

20. Adam, M. and M. Delsanti, *Dynamical behavior of semidilute polymer solutions in a ? solvent: Quasi-elastic light scattering experiments.* Macromolecules, 1985. **18**(9): p. 1760-1770.

21. Kostko, A.F., M.A. Anisimov, and J.V. Sengers, *Dynamic crossover to tricriticality and anomalous slowdown of critical fluctuations by entanglements in polymer solutions.* Physical Review E - Statistical, Nonlinear, and Soft Matter Physics, 2002. **66**(2): p. 020803/1-020803/4.

22. Brochard, F. and P.G. De Gennes, *Dynamical scaling for polymers in theta solvents.* Macromolecules, 1977. **10**(5): p. 1157-1161.

23. Jian, T., D. Vlassopoulos, G. Fytas, T. Pakula, and W. Brown, *Coupling of concentration fluctuations to viscoelasticity in highly concentrated polymer solutions.* Colloid and Polymer Science, 1996. **274**(11): p. 1033-1043.

24. Nicolai, T., W. Brown, R.M. Johnsen, and P. Stepanek, *Dynamic behavior of theta solutions of polystyrene investigated by dynamic light scattering.* Macromolecules, 1990. **23**(4): p. 1165-1174.

25. Habicht, J., M. Schmidt, J. Ruhe, and D. Johannsmann, *Swelling of thick polymer brushes investigated with ellipsometry.* Langmuir, 1999. **15**(7): p. 2460-2465.

26.   Lan, K.H., N. Ostrowsky, and D. Sornette, *Brownian dynamics close to a wall studied by photon correlation spectroscopy from an evanescent wave.* Physical Review Letters, 1986. **57**(1): p. 17-20.

27.   Garnier, N. and N. Ostrowsky, J. Phys. II (France), 1991. **1**: p. 1221.

28.   Holmqvist, P., J.K.G. Dhont, and P.R. Lang, *Anisotropy of Brownian motion caused only by hydrodynamic interaction with a wall.* Physical Review E - Statistical, Nonlinear, and Soft Matter Physics, 2006. **74**(2).

29.   Lee, J.Y., R.B. Thompson, D. Jasnow, and A.C. Balazs, *Entropically driven formation of hierarchically ordered nanocomposites.* Physical Review Letters, 2002. **89**(15): p. 155503/1-155503/4.

30.   Bockstaller, M.R., Y. Lapetnikov, S. Margel, and E.L. Thomas, *Size-selective organization of enthalpic compatibilized nanocrystals in ternary block copolymer/particle mixtures.* Journal of the American Chemical Society, 2003. **125**(18): p. 5276-5277.

31.   Berret, J.F., G. Cristobal, P. Herve, J. Oberdisse, and I. Grillo, *Structure of colloidal complexes obtained from neutral/polyelectrolyte copolymers and oppositely charged surfactants.* European Physical Journal E, 2002. **9**(4): p. 301-311.

32.   Lauga, E., M.P. Brenner, and H.A. Stone, *The No-Slip Boundary Condition: A Review.* Condens. Matter, 2005: p. 501557.

33.   Bocquet, L. and J.L. Barrat, Soft Matter, 2007. **3**: p. 658.

34.   Kim, J.U. and B. O'Shaughnessy, *Nanoinclusions in dry polymer brushes.* Macromolecules, 2006. **39**(1): p. 413-425.

35.   Filippidi, E., V. Michailidou, B. Loppinet, J. Ruhe, and G. Fytas, *Brownian diffusion close to a polymer brush.* Langmuir, 2007. **23**(9): p. 5139-5142.

36.   Koenderink, G.H., S. Sacanna, D.G.A.L. Aarts, and A.P. Philipse, *Rotational and translational diffusion of fluorocarbon tracer spheres in semidilute xanthan solutions.* Physical Review E - Statistical, Nonlinear, and Soft Matter Physics, 2004. **69**(2 1): p. 021804-1-021804-12.

37.   Sun, T., R.R. Chance, W.W. Graessley, and D.J. Lohse, *A study of the separation principle in size exclusion chromatography.* Macromolecules, 2004. **37**(11): p. 4304-4312.

Chapter 4

4. RESULTS & DISCUSSION - Dynamics of Hard Spheres

In this part of the work we investigate the dynamics of hard spheres in the bulk and close to a hard wall [1]. We used dynamic light scattering to investigate the Brownian motion of colloidal particles near a solid, planar surface. An evanescent wave scattered from a colloidal solution adjacent to the solid interface correlates with the anisotropic dynamics of particles within a penetration depth of the wall. Measurements were carried out for various volume fractions of PMMA hard-sphere suspensions over a range of scattering wave vectors. The results were analyzed using a new framework for extracting both the short-time self - diffusivity and the collective diffusivity from evanescent wave scattering data. In the dilute regime, the diffusion coefficient near the interface is much smaller than that for free diffusion in bulk solution. This is due to the hydrodynamic interactions between the sphere and the solid wall, which slows down the motion. The wall-induced reduction of the self- diffusion is negligible at higher

volume fractions due to interplay between the particle-wall and particle-particle hydrodynamic interactions. A simple model captures the basic physical mechanism responsible for such behaviour, while a quantitative prediction of the weaker decay of the near-wall self-diffusion coefficient with volume fraction is offered by Stokesian Dynamics simulations [1]. Stokesian Dynamics simulations were performed by J. Swan and J. F. Brady (Caltech University).

A similar system was also investigated using another Evanescent wave dynamic light scattering set – up, in Jülich (Prof. J. K. G. Dhont's Lab) [2, 3]. Details of this set – up used can be found in Chapter 2. This set – up allows us to independently vary the scattering vector components parallel, $q_{//}$, and normal, $q_{\perp}$, to the wall, allowing the study of the anisotropic particles' mobility near a wall. An expression for the initial decay rate Γ of the time autocorrelation functions as a function of both $q_{//}$ and $q_{\perp}$, as well as the penetration depth of the evanescent wave is used [2, 3]. Measurements were carried out for various volume fractions of PMMA hard sphere suspensions in a wide range of scattering wavenumbers. The near wall dynamics were compared to the associated bulk dynamics of the hard spheres and the main finding is that the parallel diffusivities in the concentrated suspensions behave similarly to the bulk dynamics in contrast with the perpendicular ones that are affected stronger by the presence of the wall.

4.1 Dynamics of concentrated colloidal suspensions near a hard wall [1].

Interfaces are an important ingredient of mesoscopic systems such as colloids and polymers as well as biological systems such as cells and biomembranes. Consequently, the Brownian motion of their constituents: colloidal particles, polymer chains and proteins, near a solid or liquid interface, is of central importance and determines their macroscopic properties and impacts their biological functions. Such confined dynamics are affected by direct energetic interactions between the interface and the Brownian diffuser as well as excluded volume and hydrodynamic interactions. Hydrodynamics strongly affect the diffusion (collective and single) and flow of particles near a hard wall [4-6] between two bounding surfaces [7] or in microfluidic channels [8]. In biological systems hydrodynamic coupling also plays an essential role in the collective motion of sperm cells near an interface [9], and for swimming bacteria confined in thin films. At the same time, flows of dilute or concentrated suspensions in confined environments are ubiquitous in industrial processes of high importance from food processing to petrol recovery [10]. Thus, Brownian motion of colloidal particles near surfaces is of interest from both standpoints of fundamental mesoscopic physics and interface science as well as for its high technological relevance. Its detailed understanding is required for the advancement of microfluidics and optofluidics [11, 12] and for flow and mobility control in biological systems such as protein motion inside cells or through biomembranes. A key question is how particle dynamics are affected by the existence of non-penetretable walls via hydrodynamic interactions (HIs). Experimentally, confocal microscopy [13] limited by particle size, and evanescent wave dynamic light scattering (EWDLS) [2, 4, 5, 13] combining dynamic light scattering (DLS) with the short penetration depth of an evanescent wave produced in a total internal reflection geometry, have been used to study near surface dynamics. The latter requires a careful interpretation of the intensity time autocorrelation function. Currently only its initial decay from dilute colloidal suspensions is well described taking into account both the anisotropic diffusion as well as the particular evanescent wave illumination[2, 3]. EWDLS has been utilized to also study the dynamics of polymer brushes, particles near a brush and rod-like polymers near a wall [14-17]. With increasing volume fraction (Φ) particle-particle HIs become important and modify the wall-induced drag effect. Furthermore, the liquid to solid (glass or

crystal) transition in confined systems is directly related with the way particle dynamics in highly concentrated suspensions are affected by the presence a non-penetrable wall [18]. However, near-wall dynamics in concentrated suspensions are virtually unexplored either experimentally or theoretically.

We performed conventional DLS and EWDLS with several scattering wave vectors with magnitude $q = (4\pi n_2 / \lambda_0)\sin(\theta_s / 2)$ and the inverse penetration depth denoted $\kappa / 2 = (2\pi / \lambda_0)\sqrt{(n_1 \sin \theta_i)^2 - n_2^2}$, where n_1 and n_2 are the refractive indices of the reflective interface and suspension respectively, λ is the vacuum wavelength of the laser, θ_s is the scattering angle and θ_i is the angle at which the incident beam impinges the surface, to measure the colloidal dynamics (at room temperature, T = 18 °C) in bulk (3D) and close to the wall (2D) of sterically stabilized suspensions.

The suspensions were composed of poly(methyl methacrylate) (PMMA) nearly hard-sphere particles with radius R = 183nm (determined by light scattering) in refractive index matching tetralin/cis-decalin (30%/70%) mixture (n_2 = 1.497) which minimized multiple scattering at high volume fractions. We prepared several volume fractions by progressively diluting a single batch of concentrated suspension; the volume fraction of the latter was determined both in the coexistence regime and from random close packing (RCP = 0.65). The evanescent wave was generated by a laser with a vacuum wavelength, λ_0 = 532 nm and an impingement angle, θ_i = 68.2 °, at the interface of a semi-cylindrical prism of high refractive index (n_1 = 1.627) and the suspending liquid which was confined in the cylindrical solvent cell. The cell was placed at the center of a θ_s–$2\theta_s$ goniometer that allowed for variation of both the wave vector and the penetration depth. The TCF was measured under mixed homodyne and heterodyne conditions due to the strong static scattering from the glass surface in the case of EWDLS. In these experiments, we achieved penetration depths in the range of a few particle radii (1 < $2/(\kappa R)$ < 6). This allowed us to probe the dynamics very near the wall. Similarly, we operated in a range of scattering wave vector magnitudes of just a few particle radii (1 < qR < 7).

In the experiments, we measure the time dependent light scattering intensity, $I(q,t;\kappa)$, and compute the normalized intensity time-autocorrelation function TCF $g^{(2)}(q,t;\kappa) = <I(q,t;\kappa)I^*(q,0;\kappa)> / <I>^2$, under mixed homodyne and heterodyne conditions due to the strong static scattering from the glass prism surface. We then calculate

the normalized field autocorrelation function $C(q,t;\kappa) = < E(q,t;\kappa)E^*(q,0;\kappa) > / < I >$ (where the angle brackets signify an ensemble average and the asterisk indicates the complex conjugate) from $g^{(2)}(q,t;\kappa)$, using the modified Siegert relation [13] (See also Chapter 2) and further compute its initial decay rate [19], $\Gamma = \frac{\partial}{\partial t}\ln f(q,t;\kappa)$ as t$\rightarrow$0, to determine the q-dependent short-time diffusion coefficient, $D^{3D}(\phi,q) = \Gamma / q^2$.

In EWDLS, the intensity of the scattered beam decays exponentially with distance from the boundary, and as such, the typical DLS averages [19] for the dynamics of suspensions persist, but they are modulated by the decay of the evanescent wave. In this case $D^{2d}(\phi,q,\kappa) = \dfrac{\Gamma}{k \bullet \overline{\overline{k}}}$ where k = q + e_3iκ/2 and e_3 is a vector normal to the wall pointing into the fluid. Thus, we have redefined the scattering vector for an evanescent wave as the sum of the usual scattering wave vector and an imaginary component that gives rise to the exponential decay.

Following typical DLS analysis, we can recover an "evanescent" collective diffusivity and an "evanescent" short-time self-diffusivity. In the limit that qR $\rightarrow$ 0, we can show that the decay $C(q,t;\kappa)$ measures the collective diffusivity as:

$$D_c^{2d}(\phi,\kappa) = < D_{33}^{\alpha\alpha}e^{-\kappa z_a} + (N-1)D_{33}^{\alpha\beta}e^{-\frac{\kappa}{2}(z_\beta + z_\alpha)} > / < e^{-\kappa z_a} + (N-1)e^{-\frac{\kappa}{2}(z_\beta + z_\alpha)} > \quad (1)$$

where $D_{33}^{\alpha\alpha}(= kTM_{33}^{\alpha\alpha})$ and $D_{33}^{\alpha\beta}(= kTM_{33}^{\alpha\beta})$ are the products of the thermal energy with the self hydrodynamic mobility of a particle in the ensemble and in the direction perpendicular to the wall, in an ensemble of N particles with z_α, z_β the distances of two particles from the wall.

Here $D_c^{2d}(\phi,\kappa)$ is the "evanescent" collective diffusivity and measures diffusion perpendicular to the wall. Only the dynamics perpendicular to the wall can be extracted from EWDLS since motion parallel to the wall in O(qR) while that perpendicular is O(1).

In contract, at large qR the decay of the TCF measures a weighted average of parallel and perpendicular "evanescent" short-time self-diffusivities as:

$$D_s^{2d}(\phi,\kappa) = \frac{<[q_{II}^2 D_{11}^{\alpha\alpha} + (q_\perp^2 + \frac{\kappa^2}{4})D_{33}^{\alpha\alpha}]e^{-\kappa z_\alpha}>}{(q_{II}^2 + q_\perp^2 + \frac{\kappa^2}{4})<e^{-\kappa z_\alpha}>} \quad (2)$$

where $D_{11}^{\alpha\alpha}(=kTM_{11}^{\alpha\alpha})$ reflects the self hydrodynamic mobility parallel to the wall. In particular, for $\kappa/2 << q$ (which always hold here) and $q_{||} \sim q_\perp$ (at $\theta_s = 90$ °) the short time decay of $C(q,t;\kappa)$ weights equally the components of the self-diffusivity parallel an perpendicular to the wall, yielding:

$$D_s^{2D}(\phi,\kappa) = \frac{<(D_{11}^{\alpha\alpha} + D_{33}^{\alpha\alpha})e^{-\kappa z_\alpha}>}{2<e^{-\kappa z_\alpha}>} \quad (3)$$

The above results are similar to the cumulant expansion of Holmqvist et al. [3], but apply over the entire range of volume fractions where the previous ones were only valid in the dilute regime.

Below, we first present the experimental data from both DLS and EWDLS interrogations of the decay of the TCF generated by suspensions of increasing ϕ. This reveals the effect of the particle crowding on the wall-induced HIs.

Figure 4.1.1 shows the $C(q,t;\kappa)$ at qR = 4.58 for a dilute and a concentrated suspension. In all the EWDLS results presented the penetration depth was $\frac{2}{\kappa} = 4.37R$ (corresponding to $\theta_i = 67.2°$). It is evident that while in the dilute suspension the 2D dynamics are clearly slower due to the additional wall induced drag [4, 20], for a more concentrated suspension the dynamics in 2D and 3D are essentially the same, especially in the short-time regime. This directly reveals a qualitative modification of the wall induced hydrodynamic interactions at high ϕ when compared to the dilute limit.
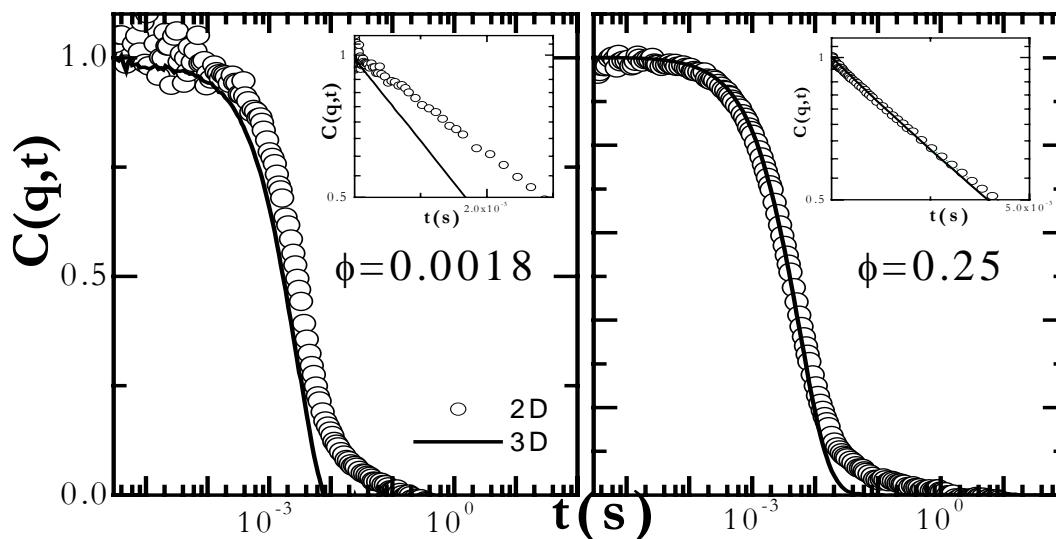
Figure 4.1.1: The TCF from DLS and EWDLS at qR = 4.58 (and $\frac{2}{\kappa} = 4.37R$ in the latter case) for a dilute ($\phi = 0.0018$) and a concentrated suspension ($\phi = 0.25$). The insets portray the initial decay of these functions.

In Figure 4.1.2 and 4.1.3 we show the q-dependent diffusivity, deduced for the short-time decay of the TCF in both 2D (Figure 4.1.3) and 3D (Figure 4.1.2), normalized by the Stokes-Einstein-Sutherland diffusivity, $D_0 = \frac{kT}{6\pi\eta R}$. At higher ϕ, the slowing of the dynamics near the peak in the structure factor ("de Gennes narrowing") is evident in both the 2D and the 3D data. In suspension of hydrodynamically interacting colloidal particles the effective short – time diffusion coefficient D^s, is determined from the initial decay of C(q, t) according to

$D^s(q) = (1/q^2)\lim_{t\to 0}[(d/dt)\ln|C(q,t)|]$ is given by: $D^s(q) = D_0 \frac{H(q)}{S(q)}$ where H(q) is the hydrodynamic factor and S(q) the structure factor [21].

To quantify the influence of ϕ on the near-wall dynamics, we extract the short-time self-diffusivity by determining $D^{2D}(\phi, q, \kappa)$ at qR=4.58 ($\theta_s = 90$ °) respectively. The parallel and perpendicular diffusivities are averaged in the ratio of one to one as shown above.
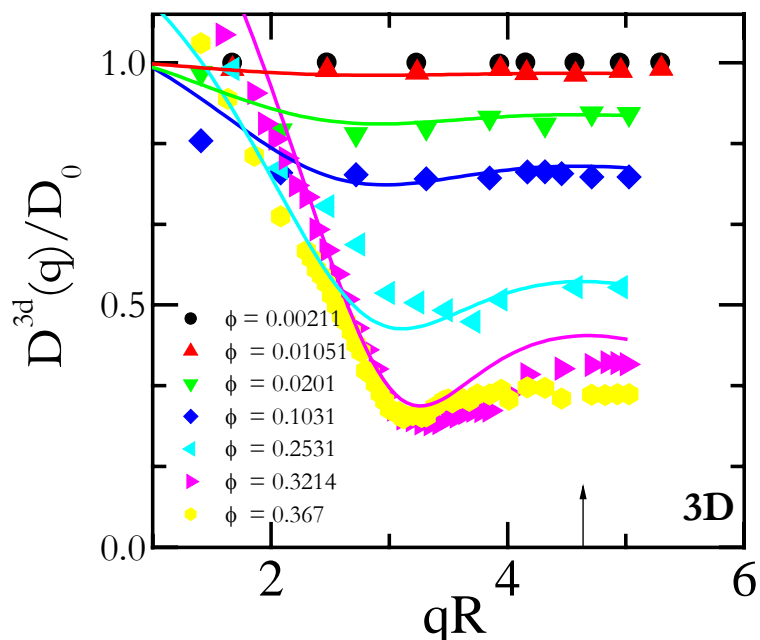
Figure 4.1.2: The decay of the intermediate scattering function (q-dependent diffusivity) as a function of qR in the bulk. The arrow denotes the 90 ° scattering point and the lines denote the theoretical predictions of Beenaker and Mazur of diffusion in the bulk.
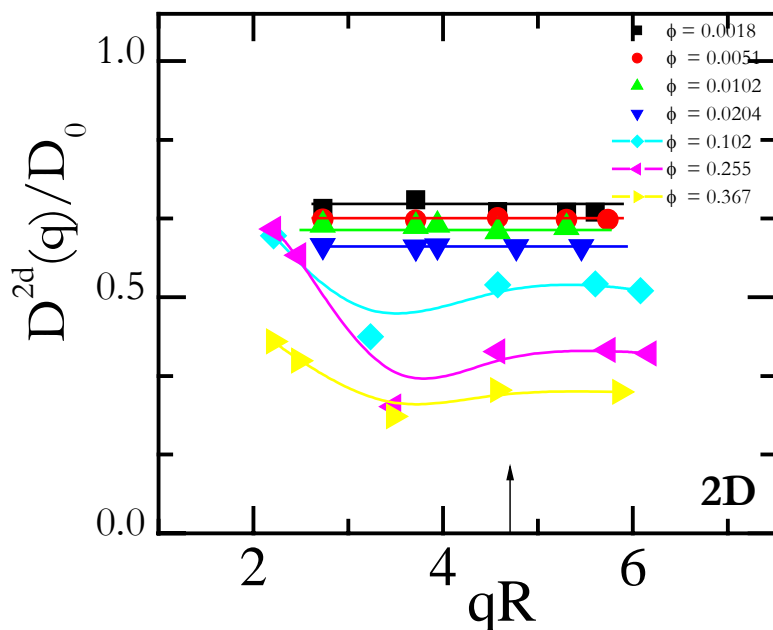
Figure 4.1.3: The decay of the intermediate scattering function (q-dependent diffusivity) as a function of qR near the wall. The arrow denotes the 90 ° scattering point. The lines are to guide the eye.

In figure 4.1.4 we show the evolution of the self-diffusion coefficient with increasing ϕ in both the bulk and near the wall. In the limit $\phi \rightarrow 0$ we recover a ratio of near-wall to bulk self-diffusivity of 0.68 (at $2/\kappa = 4.37R$) in qualitative agreement with the theoretical predictions for the hydrodynamics slowing of a particle near a hard wall (0.85) [2, 3]. It is quite interesting that above $\phi \sim 0.35$ both the single particle and collective dynamics near the wall are virtually indistinguishable from those in the bulk. Consequently the decay of the near-wall self-diffusion with respect to ϕ is weaker than self-diffusion in the bulk. We also see that the bulk diffusivities agree quite well with the results of Stokesian dynamics simulations with full hydrodynamics at high ϕ and with Batchelor's virial expansion [22, 23] up to $\phi \sim 0.1$.
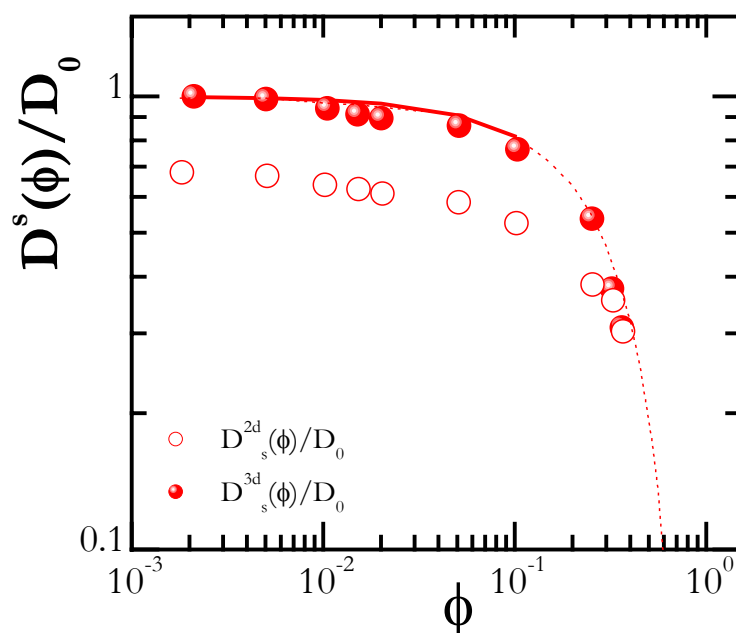
Figure 4.1.4: The ϕ-dependence of the short-time self - diffusion coefficients in bulk and near the wall. The solid lines correspond to Batchelor's dilute predictions [22, 23] and the dashed lines are the results of Stokesian dynamics simulations[24].

A simple model explains the physical origin of the diminished effect of the wall on the dynamics of particles at high ϕ. The decrease in the short-time self-diffusivity with ϕ in the bulk is caused by HIs comprising a far field ($\sim 1/r$) and a near field (lubrication) contribution [24]. The particle-wall and particle-particle near field HIs may be reasonably assumed the same (they have the same singular behavior near contact). We may then use this idea to calculate the

ratio of the bulk to the near-field self-diffusivity. In the bulk we may write the normalized diffusivity as, $D^{3D} = \left(\eta_{FF}^{3D} + \eta_{lub}^{3D}\right)^{-1}$ and $D_{FF}^{3D} = \left(\eta_{FF}^{3D}\right)^{-1}$ with *ff* and *lub* denoting the far- and near-field parts of the HIs respectively, yielding $\eta_{lub}^{3D} = 1/D_s^{3D} - 1/D_{FF}^{3D}$.

For a given penetration depth and for a dense suspension, the near-wall diffusivity may be written as $D_s^{2D}(\phi,\kappa) = \left(\eta_{FF}^{2D} + \eta_{lub}^{3D}\right)^{-1}$. We further assume that the far-field contribution to the near-wall diffusivity may be expressed as $D_{FF}^{2D}(\phi,\kappa) = D_{FF}^{3D}(\phi)\left(D_0^{2D}(\kappa)/D_0^{3D}\right)$, where $D_0^{2D}(\kappa)$ is the dilute near-wall short-time self-diffusivity. This results in a ratio of bulk to near-wall diffusivities of

$$D_s^{3D}(\phi)/D_s^{2D}(\phi,\kappa) = 1 + \left(D_s^{3D}(\phi)/D_{FF}^{3D}(\phi)\right)\left(D_0/D_0^{2D}(\kappa)-1\right) \quad (4)$$

The right hand side of this equation can be determined using the experimental dilute limit ratio $D_0/D_0^{2d}(\kappa)$ and the ratio $D_s^{3d}(\phi)/D_{ff}^{3d}(\phi)$ taken from simulations [24]. As seen in Figure 4.1.5, the above equation approximates well our experimental data and validates the proposed mechanism, although a discrepancy is observed at high volume fractions. The latter suggests that an additional mechanism might exist leading to an enhancement of the phenomenon.
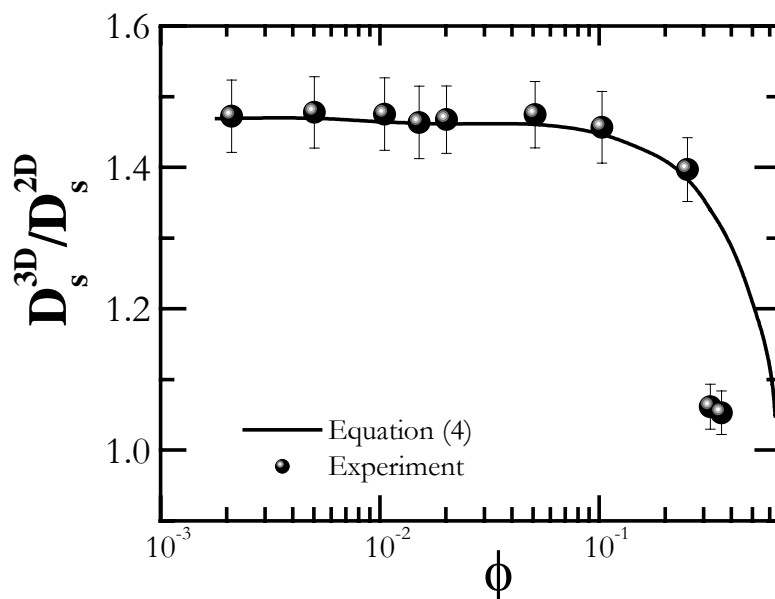
Figure 4.1.5: The ratio of the bulk to the near-wall self-diffusion as a function of volume fraction. The line corresponds to the model prediction (equation 4).

The ϕ-dependence of the near-wall self-diffusivity is also very interesting. We have already observed a weaker decay of the diffusivity than the in bulk. Stokesian dynamics simulations to calculate the order ϕ term in the virial expansion of $D_s^{2d}(\phi,\kappa)$ [1]. In the bulk, Batchelor predicts that $D_s^{3d}(\phi) = D_0(1-1.83\phi)$. Near the wall, however, this coefficient depends on the penetration depth so that in the dilute limit

$$D_s^{2d}(\phi,\kappa) = D_0^{2d}(\kappa)(1-\alpha(\kappa)\phi) \text{ (5)}$$

The coefficient $\alpha(\kappa)$ was calculated by averaging the His over all possible positions of a second particle around a first one (placed a distance h from the wall). Then this average is integrated over the height of the first particle above the wall weighted exponentially, akin to the ensemble average proposed above.
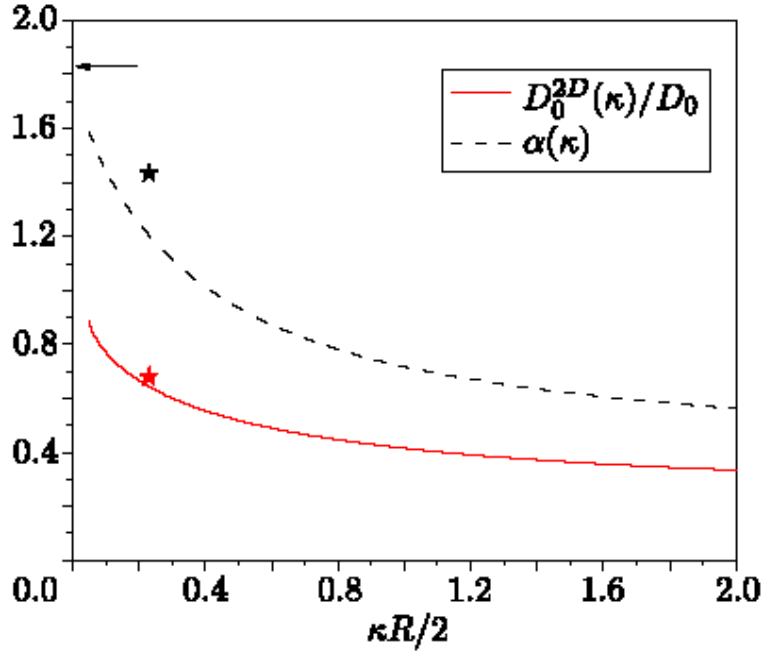
Figure 4.1.6: The contributions to the dilute limit, near-wall, short time self-diffusivity as predicted by Stokesian dynamics simulations. The stars are results from current set of experiments, and the arrow corresponds to Batchelor's prediction [19] for the decay of the self - diffusivity in the bulk (i.e. 1.83).

Figure 4.1.6 shows $D_0^{2d}(\kappa)/D_0$ and $\alpha(\kappa)$ as well as the dilute limit measurement from the experiments and the best fit dilute limit slope of the same diffusivity at $2/\kappa = 4.37R$ (these are denoted by stars on this figure). The results of simulations and the experiments are in very good agreement for both $D_0^{2D}(\kappa)/D_0$ and α(κ), while α(κ) is found to be clearly smaller than 1.83 (shown as an arrow in the figure) for all the values of κ. This suggests that the wall serves to screen out HI's among many particles in the dilute limit, reminiscent of the weaker decay of HI's near the wall $1/r^2$ versus $1/r$ in the bulk.

Concluding, we have shown that hard-sphere particle dynamics near a hard wall are significantly altered as ϕ is increased. The hydrodynamic drag that slows a particle in the vicinity of the wall in progressively weakened at high ϕ due to a counter-balancing of the wall-particle HIs by the particle-particle HIs. The wall is then felt as another, larger particle. While the convergence of near-wall and bulk dynamics at high volume fractions is observed

generically in both collective and self-diffusion, we have provided a simple model to describe the behavior of the short-time self-diffusion coefficient and further calculate the order ϕ contribution to a virial expansion of $D_s^{2d}(\phi, \kappa)$ from Stokesian dynamics simulations. The latter is found to be smaller than Batchelor's prediction in the bulk due to the screened HIs between particle pairs adjacent to a wall. In contrast, experimental data suggest that the near-wall collective diffusivity exhibits a stronger growth with ϕ when compared with the bulk. The study of the near-wall HIs on the collective diffusivity, the investigation of the ϕ-dependence of the parallel and perpendicular diffusivities, as well as an understanding of the long-time, near-wall diffusive behavior will be the subjects of future work. In particular, the investigation of the ϕ-dependence of the parallel and perpendicular diffusivities will be discussed in 4.2 in this Chapter.

4.2 Measurement of anisotropic Brownian motion near an interface by evanescent wave dynamic light scattering [25].

Within the last years, dynamic light scattering with evanescent illumination (EWDLS) has been established to study Brownian motion of particles in the close vicinity of a planar solid interface. The diffusion of colloidal particles [4, 5] has been studied in addition with the translational and rotational dynamics of stiff polymers adsorbed to the interface [26] and the collective motion of end grafted polymer brushes [27, 28]. Nevertheless, all experimental studies on Brownian motion near a hard wall by means of light scattering known so far suffer from the fact that it was not been possible to measure the particle's mobility parallel and normal to the wall independently and interpret the time autocorrelation function. A novel set - up for EWDLS with which we can change the scattering vector components parallel q_{II} and normal $q_{\perp}$ to the wall separately. Consequently the diffusivities parallel and perpendicular to the interface are experimentally available.

For these experiments, a triple axis goniometer and a spherical sample cell to construct a scattering geometry was used (Jülich)[2, 3]. The cell consists of a massive SF10-glass semispherical lens covered by a dome, which contains the sample solution as it can be seen in Figure 4.2.1 [3]. The incident beam is totally reflected from the interface between the bottom part and the solution. The upper limit is mainly set by focusing of the incoming beam in the bottom part of the sample cell and the divergence of the penetration depth at the critical angle. The nominal critical angle of total reflection α_c can be calculated from the refractive index of the SF10 glass n_1=1.7231 and of the solution n_2=1.497 for the sample solution. Experiments were performed on sterically stabilized PMMA spheres with radius R=156 nm in a mixed **tetralin/cis-decalin (30 %/ 70 %)** solution which was contained in the upper half-sphere of the sample cell. The particle volume fraction was varied between $0.002 \leq \phi \leq 0.4$. We prepared several volume fractions by progressively diluting a single batch of concentrated suspension; the volume fraction of the latter was determined both in the coexistence regime and from random close packing (RCP = 0.65).

Since we can change the observation angle in – plane θ and off – plane α_c, $q_\perp = 2\pi \sin \alpha_r / \lambda$ can be changed while $q_{II} = 2\pi \sqrt{1 + \cos \alpha_r^2 - 2 \cos \alpha_r \cos \theta} / \lambda$ is kept constant and vice versa. Here, is the wavelength of the evanescent wave and the scattered light in the sample, and the total scattering vector magnitude is given by $q = \sqrt{q_{II}^2 + q_\perp^2}$. In our experiments the illuminating beam comes from a He-Ne laser with a power of 35 mW and a vacuum wavelength of $\lambda_0 = 632.8$ nm, which is mounted on the source arm of the triple axis goniometer. Scattered light is collected with a single mode fiber and detected with an avalanche diode (ALV-APD, ALV-Laservertriebsgesellschaft, Germany). The diode's transistor-transistor logic (TTL) output is correlated with an ALV-6010 multiple tau correlator. Varying the angle of incidence, the penetration depth of the evanescent wave $\Xi = (2\pi \sqrt{(n_1 \sin \alpha_i)^2 - n_2^2})^{-1}$ can be changed approximately in the range $100nm < \Xi < 1\mu m$.
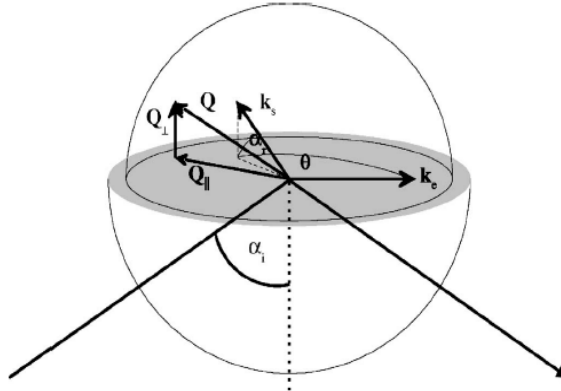
Figure 4.2.1: Spherical sample cell with total scattering vector Q and scattering vector components parallel $q_{//}$ and normal $q_\perp$ to the reflecting interface [3].

In figure 4.2.2 we show the effective short-time diffusion coefficient, $D^s(q)$, for the 3D measurements normalized by the corresponding dilute limit values. From the 3D dynamics shown in Fig. 4.2.2 we deduce the values of $D^sq)$ at the highest q that define the cooperative diffusion coefficient probing relaxation of concentration fluctuations via collective motions.
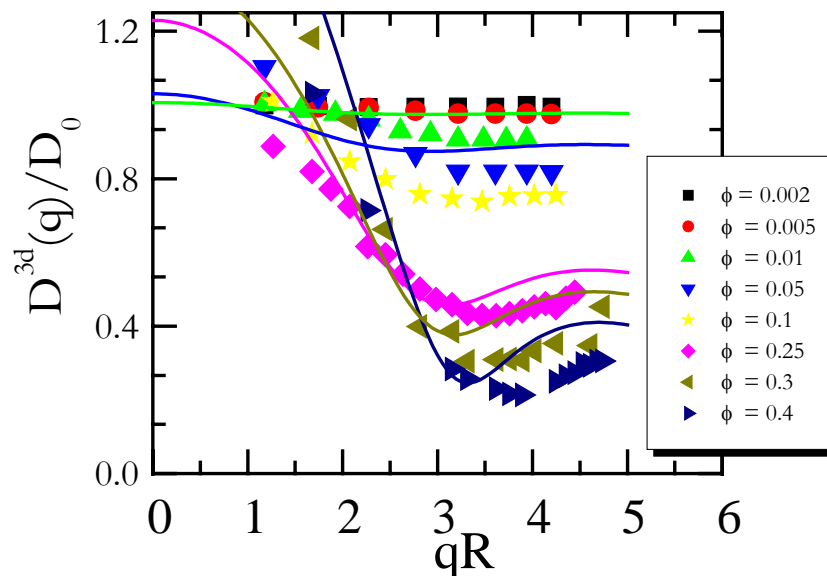
**Figure 4.2.2:** Normalized effective diffusion coefficients as a function of qR for indicative volume fractions in bulk. The solid lines are the theoretical predictions according to Beenaker and Mazur.

A wide range of q scan (either parallel or normal) was carried out for all the different volume fractions. Figure 2.4.3 below demonstrates the $q_{//}$ dependence of a dilute suspension as well as Figure 2.4.4 demonstrated the $q_{\perp}$ dependence of the same suspension. The same volume fraction's bulk correlation function at 90 ° lies in the same plots represented by a solid black line, in order to see the effect of the wall in the dynamics of the colloids. The slowing down is stronger in the normal component rather than the parallel in all cases. In the insets of Figures 4.2.3 & 4.2.4, the initial slope of the correlations is represented, where the strong effect of the wall in the dynamics is more pronounced.
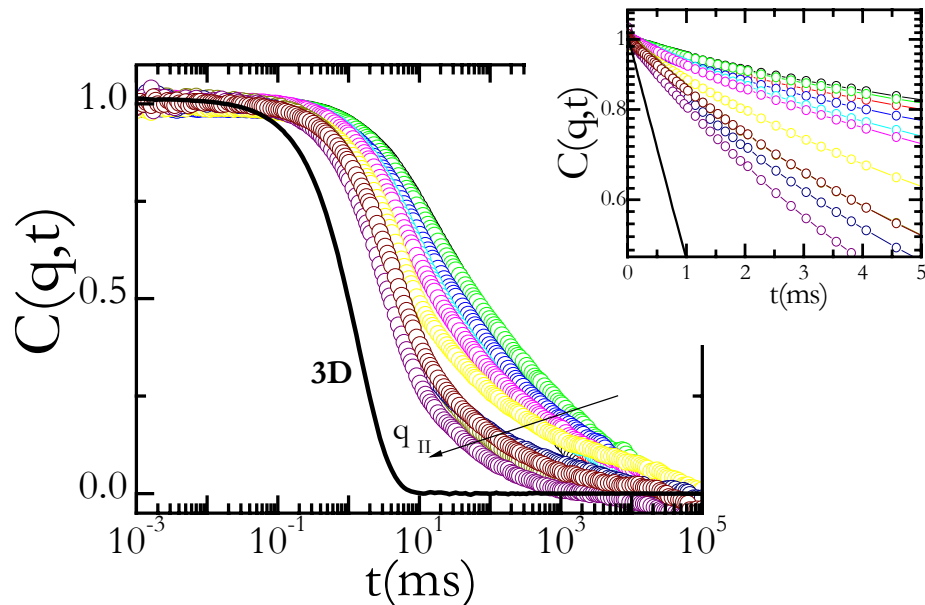
Figure 4.2.3: Correlation functions of bulk (3D, solid line) at 90 ° and near hard wall (2D) q‖ dependence, increasing with the direction of the arrow, for a dilute suspension (ϕ = 0.05). Insets: Log-lin plot of the initial decay.
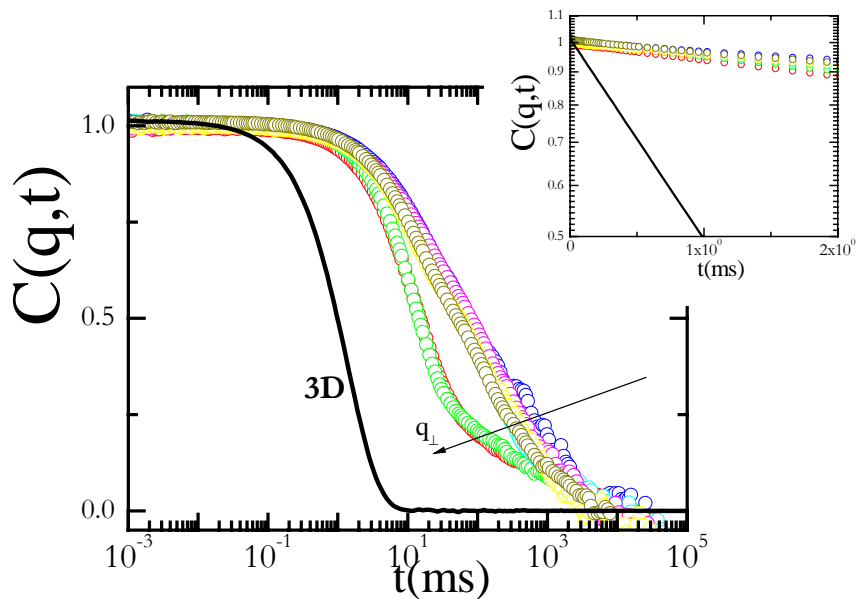
Figure 4.2.4: Correlation functions of bulk (3D, solid line) at 90 ° and near hard wall (2D) q⊥ dependence, increasing with the direction of the arrow, for a dilute suspension (ϕ = 0.05). Insets: Log-lin plot of the initial decay.

First cumulant analysis was used and the resulting values for the first cumulant were plotted versus q_{II}^2 and $(q_{\perp}^2 + \frac{1}{\Xi^2})$ (Figure 4.2.5). In both sets of data, Γ depended linearly on q_{II}^2 and $(q_{\perp}^2 + \frac{1}{\Xi^2})$ as expected. $\Gamma = q_{II}^2 <D_{II}>(\Xi) + (q_{\perp}^2 + \frac{1}{\Xi^2}) <D_{\perp}>(\Xi)$

In the latter case the slope is evidently smaller than in the first, which shows that, close to the wall, the diffusivity of the particles is anisotropic in the range of separation distances that are probed. Corresponding results were obtained at different penetration depths.

One should consider two different diffusivities parallel and normal to the wall, which depends differently on the separation distance z of a colloidal sphere to the wall. An average then diffusivity for each specific qR may be the sum of $D = \left(\frac{2}{3} D_{II}\right) + \left(\frac{1}{3} D_{\perp}\right)$.
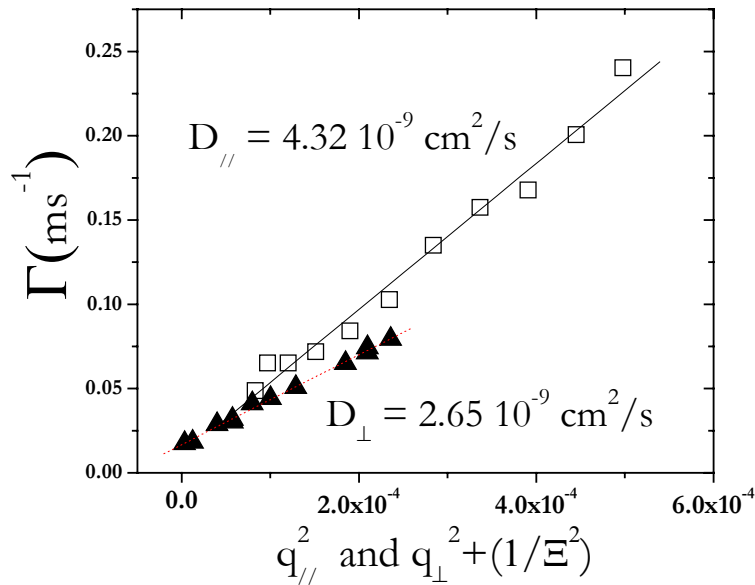
Figure 4.2.5: Initial relaxation rates Γ recorded at a penetration depth 900 nm for $\Phi = 0.05$. The symbol (▲) relates to the different values of $q_{\perp}$ at constant q_{II} vs $(q_{\perp}^2 + \frac{1}{\Xi^2})$ while the symbol (□) relates to the different values of q_{II} at constant $q_{\perp}$ vs q_{II}^2. The straight lines represent linear fits.

Figure 4.2.6 and 4.2.7 below show the correlation functions measured in 3D and 2D for four different volume fractions, from a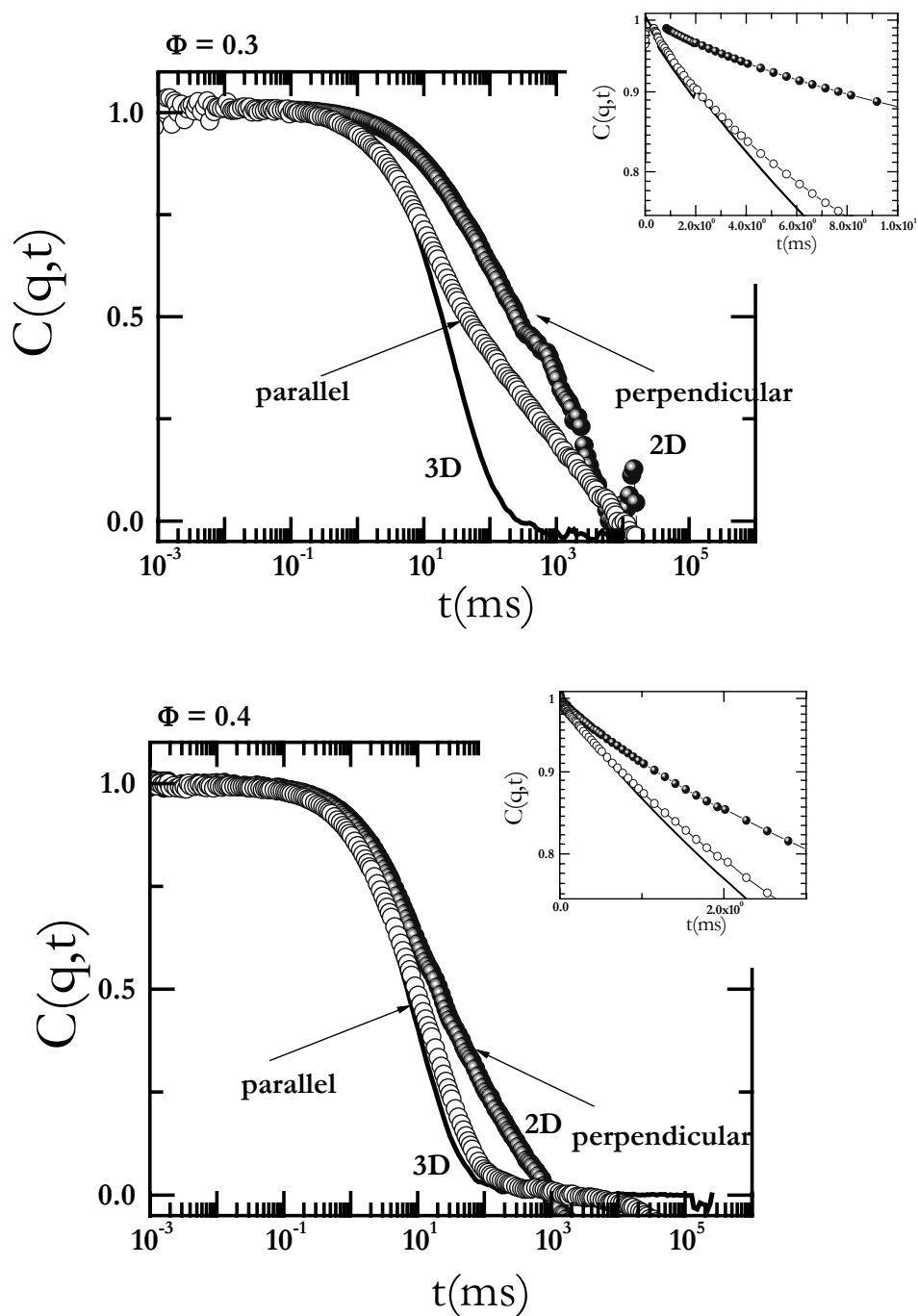 dilute to a concentrated suspension at $\theta \sim 60^\circ$ for the parallel and the perpendicular component (where in EWDLS $q_\parallel \sim q_\perp$). It is evident that in the dilute suspension both the parallel and the perpendicular dynamics near the wall are clearly slower due to hydrodynamic wall drag effect. In contrast, at higher volume fractions, the short time part of the 3D and the 2D parallel component, are virtually the same.

Also, in the concentrated suspensions, $\varphi = 0.25, 0.3, 0.4$, it is noticeable the different dynamics of the parallel and the perpendicular component as compared to the bulk. The parallel one seems to follow the 3D dynamics whereas the perpendicular is still slower than the bulk. As we have already reported previously, a similar effect was noticed in a dilute hard sphere suspension, where the average dynamics near the wall (parallel and perpendicular) became the same at around $\varphi = 0.35$.
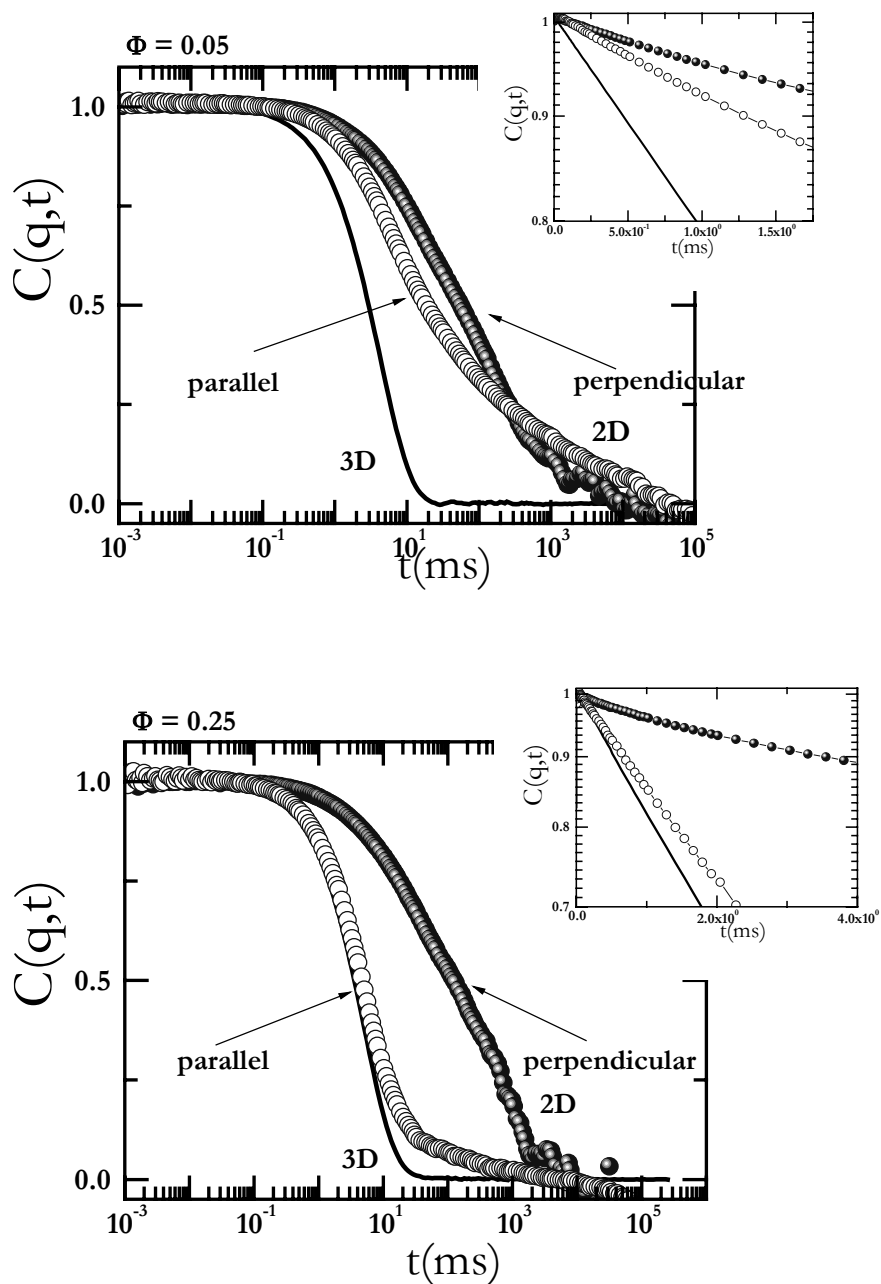
Figure 4.2.6: Correlation functions in bulk (3D) and near a hard wall (2D) at q=0.015nm^{-1} (q∥~ q⊥ at θ~60º) for a dilute (ϕ = 0.05) suspension and a concentrated suspension (ϕ = 0.05). Insets: Log-lin plot of the initial decay. (α_r = 60 ° and θ = 60 ° for the parallel, and α_r = 60 ° and θ = 0 ° for the perpendicular component.)
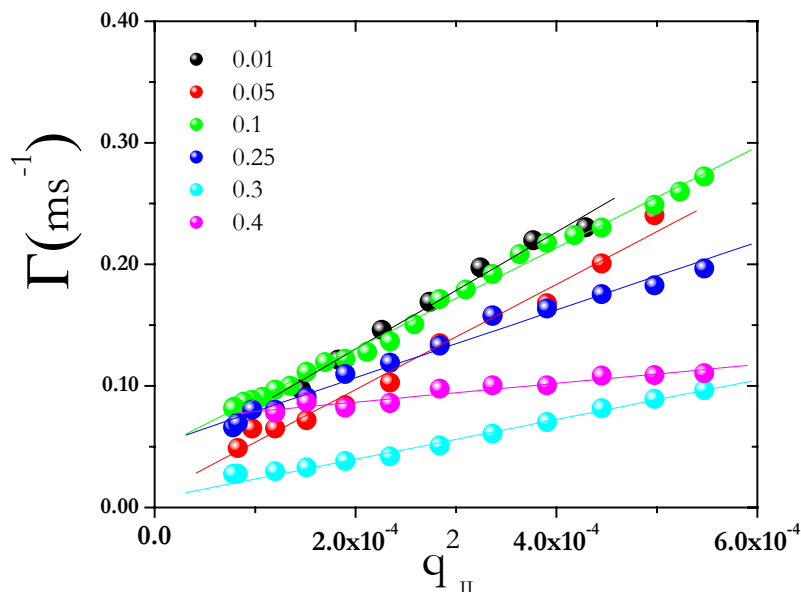
Figure 4.2.7: Correlation functions in bulk (3D) and near a hard wall (2D) at q=0.015nm^{-1} (q$_\parallel$ ~ q$_\perp$ at θ~60°) for two concentrated suspensions (ϕ = 0.3 and 0.4). Insets: Log-lin plot of the initial decay. (α_r = 60 ° and θ = 60 ° for the parallel, and α_r = 60 ° and θ = 0 ° for the perpendicular component.)

Figure 4.2.8: Initial relaxation rates Γ related to the different values of q_{II} at constant $q_{\perp}$ vs q_{II}^2 recorded at a penetration depth 900 nm for a range of ϕ's. The straight lines represent linear fits.
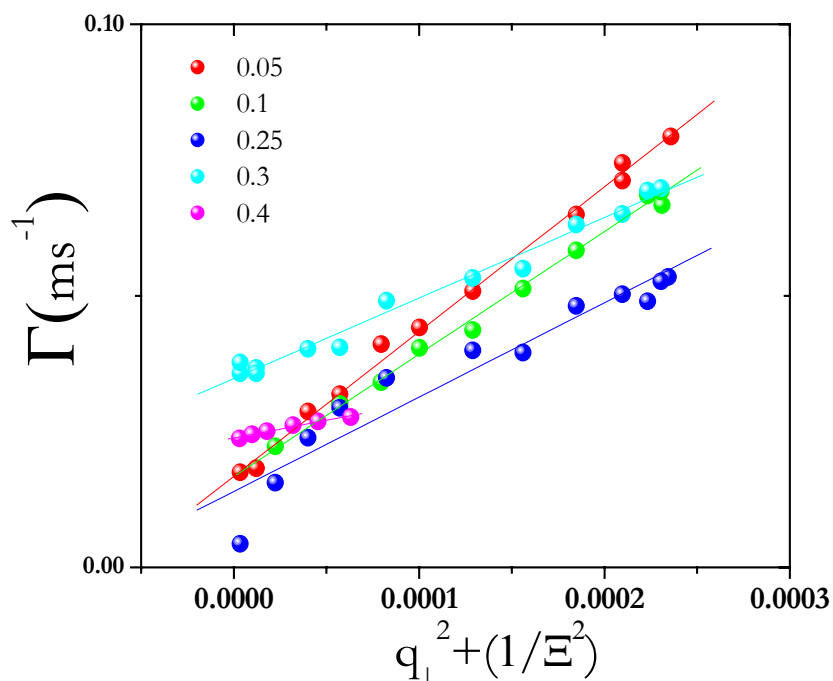
Figure 4.2.9: Initial relaxation rates Γ related to the different values of $q_{\perp}$ at constant q_{II} vs $(q_{\perp}^2 + \frac{1}{\Xi^2})$, recorded at a penetration depth 900 nm for a range of ϕ's. The straight lines represent linear fits.

Resulting values for the first cumulant Γ are plotted versus q_{II}^2 and $(q_{\perp}^2 + \frac{1}{\Xi^2})$ in Figure 4.2.8

and 4.2.9 for a penetration depth of 900 nm. In both data sets, Γ depends linearly on q_{II}^2

and $(q_{\perp}^2 + \frac{1}{\Xi^2})$. In the latter case the slope is smaller than the first, which shows that, close to

the wall, the diffusivity of the particles is anisotropic in the range of separation distances that

are probed. The mean diffusivities can be determined by the slopes of each fit.

Volume fraction (φ)	$D_{//}^{mean}(10^{-9}cm^2/s)$	$D_{\perp}^{mean}(10^{-9}cm^2/s)$
0.01	4.8	2.8
0.05	4.32	2.65
0.1	4.15	2.25
0.25	2.78	1.73
0.3	1.65	1.48
0.4	0.8	0.68

Table 4.2.1: The mean parallel and the normal diffusivities of the colloids near the hard wall at different volume fractions.
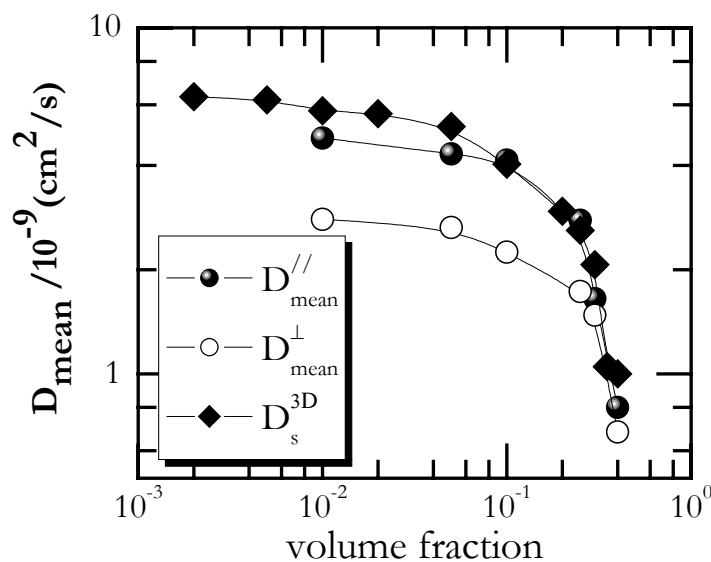
Figure 4.2.10: The parallel and the normal mean diffusivities of the colloids near the hard wall as a function of volume fraction together with the self – diffusivities of the bulk suspensions.

Table 4.2.1 above summarizes the mean diffusivities of the parallel and the perpendicular component as obtained by the slopes from Figures 4.2.8 & 4.2.9 for different volume fractions. In addition, the same obtained mean diffusivities are plotted as a function of volume fraction in Figure 4.2.10 together with the self – diffusivities of the bulk dynamics of the particles.
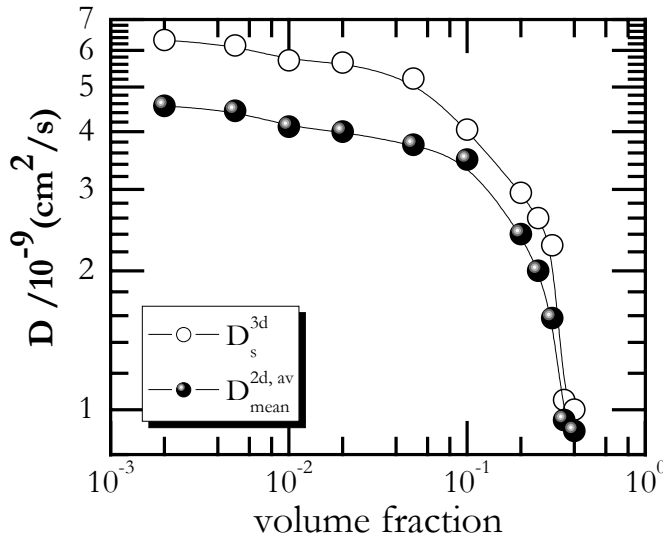
Figure 4.2.11: Volume fraction dependence of the short-time diffusion coefficients in bulk (3D) and near the wall mean diffusivities (2D). Lines are to guide the eye.

In figure 4.2.11 we show the evolution of the self-diffusion coefficient (determined at the highest q's) with increasing volume fraction for the 3D and near wall case. At the limit $\varphi \rightarrow 0$ we get $D^{2D}/D^{3D}=0.72$ in qualitative agreement with the theoretical predictions for the hydrodynamic slowing down of particle near a hard wall (giving 0.85).

In figure 4.2.12 we show the self - diffusion coefficients in 3D and the mean diffusive coefficient of the 2D normalized by D_0^{3D}. As expected, in both cases the self-diffusion slows down with increasing φ. However, interestingly, while both are slower near the wall at low φ as particle density increases they merge towards each other so that above $\varphi \sim 0.25$ the dynamics are virtually indistinguishable (see also Figure 4.2.6 & 4.2.7). Therefore the near wall self-diffusion (D^{2D}) decays with φ weaker than the 3D one (D^{3D}). As shown in Figure 4.2.12 the 3D self diffusion, follows very well the Batchelor's virial expansion up to $\varphi \sim 0.1$.
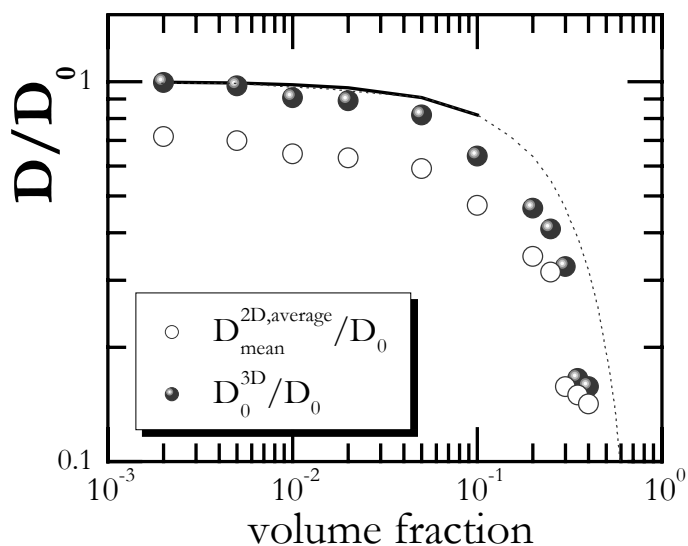
Figure 4.2.12: The ϕ-dependence of the short-time self - diffusion coefficients in bulk and near the wall (mean average over parallel and normal) diffusivities. The solid lines correspond to Batchelor's dilute predictions and the dashed lines are the results of Stokesian dynamics simulations [24].

In a previous work, a simple model was used to describe the physical origin of the diminished hydrodynamic wall effect on the dynamics at high φ's provided by Swan and Brady [1].
In Figure 4.2.13 below, the simple model is in good agreement with our experimental data.
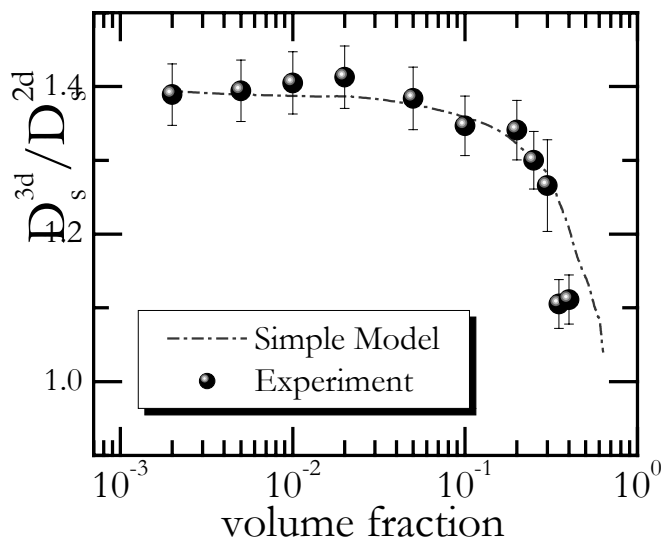
Figure 4.2.13: The ratio of the bulk to the near-wall self-diffusion as a function of volume fraction. The line corresponds to the model prediction [1].
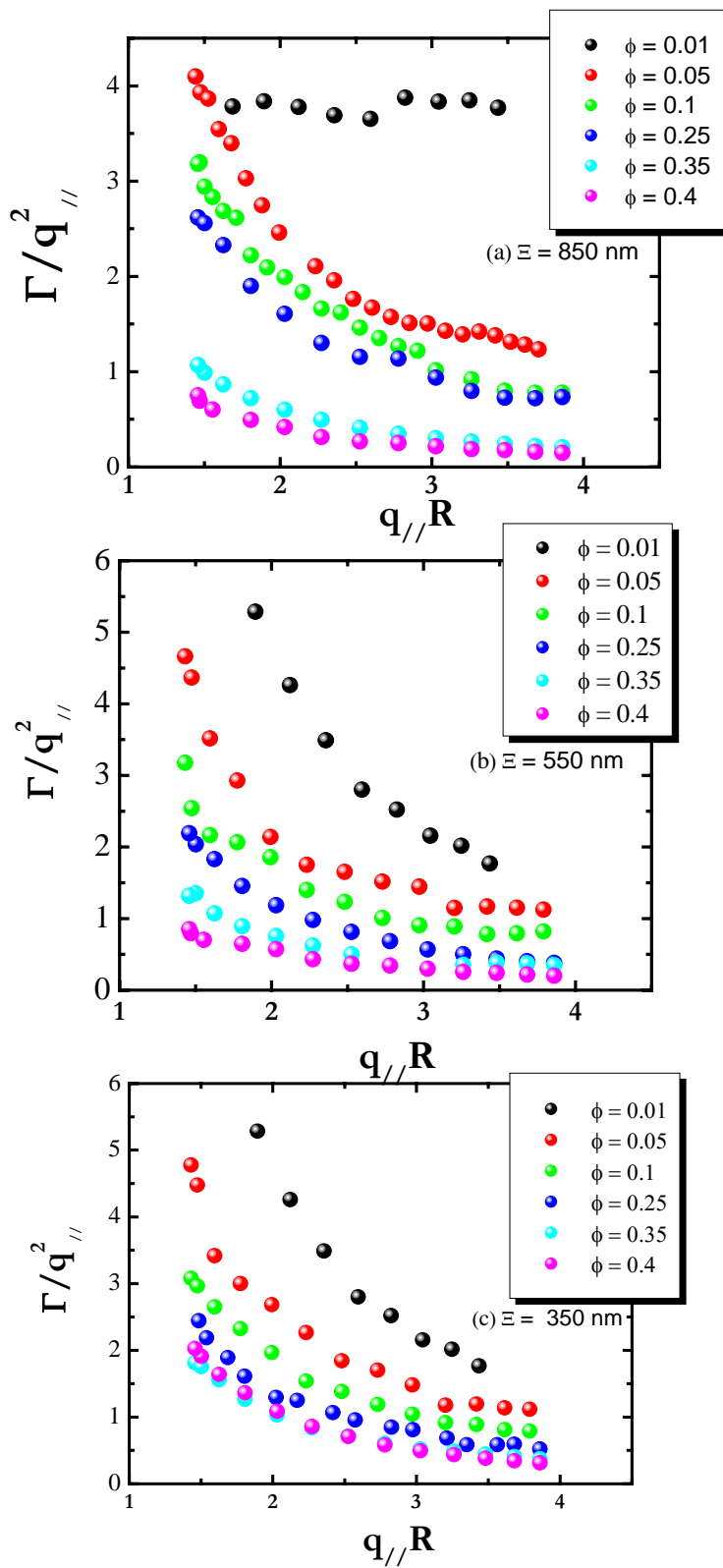
Figure 4.2.14: $\Gamma / q_{//}^2$ vs $q_{//}R$ at constant $q_\perp$ for three different penetration depths: (a) 850 nm (b) 550 nm and (c) 350 nm for different volume fractions.
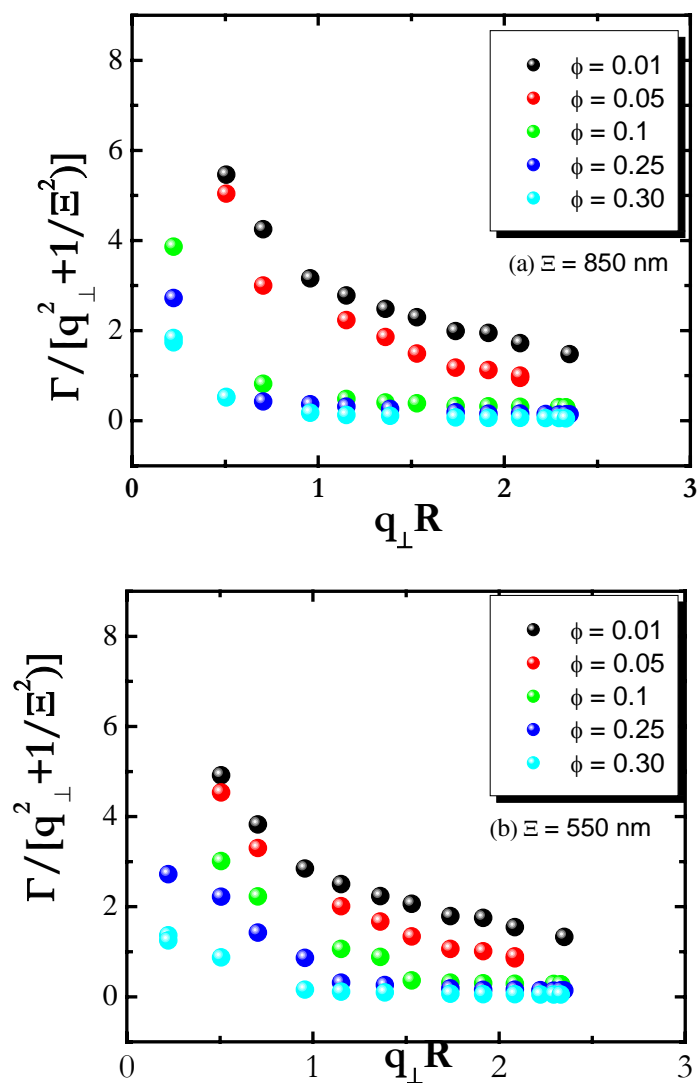
Figure 4.2.15: $\Gamma/[q_\perp^2 + \left(1/\Xi^2\right)]$ vs $q_\perp R$ for two different penetration depths: (a) 850 nm and (b) 550 nm for different volume fractions.

One could proceed with the interpretation of such rich data using two different approaches. First, we examine the data treating each component $(q_{//}, q_\perp)$ separately. Figure 4.2.14 summarizes the results of the relaxation rate Γ obtained by initial slope analysis and $\Gamma/q_{//}^2$ is plotted vs $q_{//}R$ for three different penetration depths: 850 nm, 550 nm and 350 nm. Similarly,

Figure 4.2.15 demonstrates the results of $\Gamma/[q_\perp^2 + \left(\frac{1}{\Xi^2}\right)]$ vs $q_\perp R$ for two different penetration depths: 850 nm and 550 nm. In all cases, we find a strong increase of the either $\Gamma/q_{//}^2$ or $\Gamma/[q_\perp^2 + \left(\frac{1}{\Xi^2}\right)]$ as the associated qR's decreases as the volume fraction increases. This effect resembles the same finding in the 3D bulk dynamics.

On the other hand, we can treat the experimental data having a total q component instead of the two $(q_{//}, q_\perp)$. The total q component is given by $q = \sqrt{q_{II}^2 + q_\perp^2}$ as mention before.
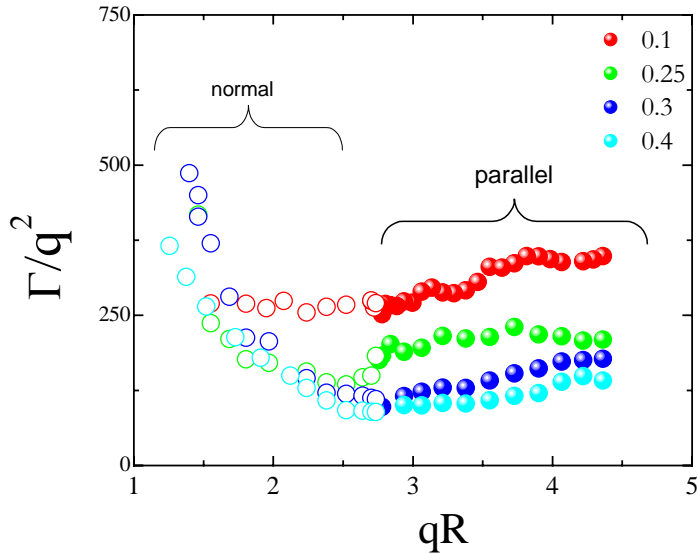
Figure 4.2.16: Γ/q^2 vs qR for a penetration depth of 850 nm for four different volume fractions where q stands for the total q ($q = \sqrt{q_{II}^2 + q_\perp^2}$).

Figure 4.2.16 illustrates the Γ/q^2 vs qR for a penetration depth of 850 nm for four different volume fractions. In this plot, the relaxation rates results from the experimental series (parallel and the normal) are plotted vs the total scattering wavevector q. As we can see, we have clear satisfactory continuous data points as we gradually shift from the parallel to the normal limits.

Further analysis is currently underway in order to understand the rich and complex data sets.

Concluding, we have shown experimentally, that the effect of wall viscous drag gives rise to anisotropy of the mobility of Brownian particles. With this set – up, it was possible to measure mean diffusivities parallel and normal to the wall independently. We have found that the wall drag effect has a pronounced effect on the diffusive properties of colloidal hard spheres.

In the dilute suspension both the parallel and the perpendicular dynamics near the wall are clearly slower due to hydrodynamic wall drag effect. In contrast, at higher volume fractions the correlation functions in 3D and 2D, especially the 3D with the short-time part of the parallel components, are virtually the same.

4.3 REFERENCES

1.   Michailidou, V., G. Petekidis, J. Swan, and J.F. Brady, *Dynamics of concentrated colloidal suspensions near a hard wall.* Physical Review Letters, 2008. **Submitted**.

2.   Holmqvist, P., J.K.G. Dhont, and P.R. Lang, *Colloidal dynamics near a wall studied by evanescent wave light scattering: Experimental and theoretical improvements and methodological limitations.* Journal of Chemical Physics, 2007. **126**(4).

3.   Holmqvist, P., J.K.G. Dhont, and P.R. Lang, *Anisotropy of Brownian motion caused only by hydrodynamic interaction with a wall.* Physical Review E - Statistical, Nonlinear, and Soft Matter Physics, 2006. **74**(2).

4.   Lan, K.H., N. Ostrowsky, and D. Sornette, *Brownian dynamics close to a wall studied by photon correlation spectroscopy from an evanescent wave.* Physical Review Letters, 1986. **57**(1): p. 17-20.

5.   Lobry, L. and N. Ostrowsky, *Diffusion of Brownian particles trapped between two walls: Theory and dynamic-light-scattering measurements.* Physical Review B - Condensed Matter and Materials Physics, 1996. **53**(18): p. 12050-12056.

6.   Squires, T.M. and M.P. Brenner, *Like-charge attraction and hydrodynamic interaction.* Physical Review Letters, 2000. **85**(23): p. 4976-4979.

7.   Pesche, R. and G. Nagele, *Stokesian dynamics study of quasi-two-dimensional suspensions confined between two parallel walls.* Physical Review E - Statistical Physics, Plasmas, Fluids, and Related Interdisciplinary Topics, 2000. **62**(4 B): p. 5432-5443.

8.   Beatus, T., R. Bar-Ziv, and T. Tlusty, *Anomalous microfluidic phonons induced by the interplay of hydrodynamic screening and incompressibility.* Physical Review Letters, 2007. **99**(12).

9.   Riedel, I.H., K. Kruse, and J. Howard, *Biophysics: A self-organized vortex array of hydrodynamically entrained sperm cells.* Science, 2005. **309**(5732): p. 300-303.

10.   Russel W. B., S.D.A., and. Schowalter W. R., *Colloidal Dispersions.* 1989, Cambridge: Cambridge University Press.

11.   Whitesides, G.M. and A.D. Stroock, *Flexible methods for microfluidics.* Physics Today, 2001. **54**(6): p. 42.

12. Psaltis, D., S.R. Quake, and C. Yang, *Developing optofluidic technology through the fusion of microfluidics and optics.* Nature, 2006. **442**(7101): p. 381-386.

13. Carbajal-Tinoco, M.D., R. Lopez-Fernandez, and J.L. Arauz-Lara, *Asymmetry in colloidal diffusion near a rigid wall.* Physical Review Letters, 2007. **99**(13).

14. Filippidi, E., V. Michailidou, B. Loppinet, J. Ru?he, and G. Fytas, *Brownian diffusion close to a polymer brush.* Langmuir, 2007. **23**(9): p. 5139-5142.

15. Fytas, G., S.H. Anastasiadis, R. Seghrouchni, D. Vlassopoulos, J. Li, B.J. Factor, W. Theobald, and C. Toprakcioglu, *Probing collective motions of terminally anchored polymers.* Science, 1996. **274**(5295): p. 2041-2044.

16. Michailidou, V.N., B. Loppinet, O. Prucker, J. Ruhe, and G. Fytas, *Cooperative diffusion of end-grafted polymer brushes in good solvents.* Macromolecules, 2005. **38**(21): p. 8960-8962.

17. Michailidou, V.N., B. Loppinet, D.C. Vo, O. Prucker, J. Ruhe, and G. Fytas, *Dynamics of end-grafted polystyrene brushes in theta solvents.* Journal of Polymer Science, Part B: Polymer Physics, 2006. **44**(24): p. 3590-3597.

18. Nugent, C.R., K.V. Edmond, H.N. Patel, and E.R. Weeks, *Colloidal glass transition observed in confinement.* Physical Review Letters, 2007. **99**(2).

19. Brady, J.F., *Response to "comment on 'the rheological behavior of concentrated colloidal dispersions'" [J. Chem. Phys. 101, 1757 (1994)].* The Journal of Chemical Physics, 1994. **101**(2): p. 1758.

20. Faxen, H., *Die bei Interferenz von Rontgenstrahlen infolge der Warmebewegung entstehende Streustrahlung.* Zeitschrift fur Physik, 1923. **17**(1): p. 266-278.

21. Pusey, P.N. and D.L. edited by J. P. Hansen, and J. Zinn-Justin, *Freezing and the Glass Transition in Liquids.* 1991, Amsterdam: Elsevier.

22. Batchelor, G.K., *Brownnian diffusion of particles with hydrodynamic interaction.* Journal of Fluid Mechanics, 1976. **74**(pt 1): p. 1-29.

23. Batchelor, G.K., *Brownnian diffusion of particles with hydrodynamic interaction.* Journal of Fluid Mechanics, 1976. **74**(1).

24. Banchio, A.J. and J.F. Brady, *Accelerated stokesian dynamics: Brownian motion.* Journal of Chemical Physics, 2003. **118**(22): p. 10323-10332.

25.   Michailidou, V., G. Petekidis, J. Swan, J.F. Brady, P.R. Lang, and J.K.G. Dhont, *Measurement of anisotropic Brownian motion near an interface by evanescent wave dynamic light scattering.* In preparation, 2008.

26.   Loppinet, B., G. Petekidis, G. Fytas, R. Rulkens, and G. Wegner, Langmuir, 1998. **14**: p. 4858.

27.   Semenov, A.N. and S.H. Anastasiadis, *Collective dynamics of polymer brushes.* Macromolecules, 2000. **33**(2): p. 613-623.

28.   Yakubov, G.E., B. Loppinet, H. Zhang, J. Ruhe, R. Sigel, and G. Fytas, *Collective Dynamics of an End-Grafted Polymer Brush in Solvents of Varying Quality.* Physical Review Letters, 2004. **92**(11): p. 115501-1.

Chapter 5

5. CONCLUSIONS

During this work we have studied the interfacial dynamics of different soft matter systems including polymer brushes, colloidal particles and mixtures. The main technique employed was the Evanescent Wave Dynamic Light Scattering, used to probe dynamics near a surface.

In this work, a comprehensive study on the collective dynamics of end-grafted polystyrene brushes in pure solvents, including good solvents and a theta solvent using the powerful technique of evanescent wave dynamic light scattering was reported.

Synthesis of a wide range of polymer brushes was carried out using the "grafting from" technique. We have used different monomers such as polystyrene and polymethylmethacrylate and a variation of well defined polymer brushes were achieved. All brushes had high molecular

weight (10^6 g/mol) and different dry thickness, which were measured by ellipsometry as well as atomic force microscopy (AFM).

First, using chemically end grafted polydisperse polymer brushes (three polystyrene and one poly (n-butylacrylate) samples), in good solvent, we have identified the theoretically predicted cooperative diffusion. The concentration fluctuations of a given wave vector q decay slower with decreasing grafting density σ and the associated intensity increased rather strongly with σ.

We have prolonged our studies of polymer brushes in theta solvent resulting in slow and broad dynamics when the solvent environment changes, from good to theta conditions. The decay of the relaxation function for the polymer density fluctuations becomes bimodal and is well described by a sum of one single exponential and a broad stretched exponential decay. The diffusive relaxation rate of the fast mode was related to the cooperative diffusion whereas the origin of the slower process with a q-independent rate was not certain. The results of the study showed that measurements of the brush dynamics provide detailed local structural information and allow quantifying the solvent quality directly, which is not possible based on static measurements alone.

Carrying on our extended studies we have investigated, both the penetration and diffusivities of particles of different sizes in contact with a swollen polymer brush in a good solvent environment. The penetration depth dependence of the scattered intensity evidenced a size selective penetration of the particles within the brush. Large hard spheres were found to be largely expelled from the brush and their diffusivities were only slightly slowed down, reflecting a certain drag reduction from the brush. Small softer particles showed a partial penetration of the brush. The slower diffusivities of the penetrating particles reflected their increased friction within the brush, providing an indirect structural characterization of the brush. Extending these studies on a polymer brush/particle system, we have shown how particle penetration in the brush can be measured and offer an estimate of the brush height and how different degree of penetration affected the measured surface diffusivities. In addition, we have further investigated the diffusivities of colloidal particles within swollen brushes, focusing on the effect of the brushes grafting density on both particle penetration and diffusivity.

Finally, we use evanescent wave dynamic light scattering to investigate the Brownian motion of colloidal particles near a solid, planar surface. A simple model was proposed that captured

the basic physical mechanism responsible for particles' behavior, while a quantitative prediction of the weaker decay of the near-wall self-diffusion coefficient with volume fraction was offered by Stokesian Dynamics simulations. At high volume fractions, it seems that the particles exhibit similar behaviour either when in close proximity to another particle or to the wall.

The same system was used to study the anisotropic diffusion of colloidal suspensions, varying the volume fraction of the colloidal suspensions, from the dilute to a concentrated regime. With this set – up used (Juelich) it was possible to measure mean diffusivities parallel and normal to the wall independently. We have found that the wall drag effect has a pronounced effect on the diffusive properties of colloidal hard spheres. In the dilute suspension both the parallel and the perpendicular dynamics near the wall are clearly slower due to hydrodynamic wall drag effect. In contrast, at higher volume fractions the correlation functions in 3D and 2D, especially the 3D with the short-time part of the parallel components, are virtually the same.